12-2016

Coarse-Grained Simulations of the Self-Assembly of DNA-Linked Gold Nanoparticle Building Blocks

Charles Wrightsman Armistead
University of Arkansas, Fayetteville

Coarse-Grained Simulations of the Self-Assembly of
DNA-Linked Gold Nanoparticle Building Blocks

A thesis submitted in partial fulfillment
of the requirements for the degree of
Master of Science in Cell and Molecular Biology

by

Charles Armistead
University of Arkansas
Bachelor of Science in Biomedical Engineering, 2014

December 2016
University of Arkansas

This thesis is approved for recommendation to the Graduate Council.

Dr. Jin-Woo Kim
Thesis Director

Dr. Matthew Patitz
Committee Member

Dr. Joshua Sakon
Committee Member

Abstract

The self-assembly of nanoparticles (NPs) of varying shape, size, and composition for the purpose of constructing useful nanoassemblies with tailored properties remains challenging. Although progress has been made to design anisotropic building blocks that exhibit the required control for the precise placement of various NPs within a defined arrangement, there still exists obstacles in the technology to maximize the programmability in the self-assembly of NP building blocks. Currently, the self-assembly of nanostructures involves much experimental trial and error. Computational modeling is a possible approach that could be utilized to facilitate the purposeful design of the self-assembly of NP building blocks into a desired nanostructure. In this report, a coarse-grained model of NP building blocks based on an effective anisotropic mono-functionalization approach, which has shown the ability to construct six building block configurations, was used to simulate various nanoassemblies. The purpose of the study was to validate the model's ability to simulate the self-assembly of the NP building blocks into nanostructures previously produced experimentally. The model can be programmed to designate up to six oligonucleotides attached to the surface of a Au NP building block, with a modifiable length and nucleotide sequence. The model successfully simulated the self-assembly of Au NP building blocks into a number of previously produced nanostructures and demonstrated the ability to produce visualizations of self-assembly as well as calculate interparticle distances and angles to be used for the comparison with the previous experimental data for validation of the model. Also, the model was used to simulate nanoassemblies which had not been produced experimentally for its further validation. The simulations showed the capability of the model to use specific NP building blocks and self-assemble. The coarse-grained NP building block model

shows promise as a tool to complement the purposeful experimental design of functional nanostructures.

Acknowledgements

Special thanks are extended to my parents for their constant support during my time at the University of Arkansas. I would also like to thank my advisor, Dr. Jin-Woo Kim, and the other members of the Bio/Nano Technology Group, Arvind Sinha, Joseph Batta-Mpouma, and Betty Martin.

Also, a special thanks goes out to my committee members, Dr. Patitz and Dr. Sakon, and the members of the Self-Assembly Computer Science Group, Jacob Hendricks and Tyler Fochtman. This work was supported in part by National Science Foundation (CMMI 1235100).

Table of Contents

List of Figures

List of Tables

Chapter 1: Introduction

Nanotechnology is an interdisciplinary field that concentrates its efforts on manipulating atoms and molecules to engineer materials of particular size, shape, and composition at the nanometer level, offering far-reaching possibilities and challenges (Cai, Gao, Hong, & Sun, 2008; Cao, 2004; Ochekpe, Olorunfemi, & Ngwuluka, 2009; Varadan et al., 2010). With the correct specifications, these materials can be designed by arranging atomic or molecular components into innovative structures, devices, and systems, exhibiting unique characteristics due to their chemical, biological, electrical, and magnetic properties (Cai, Gao, Hong, & Sun, 2008; Cao, 2004; Cuenca et al., 2006; Ochekpe, Olorunfemi, & Ngwuluka, 2009; Sharma, Dutta, & Pandey, 2011; Varadan et al., 2010). Taking advantage of their noteworthy properties, these nanomaterials can be applied to practical applications in many different fields such as biomedical engineering with clinical objectives for drug delivery, cancer theranostics, and bio-imaging (Varadan et al., 2010; Cuenca et al., 2006; Sharma, Dutta, & Pandey, 2011).

The beginnings of nanoscience can be attributed to the preliminary works of Feynman, Taniguchi, and Drexler (Varadan et al., 2010). The manipulation of specific atoms and molecules and its possible innovations was first described by Feynman in his paper, "*There's Plenty of Room at the Bottom: An Invitation to Enter a New Field of Physics*," in 1959 (Feynman, 1960; Ochekpe et al., 2009; Varadan et al., 2010). Although Feynman is considered the father of nanotechnology, the term actually originated in 1974, with Taniguchi (Varadan et al., 2010). Later, Drexler would present a series of notable publications on molecular nanotechnology, publishing its first technical paper in 1981, describing a molecular computer in 1983, and printing its first book, *Engines of Creation*, in 1986 (Drexler, 1986; Varadan et al., 2010).

To appreciate the field of nanotechnology and investigate its many possible applications, it is essential to understand what occurs at the nanoscale that affects a particular nanomaterial's properties (Cao, 2004; Varadan et al., 2010; Wilson, Kannangara, Smith, Simmons, & Raguse, 2002). When a material has at least one dimension in the nanometer range, its properties become size-dependent, which leads to changes in atomic structure, chemical reactivity, and its optical and physical properties (Varadan et al., 2010).

Since nanomaterials offer many unique, size-dependent properties that can be tailored for a given application, a great deal of research aims to obtain precise control over the positions of each component within a desired nanostructure (Alivisatos, 1996, "*Semiconductor"*; Alivisatos, Johnsson, Peng, Wilson, Loweth, Bruchez, & Schultz, 1996; Bethune et al., 1993; Iijima, 1991; Iijima & Ichihashi, 1993; Jones, Seeman, & Mirkin, 2015; Kelsall, Hamley, & Geoghegan, 2005). To accurately predict the final arrangement of each component, the interactions that occur between molecules in the system must be fully understood and sufficiently directional, so as to ensure greater control over the system and increase the probability of obtaining the desired product(s) (Jones et al., 2015).

When considering the manufacturing of nanoscale materials, there are generally two techniques: the top-down and bottom-up approaches (see Figure 1; Bhushan, Luo, Schricker, Sigmund, & Zauscher, 2014; Hsu, 2010; Niemeyer, 2001; Varadan et al., 2010). The top-down approach involves the removal or breakdown of the initial material to produce a desired structure in the nanometer range (Hsu, 2010; Zhang, 2003). Since this approach is limited to two-dimensional surfaces, the bottom-up approach has attracted many due to its usage of nanoscale components that are designed to spontaneously self-assemble into a final structure (Hsu, 2010; Varadan et al., 2010; Zhang, 2003). Self-assembly is regulated by differentiated and controllable

interactions and driven by a reduction in Gibbs free energy to cause a system's building blocks to organize themselves in a controlled fashion with the precision to form a defined structure (Cao, 2005; Hsu, 2010; John & Bär, 2005; Varadan et al., 2010).

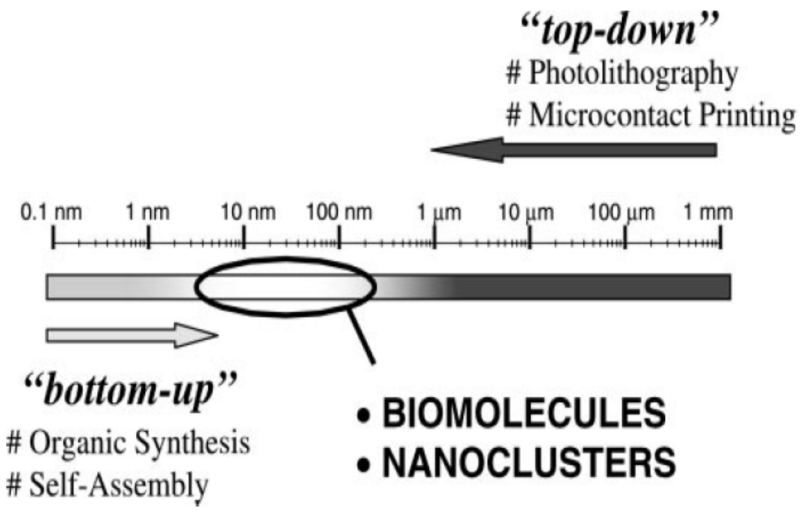

Figure 1. Top-down and bottom-up strategies for nanoscale fabrication. For nanoscale building blocks, biomolecules, such as nucleic acids, and metal and semiconductor material colloidal nanoparticles (NPs) are well-suited for bridging the gap between bottom-up and top-down processes. Adapted with permission from "Nanoparticles, proteins, and nucleic acids: biotechnology meets materials science," by C. M. Niemeyer, 2001, *Angewandte Chemie International Edition, 40,* p. 4131.

Self-assembly can be seen occurring in biological settings, notably with deoxyribonucleic acid (DNA) (Varadan et al., 2010). A single strand of this complex biological molecule has the ability to selectively recognize another strand of a complementary sequence and to be modified at either its 5' or 3' ends (Varadan et al., 2010). These properties make DNA an ideal candidate to be incorporated into building blocks, acting as a molecular glue to assemble nanoscale components into a desired structure (Varadan et al., 2010).

Nanoparticles (NPs) are another possible component to be utilized in the self-assembly process. The behavior of their properties at the nanoscale could realize many new materials to be applied towards specific applications (Alivisatos et al., 1996; Kyrychenko, Karpushina, Bogatyrenko, Kryshtal, & Doroshenko, 2011; Vardan et al., 2010). One possible way to incorporate NPs into nanoscale building blocks is to functionalize single-stranded DNA (ssDNA) to the surface of the NP (Alivisatos, 1996, "Perspectives"; Alivisatos, 1996, "*Semiconductor"*; Kyrychenko et al., 2011; Varadan et al., 2010). A building block composed of a single NP and ssDNA would provide the opportunity to take advantage of DNA's selective molecular recognition to self-assemble various NPs into a desired final structure (Alivisatos, 1996, "Perspectives"; Alivisatos, 1996, "*Semiconductor"*; Kryrchenko et al., 2011). Various researchers have demonstrated the ability to arrange Au NPs into defined structures using DNA as a linker (Alivisatos, 1996, "Perspectives"; Alivisatos, 1996, "*Semiconductor"*; Kryrchenko et al., 2011). These assemblies increase the wavelength of the surface plasmon resonance of the Au NPs from about 520 to 574 nm, changing the color of the solution they are in from red to purple (see Figure 2; Alivisatos, 1996, "Perspectives"; Alivisatos, 1996, "*Semiconductor"*; Kryrchenko et al., 2011). Since the properties of a nanoassembly depend on the size, shape, and composition of each NP component, the ability to produce arrangements of two or more unique NPs would offer an opportunity for the systematic study of physical properties of nanostructures and the capacity to tune a structure's optical characteristics (Alivisatos, 1996, "Perspectives"; Alivisatos, 1996, "*Semiconductor"*; Kryrchenko et al. 2011; Varadan et al., 2010).

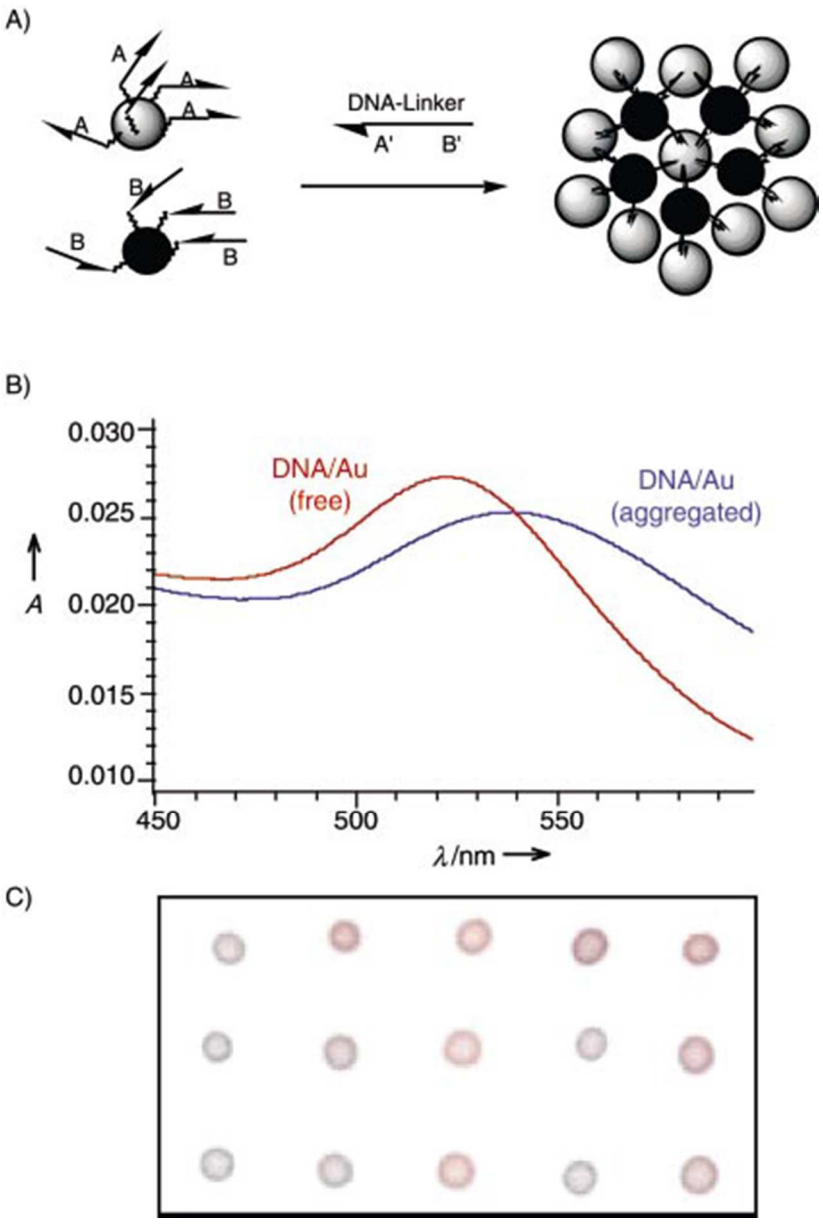

Figure 2. DNA self-assembly of gold colloids. A) Two samples of Au NPs functionalized with non-complementary ssDNA aggregate using a complementary oligonucleotide linker, (B) aggregation leads to a characteristic red shift and broadening in plasmon absorption, and (C) shows changes the color change associated with DNA hybridization of the NPs. Red indicates the absence of hybridization, and blue indicates aggregation. Adapted with permission from "Nanoparticles, Proteins, and Nucleic Acids: Biotechnology Meets Materials Science," by C. M. Niemeyer, 2001, *Angewandte Chemie International Edition, 40,* p. 4137.

1.1 Molecular Self-Assembly

The anisotropy occurring in biological systems has motivated nanotechnology research to produce similarly complicated structures and functions (Adleman, 1998; Aldaye, Palmer, & Sleiman, 2008; Kim & Deaton, 2013; Whitesides & Boncheva, 2002). Researchers have used the template-matching hybridization of DNA self-assembly to develop biologically based "Turing-universal computation," which may enable the technology to compute intricate structures with complex functions (Adleman, 1998; Aldaye, Palmer, & Sleiman, 2008; Kim & Deaton, 2013; Whitesides & Boncheva, 2002; Winfree, 1998). Also, self-assembly occurs anywhere from the construction of biological structures to the formation of social contact networks (Kim & Deaton, 2013; Rosvall & Sneppen, 2006; Whitesides & Boncheva, 2002). Therefore, computable self-assembly, guided by DNA, has the potential to manufacture complex, anisotropic, nano-biomolecular materials by arranging NPs into discrete assemblies to realize a specific purpose (Adleman, 1998; Aldaye, Palmer, & Sleiman, 2008; Kim & Deaton, 2013; Whitesides & Boncheva, 2002).

DNA's candidacy to control self-assembly was first proposed by Seeman in 1982, due to the precision of its unique self-recognition properties (Hsu, 2010). This biomolecule consists of four different units known as nucleotides, which each have three distinct parts (Lodish, Berk, Kaiser, Kriger, Scott, Bretscher, Ploegh, & Matsudaira, 2000; Snodin, Randisi, Mosayebi, Sulc, Schreck, Romano, Ouldridge, Tsukanov, Nir, Louis & Doye, 2015). Each nucleotide contains a nitrogenous base, either adenine (A), thymine (T), cytosine (C), or guanine (G), bound to the pentose sugar deoxyribose linked to a phosphate group by a phosophoester bond (Lodish et al., 2000; Snodin et al., 2015). The molecular recognition of DNA is due to the specificity of the hydrogen bonding patterns that occur between an A-T pair and a C-G pair, which is known as

Watson-Crick base pairing (bp) (Hsu, 2010; Jones et al., 2015; Snodin et al., 2015). These interactions along with planar stacking between bases and the constraints of the sugar-phosphate backbone direct complementary binding of single strands of DNA into the double helix with high selectivity and a global free-energy minimum (Hsu, 2010; Jones et al., 2015; Snodin et al., 2015). Also, it is important to note that this double-stranded DNA (dsDNA) structure has a persistence length of around 150 bp (~50 nm), whereas ssDNA has the flexibility to act as a hinge (Bhushan et al., 2014; Hsu, 2010; Niemeyer, 2000; Ouldridge, Louis, & Doye 2011). With researcher's ability to program the sequence of bases and its selective interactions, DNA is an ideal candidate for obtaining nanometer precision in the spontaneous self-assembly of building blocks into desired nanostructures of specific shapes, sizes, and compositions with new properties (Hsu, 2010; Kim & Deaton, 2013; Kim, Kim, & Deaton, 2011; Ouldridge et al., 2011; Zhang, 2003).

DNA-based building blocks can be programmed to cooperatively arrange themselves to construct a final structure (Kim et al., 2011). Programmability suggests that the building blocks can be designed in such a way as to control the final outcome of an assembly (Kim et al., 2011). The ability to control the final product's shape and size and its intended function is the inherent challenge associated with programmability (Kim et al., 2011). If the hurdles of programmability can be overcome, properly designed DNA building blocks could be utilized to achieve three-dimensional (3D) self-assembly (Kim et al., 2011).

1.1.1 Hybridization-based DNA bonds. The concept of using DNA as a tool for the molecular self-assembly of programmable materials can be traced back to 1996 (Jones et al., 2015). This approach involved using DNA to carefully design branched architectures with multiple crossover junctions to create rigid building blocks with programmable bonding

characteristics, forming the basis of structural DNA nanotechnology (Jones et al., 2015; Li, Yang, Qi, & Seeman, 1996). These building blocks became known as double crossover tiles and were used to self-assemble large two-dimensional crystals (Jones et al., 2015). Multiple crossover junctions and other complex motifs have been used to self-assemble lattices, ribbons, cubes, and truncated octahedrons (Hsu, 2010; Ouldridge et al., 2011). The selectivity of DNA binding has also been used to drive nanomachines, which utilize a strand that replaces another in a partially formed duplex to form a more complete duplex, known as toehold-mediated strand displacement, and to perform simple logic operations (Ouldridge et al., 2011).

Another popular method for hybridization-based self-assembly developed by Rothemund (2006) involves the combination of a long ssDNA molecule, which acts as a scaffold, and numerous shorter single strands to generate the duplexes needed to provide the rigid segments required to construct the final 3D nanostructures (Bhushan et al., 2014; Jones et al., 2015; Ouldridge et al., 2011; Rothemund, 2006). The short strands are known as a "staple strands," and the sequence of each strand can be designed to be different to match corresponding sections along the scaffold (Jones et al., 2015). Also, the final structure can be designed to include locations for the addition of other nano-objects (Jones et al., 2015). With careful sequence design, this approach can be utilized to construct intricate structures ranging from defined shapes to large infinite structures with or without NPs (Chen & Seeman, 1991; Erben, Goodman, & Tuberfield, 2007; Seeman, 2003; Rothemund, Papdakis, & Winfree, 2004; Shih, Quispe, & Joyce, 2004; Yang, Wenzler, Qi, Li, & Seeman 1998; Zhang & Seeman, 1994; Zheng et al., 2006). However, this technique (Rothemund, 2006) differs from the tile method (Jones et al., 2015) because it focuses on assembling a defined nanostructure design instead of having a small number of building blocks to assemble a large periodic structure.

1.1.2 Nanoparticle-templated DNA bonds. Another approach to self-assembly utilizes building blocks consisting of ssDNA functionalized to the surface of NPs (Mirkin, Letsinger, Mucic, & Storhoff, 1996). The ssDNA facilitates the assembly of the NPs into the final product (Mirkin, Letsinger, Mucic, & Storhoff, 1996). The DNA must be attached chemically to the surface of the NP either singularly or to fully cover the surface (Mirkin, Letsinger, Mucic, & Storhoff, 1996). This is done by modifying one end of the DNA strand with a functional group, such as an alkylthiol linker (Mirkin, Letsinger, Mucic, & Storhoff, 1996). Mirkin and his colleagues described the isotropic functionalization of DNA to the surface of a non-nucleic acid core as "spherical nucleic acids," which were shown to be assembled into arrays through the use of a complementary linker DNA strand (Mirkin, Letsinger, Mucic, & Storhoff, 1996). Due to the large variety of NPs available, which vary in size, shape, and composition, this prospective approach could realize a plethora of NP building blocks to self-assemble into either discrete nanoparticle assemblies or extended 3D periodic structures (Jones et al., 2015; Macfarlane, O'Brien, Petrosko, & Mirkin, 2013).

1.1.3 Discrete nanoparticle assemblies. DNA-NP building blocks have great potential to produce new materials for novel applications (Aldaye & Sleiman, 2007, "*DNA-mediated*"; Aldaye & Sleiman, 2007, "*Dynamic*"). When these building blocks are assembled, many properties begin to surface, such as optical coupling and electron transport, due to the relative arrangement of the NPs (Aldaye & Sleiman, 2007, "*DNA-mediated*"; Aldaye & Sleiman, 2007, "*Dynamic*"; Maier, Brongersma, Kik, Meltzer, Requicha, & Atwater, 2001; Pileni, 2001). Typically, these properties are studied collectively in extended assemblies because of the lack of methods to systematically arrange the NPs, but a method to organize the DNA-NP building blocks into discrete structures could enable further investigation into the phenomena (Aldaye &

Sleiman, 2007, "*DNA-mediated*"; Aldaye & Sleiman, 2007, "*Dynamic*"; Collier, Vossmeyer, & Heath, 1998; Kim, Carignano, Tripp, & Wei, 2004; Pileni 2001; Schmid, 2011).

Being able to attach a DNA-containing molecule modified with the appropriate functional group to the surface of each NP would allow each NP to be placed in a precise location within an evolving structure due to the sequence programmability, complementarity of nucleotides, and relative stiffness of the double-helix between building blocks (Aldaye & Sleiman 2006; Alivisatos et al., 1996; Collier et al., 1998; Kim et al., 2004; Li, Park, Reif, LaBean, & Yan, 2004; Loweth, Caldwell, Peng, Alivisatos, & Schultz, 1999; Mastroianni, Claridge, & Alivisatos, 2009; Mirkin et al., 1996; Niemeyer, 2000; Pileni, 2001; Pinto, Seeman, Musier-Forsyth, Taton, & Kiehl, 2004; Rosi & Mirkin, 2005; Seeman, 1998, 2003). This ability to organize NPs into discrete patterns would contribute to the bottom-up approach to the manufacture of nanostructures for various applications (Aldaye & Sleiman, 2006; Collier et al., 1998; Kim et al., 2004; Li et al., 2004; Mirkin et al., 1996; Niemeyer, 2000; Pileni, 2001; Pinto, Seeman, Musier-Forsyth, Taton, & Kiehl, 2004; Rosi & Mirkin, 2005; Seeman 1998, 2003; Storhoff & Mirkin, 1999).

Researchers have been using ssDNA to self-assemble Au NPs into discrete arrangements since 1996 (Alivisatos et al., 1996). At that time, Alivisatos et al. prepared oligonucleotides with a thiol modification to mono-functionalize Au NPs to either the 5' or 3' side of oligonucleotides and used a template strand to direct the self-assembly of DNA-Au NP conjugates into parallel and antiparallel dimers and parallel homotrimers (see Figure 3A; Alivisatos et al., 1996).

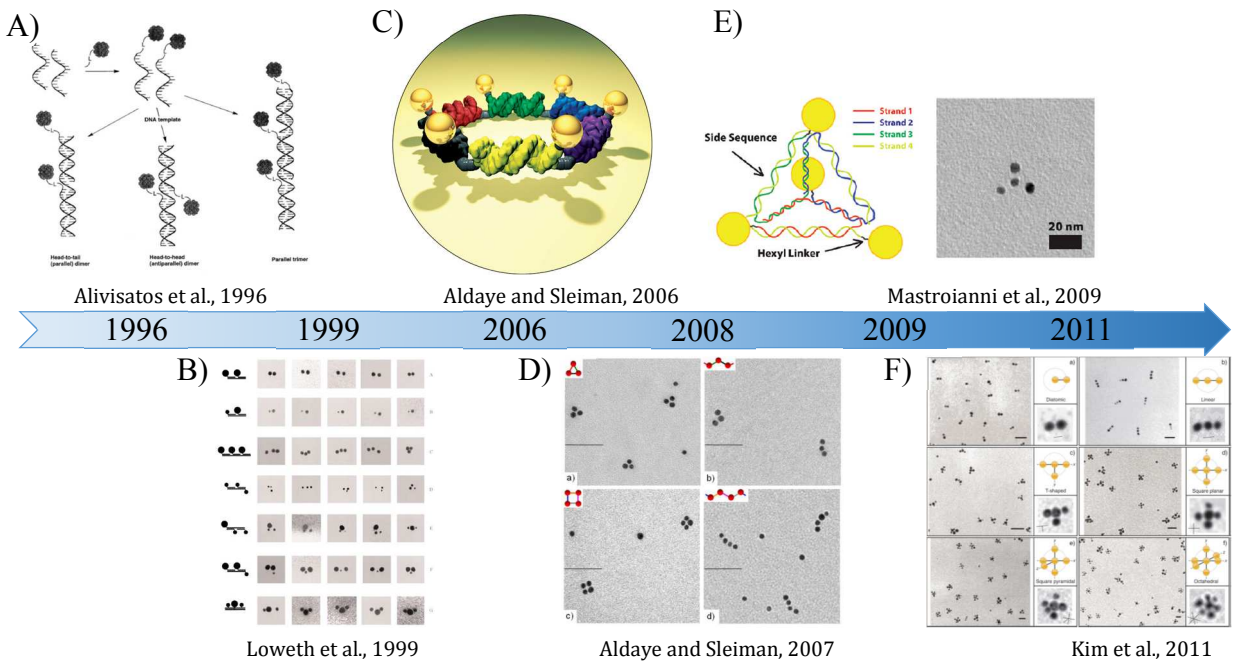

Figure 3A-F. Timeline of discrete arrangements of DNA-linked nanoparticle building blocks. A) is the organization of NPs into parallel and antiparallel homodimers and parallel homotrimers utilizing a template strand, (B) shows the heterodimeric and heterotrimeric Au NP assemblies, (C) shows a representation of the DNA hexagon, (D) shows the trimer, tetramer, triangle, and square created using linear and cyclic DNA templates, (E) shows the schematic and TEM image of a tetrahedron structure, and (F) shows the 1-, 2-, and 3D assemblies created using a sequential mono-functionalization strategy. Adapted with permission from "Organization of 'nanocrystal molecules' using DNA," by A. P. Alivisatos, 1996, *Nature, 382*, p. 610; "DNA-Based Assembly of Gold Nanocrystals," by C. J. Loweth, 1999, *Angewandte Chemie International Edition, 38,* p. 1810; "Sequential Self-Assembly of a DNA Hexagon as a Template for the Organization of Gold Nanoparticles," by F. A. Aldaye & H. F. Sleiman, 2006, *Angewandte Chemie International Edition, 45,* p. 2204; "DNA-mediated patterning of gold nanoparticles into discrete structures: modularity, write/erase and structural switching," by F. A. Aldaye & H. F. Sleiman, 2007, *NanoScience + Engineering,* p. 664203-4; "Pyramidal and Chiral Groupings of Gold Nanocrystals Assembled Using DNA Scaffolds," by A. J. Mastroianni et al., 2009, *Journal American Chemical Society, 131,* p. 8456; and "DNA-Linked Nanoparticle Building Blocks for Programmable Matter," by J.-W. Kim et al., 2011, *Angewandte Chemie International Edition, 50*, p. 9188.

After this preliminary report, Loweth et al. (1999) continued the 1D self-assembly of discrete nanostructures by using DNA in three different synthesis strategies (see Figure 4) to

control the relative spatial arrangement of specific, designed, non-periodic assemblies of Au NPs (Loweth et al., 1999). These methods also used the thiol-DNA modification to fixate the oligonucleotide to the surface of the Au NPs. The researchers used these methods to create heterodimeric and heterotrimeric assemblies of Au NPs, which were characterized using transmission electron microscopy (TEM; see Figure 3B). This group was also able to show a level of control over the spacing between NPs in homodimers by varying the number of base pairs in the duplex from 18 to 38 base pairs and to characterize the optical properties of the assemblies with UV/VIS spectrophotometry (Loweth et al., 1999). The optical properties of NP assemblies depend upon the size, shape, and or spacing between the NPs (Loweth et al., 1999). The changes in the optical properties from monodisperse NP to assembled NPs can be predicted with Generalized Mie theory (Vollmer & Kreibig, 1995; Loweth et al., 1999). For an Au-NP pair, the theory predicts that the plasmon band should red shift slightly, decrease the intensity, and broaden as the distance between the two NPs becomes smaller than the sum of their radii (Vollmer & Kreibig, 1995; Loweth et al., 1999). When the Au NPs are separated by distances greater than the sum of their radii, the electronic interactions result in a slight broadening of the spectrum and no noticeable red shift (Vollmer & Kreibig 1995).

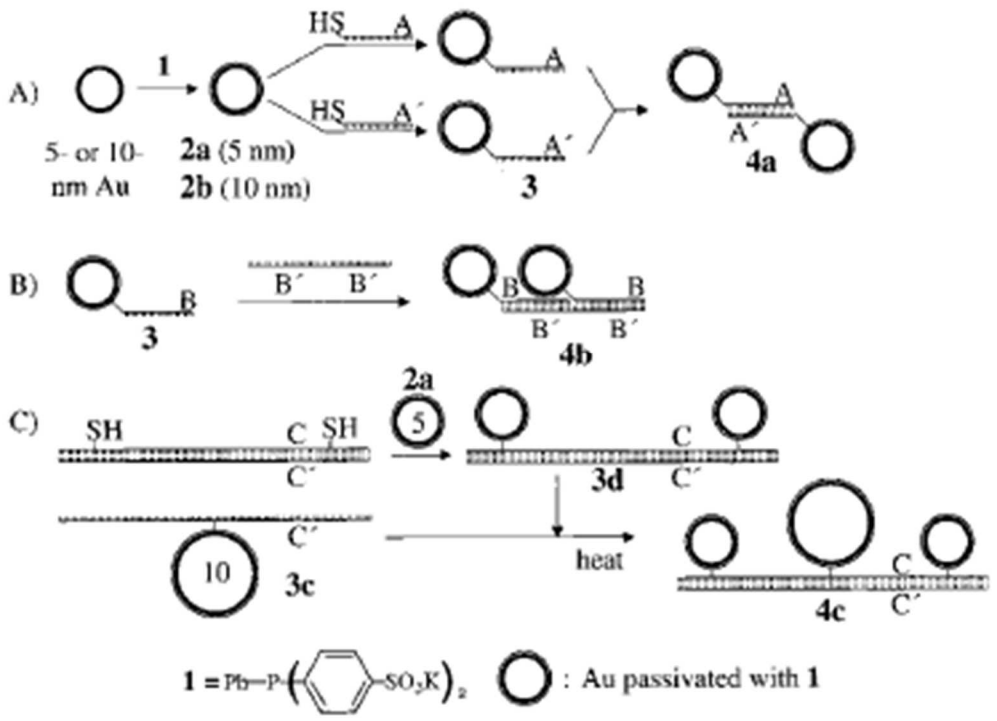

Figure 4. Synthesis strategies A-C for nanocrystal assembly. A) utilizes complementary oligonucleotides mono-functionalized to NPs, (B) utilizes complementary sections on a free template strand, and (C) utilizes thiol groups at specific locations along dsDNA for NPs to be attached. The labels A', B', and C' denote complementary oligonucleotide sequences to A, B, and C sequences, respectively. Adapted with permission from "DNA-Based Assembly of Gold Nanocrystals," by C. J. Loweth et al., 1999, *Angewandte Chemie International Edition, 38,* p. 1809.

In 2006, Aldaye and Sleiman demonstrated a unique approach to design building blocks for the sequential fabrication of NPs into the first 2D organization of Au NPs into a hexagonal structure (see Figure 3C; Aldaye & Sleiman, 2006). Their building blocks consisted of a DNA molecule with two distinct arms connected by an organic vertex, which was later mono-functionalized to the Au NP (Aldaye & Sleiman, 2006). To realize this building block, one of the DNA arms was terminated with an amine unit for covalent mono-functionalization of the Au

NPs with a succinimidyl ester moiety (Aldaye & Sleiman, 2006). Their purpose for the development of this hexagonal nanoassembly was for its potential to produce unique nanoelectronic properties and enhanced conformational rigidity compared to 1D structures, resulting in improved control over the relative orientation of each NP (Aldaye & Sleiman, 2006).

In 2007, Aldaye and Sleiman reported a different method that utilized ssDNA combined with organic vertices to form cyclic templates used to produce either triangular and square Au NP assemblies (see Figure 3D; Aldaye & Sleiman, 2007, "*DNA-mediated*"; Aldaye & Sleiman, 2007, "*Dynamic*"). To hybridize the Au NPs to the DNA templates, the Au NPs had to be mono-functionalized with the correct complementary thiolated ssDNA (Aldaye & Sleiman, 2007, "*DNA-mediated*"; Aldaye & Sleiman, 2007, "*Dynamic*"). This approach allowed for structural switching and write/erase functions and demonstrated further control over the geometry and positioning of each NP (Aldaye & Sleiman, 2007, "*DNA-mediated*"; Aldaye & Sleiman, 2007, "*Dynamic*").

More recently, Mastroianni et al. (2009) controlled the placement of Au NPs by using DNA as a scaffold to build discrete, pyramidal nanostructures with Au NPs at each tip (See Figure 3E). X-ray scattering measurements, TEM images, and gel electrophoresis confirmed the creation of four-particle assemblies with tetrahedral geometry (Mastroianni et al., 2009). Furthermore, the center-to-center distances between Au NPs indicated that the pyramidal structure enhanced the rigidity even though the Au NPs were functionalized to ssDNA via flexible alkyl linkers (Mastroianni et al., 2009).

DNA has been shown to facilitate the self-assembly of Au NPs as building blocks into controlled extended aggregations (Aldaye & Sleiman, 2006; Le et al., 2004; Li et al., 2004; Mirkin et al., 1996; Rosi & Mirkin, 2005), 1D linear groupings (Alivisatos et al., 1996; Claridge

et al., 2005; Fu et al., 2004; Loweth et al., 1999; Niemeyer 2001), 2D cyclic structures (Aldaye & Sleiman, 2006; Aldaye & Sleiman, 2007; "*DNA-mediated*"; Aldaye & Sleiman, 2007, "*Dynamic*"), and 3D pyramids (Mastroianni et al., 2009). These building blocks and their assemblies have demonstrated many unique physicochemical properties (Alivisatos, 1996, "*Semiconductor"*; Lee & Schatz, 2009). Even though the methods described were used to assemble Au NPs, they should not be limited to Au NPs and should be applied to nanoparticles composed of other various materials and shapes (Loweth et al., 1999). Although there has been some progress in controlling the spatial arrangement of NPs, achieving specific shapes and functions remains difficult to attain for a number of reasons (Kim & Deaton, 2013). This being the case, there is a need to develop an efficient method for constructing versatile DNA-NP building blocks that in turn can enhance the ability to control the outcome of the final product. Clearly, methods to improve the efficiency of nanostructure design and analysis are needed (Kim & Deaton, 2013).

1.2 Fundamental Challenges in Nanostructure Self-Assembly

DNA-NP building blocks with the ability to self-assemble into discrete nanostructure assemblies have the potential to be utilized for many applications (Toffoli & Margolus, 1991; Winfree, Liu, Wenzler, & Seeman, 1998). Many have made great progress in utilizing DNA in various ways to be used in DNA-based computation and nanotechnology (Alivisatos et al., 1996; Auyeung et al., 2012; Chen & Seeman, 1991; Kim & Deaton, 2013; Macfarlane et al., 2011; Mirkin et al., 1996; Nykypanchuk, Maye, van der Lelie, & Gang, 2008; Park et al., 2008; Winfree, Liu, Wenzler, & Seeman, 1998; Zhang & Seelig, 2011). However, this technology is still in its initial stages, and there are still opportunities to reduce trial and error and create more

efficient methods to aid in the experimental self-assembly of NPs into defined assemblies through the use of DNA (Kim & Deaton, 2013).

There are two central challenges associated with the manufacture of nanostructure self-assembly (Kim & Deaton, 2013). The first challenge involves developing components consisting of various NP compositions and geometry to be used in self-assembly (Kim & Deaton, 2013). The second challenge is to assemble the components into a structure with the necessary function(s) based of the requirements for an application (Kim & Deaton, 2013). A given nanostructure's function(s) depends on the properties of each NP utilized in the building blocks (Kim & Deaton, 2013). Therefore, the building blocks should be well-defined to maximize control of the final assembly, taking advantage of each NP's relative position and orientation (Kim & Deaton, 2013).

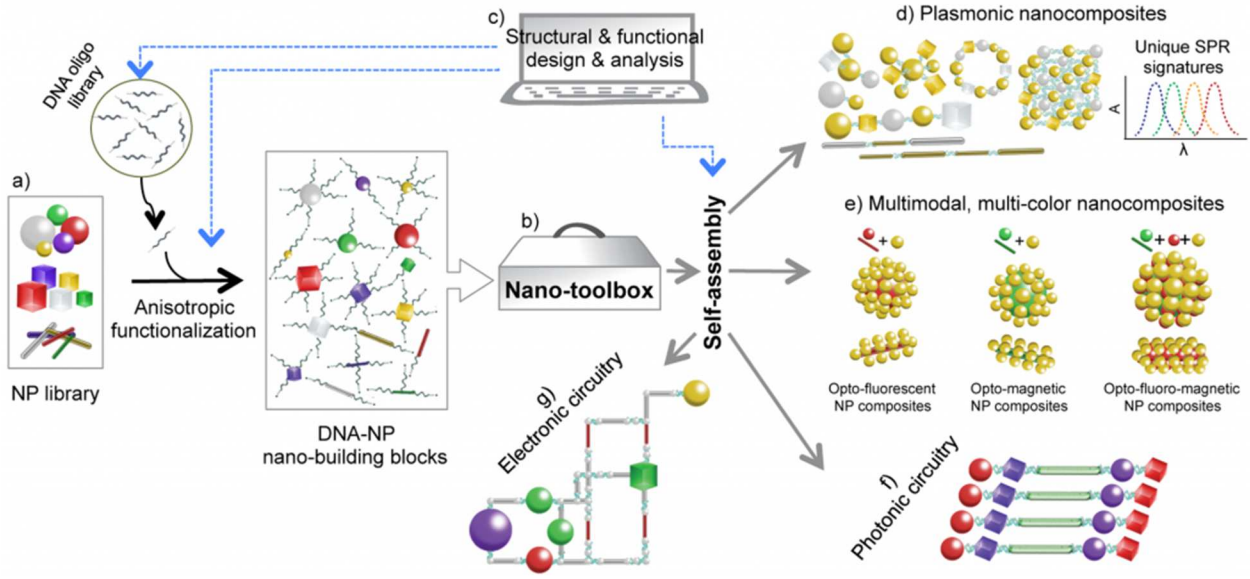

Figure 5. Schematic for the programmable self-assembly of DNA-NP building blocks created from NP and oligonucleotide libraries by the anisotropic mono-functionalization strategy to create a toolbox (nano-toolbox) to construct multifunctional nanostructures for plasmonics, photonics, and electronic nanocircuitry and multimodal nanocomposites. Adapted with permission from "Molecular Self-Assembly of Multifunctional Nanoparticle Composites with Arbitrary Shapes and Functions: Challenges and Strategies," by J.-W. Kim and R. Deaton, 2013, *Particle & Particle Systems Characterization, 30,* p. 119.

To maximize programmability for anisotropic nanostructures, building blocks should incorporate non-interfering DNA oligonucleotide sequences with control over number, location, and relative position on the NP's surface, reducing errors and defects in the final assembly (Hsu, 2010; Kim & Deaton, 2013; Kim et al., 2011). Also, incorporating various NPs in the building blocks would generate a "nanotoolbox" for the design of nanostructures (Kim & Deaton, 2013). With precise control over the placement of oligonucleotides on the NP surface, the geometry of each building block could be used to predict the local geometry of the desired structures (Kim & Deaton, 2013). Also, with a small number of DNA strands, the interparticle spacing could be controlled more efficiently (Hsu, 2010). Despite the recent progress in self-assembly methods

and NP synthesis (Aldaye & Sleiman 2006; Aldaye & Sleiman, 2007, "*DNA-mediated*"; Aldaye & Sleiman, 2007, "*Dynamic*"; Alivisatos et al., 1996; Loweth et al., 1999; Kim et al., 2011; Mastroianni et al., 2009), approaches to develop an efficient method of directed nanostructure design has been limited (Kim & Deaton, 2013). Replacing a trial and error approach with an approach that utilizes computer modeling to simulate nanostructure self-assembly could help establish control over the process and improve its efficiency (Kim & Deaton, 2013).

1.3 DNA-Programmable NP Building Blocks

Precise control over the construction of nanoscale structures to achieve desired physicochemical characteristics or biological functions would influence many areas of research (Armistead, Hendricks, Fochtman, Batta-Mpouma, Patitz, Deaton, Han, & Kim, 2015; Kim & Deaton, 2013). However, many challenges remain before the full potential of nanoscale building block self-assembly can be realized (Armistead et al., 2015; Kim & Deaton, 2013). In particular, spatial configuration of the NP building blocks must be controlled (Kim & Deaton, 2013). In order to do this, DNA must be functionalized to the NP surface at specific sites that do not interfere with the DNA's ability to hybridize with its complementary target (see Figures 5 and 6; Kim & Deaton, 2013). Improvements in the precise manipulation of matter at nanoscale levels may eventually lead to efficient production of programmable NP building blocks that are able to cooperatively self-assemble and thus overcome some of the challenges facing experimental production of multifunctional nanostructures (John & Bär, 2005; Kim & Deaton, 2013).

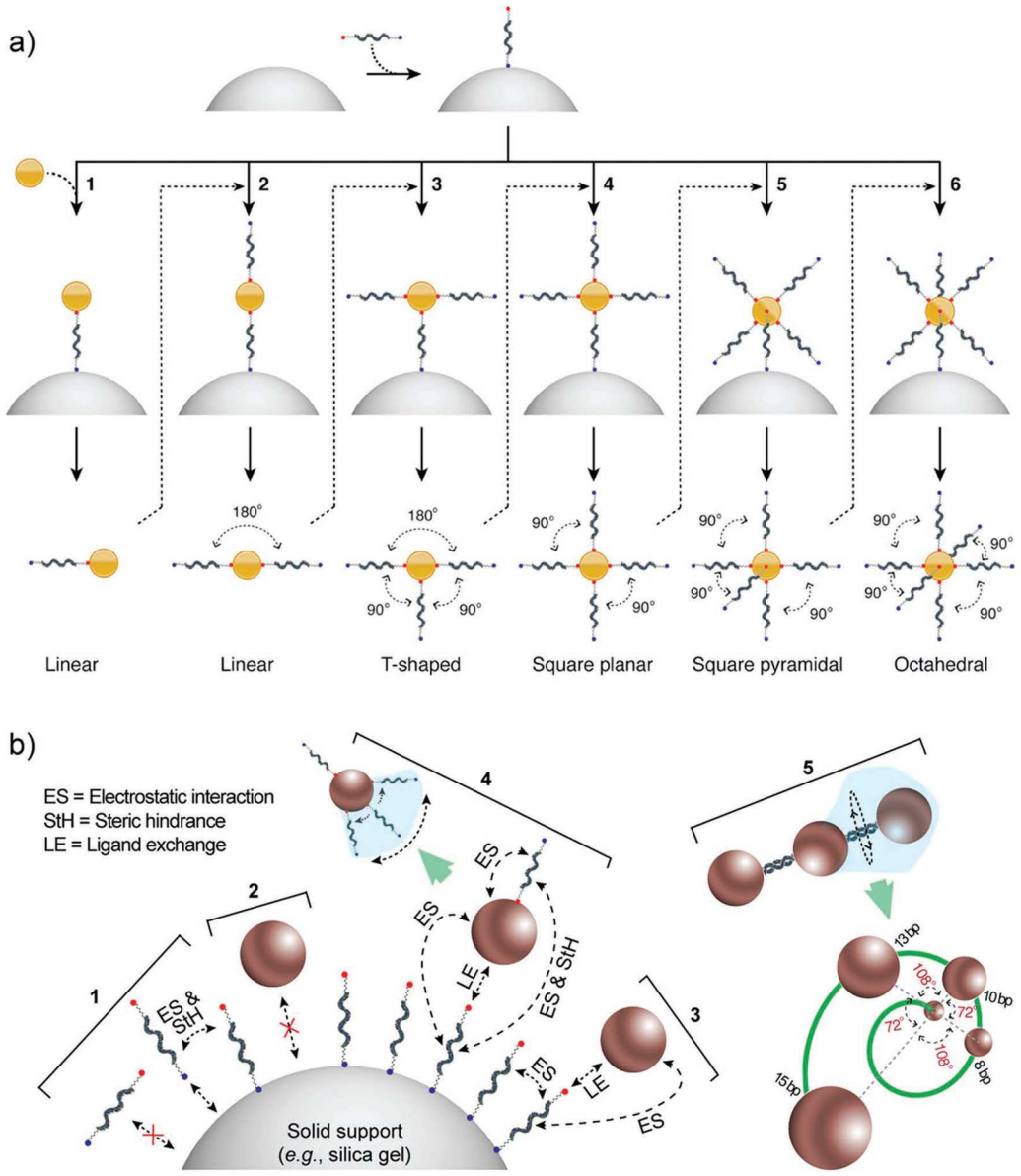

Figure 6. The anisotropic mono-functionalization of DNA onto the surface of a NP. A) is a schematic of the sequential approach to synthesize DNA-NP building blocks of six different configurations for programmable self-assembly. B) is a schematic representing the physicochemical factors of electrostatic interaction, steric hindrance, and ligand exchange that influence the spatial orientation of DNA on the surface of a NP. Adapted with permission from "Molecular Self-Assembly of Multifunctional Nanoparticle Composites with Arbitrary Shapes and Functions: Challenges and Strategies," by J.-W. Kim and R. Deaton, 2013, *Particle & Particle Systems Characterization, 30,* p. 121.

The sequential mono-functionalization of DNA to a single NP would allow the management of the number of DNA and angles between the DNA linkers on the surface of the NP (Kim & Deaton, 2013). This is managed through careful consideration of steric hindrance and electrostatic interactions in the system with the addition of each DNA (see Figure 6), marking the initial steps in the development of multifunctional anisotropic nanostructures (Kim & Deaton, 2013). Maximal programmability can be achieved through further adjustments in NP organization within a final assembly by utilizing DNA's natural twist to control the angle or changing the number of nucleotides in a DNA sequence to control the interparticle spacing (Kim & Deaton, 2013). The rational design of building blocks for self-assembly involves many interactions that should be considered and exploited to take full advantage of the technology to produce multifunctional nanostructures (Kim & Deaton, 2013).

The initial effort for mono-functionalization of DNA to Au NPs was accomplished by Alivisatos and coworkers' in 1996, through maleimide conjugation for the self-assembly of discrete nanoassemblies (Alivisatos et al., 1996). Since this preliminary work, other strategies have been employed to control the number of oligonucleotides on the NP surface to be assembled in discrete arrangements (Aldaye & Sleiman, 2007; "*DNA-mediated*"; Aldaye & Sleiman, 2007, "*Dynamic*"; Alivisatos et al., 1996; Claridge et al., 2005; Claridge et al., 2008; Fu et al., 2004; Loweth et al., 1999; Mastroianni et al., 2009; Zanchet et al., 2001; 2002). Only recently, Kim et al. (2011) developed a mono-functionalization method that sequentially attaches ssDNA to the surface of a Au NP capped in a mixed monolayer of dimethyl aminopyridine (DMAP) and mercaptoethane sulfonic acid (MESA) through aqueous-phase ligand replacement (see Figure 6; Kim & Kim, 2010; Kim et al., 2011). This method can attach up six ssDNA to the NP surface, resulting in six different building block configurations: diatomic, linear, t-shaped,

square planar, square pyramidal, and octahedral. This strategy overcomes some of the challenges associated with self-assembly, exhibiting excellent control over the placement of ssDNA on the NP surface and maximizing programmability of the building blocks (Hsu, 2010; Kim & Deaton, 2013; Park, Yan, Reif, LaBean, & Finkelstein, 2004).

Although this method for the development of NP building blocks and the construction of multifunctional nanoassemblies is promising, there are still obstacles to overcome to realize the its full potential (Kim & Deaton 2013). For example, the approach has yet to be extended to other kinds NPs, and the strategy would need to be adapted for their incorporation. Even though modifications and optimization will be needed, the sequential anisotropic mono-functionalization technique developed by Kim et al. (2011) is a viable approach for programmable self-assembly (see Figure 5; Kim et al., 2011, Kim & Deaton, 2013).

1.4 DNA & Nanostructure Modeling

Efforts to design more sophisticated nanoassembly systems are hampered by a limited understanding of the process involved in DNA self-assembly (Ouldridge, 2011; Ouldridge et al., 2011). For example, the information about the intermediate states in the assembly process is often difficult to resolve experimentally, but crucial to the process as a whole (Ouldridge, 2011; Ouldridge et al., 2011). One approach to alleviating the inefficiencies associated with experimental trial and error is utilizing computer modeling (Ouldridge, 2011; Ouldridge et al., 2011). Computational modeling can offer significant insight into self-assembly processes, such as the intermediate states occurring during the transition from ssDNA to dsDNA (Armistead et al., 2015; Ouldridge, 2011; Ouldridge et al., 2011). This approach could potentially be extended to modeling the self-assembly of NP building blocks into anisotropic nanostructures, which

could provide a more efficient way to test ideas and reduce trial and error (Ouldridge, 2011; Ouldridge et al., 2011).

Computer simulation has been used to study the behavior of DNA. There are many modeling strategies that can be employed to study biological systems (Orozco et al., 2003). On one end of the spectrum, there exists fully atomistic models, which display great detail (see Figure 7; Orozco et al., 2003). Due to the high degree of computational complexity and degrees of freedom, these models are capable of retaining the most chemical details but limit simulations to shorter timescales (Hsu, 2010; Mura & McCammon, 2008; Ouldridge, 2011; Perez, Luque, & Orozco, 2007). On the other end of the spectrum, there are continuum or theoretical models, which integrate out the degrees of freedom (Bustamante, Marko, Siggia, & Smith, 1994; Swigon, 2009). This allows larger systems to be studied but restricts access to the details of processes such as DNA melting or hybridization (Ouldridge, 2011; Snodin et al., 2015).

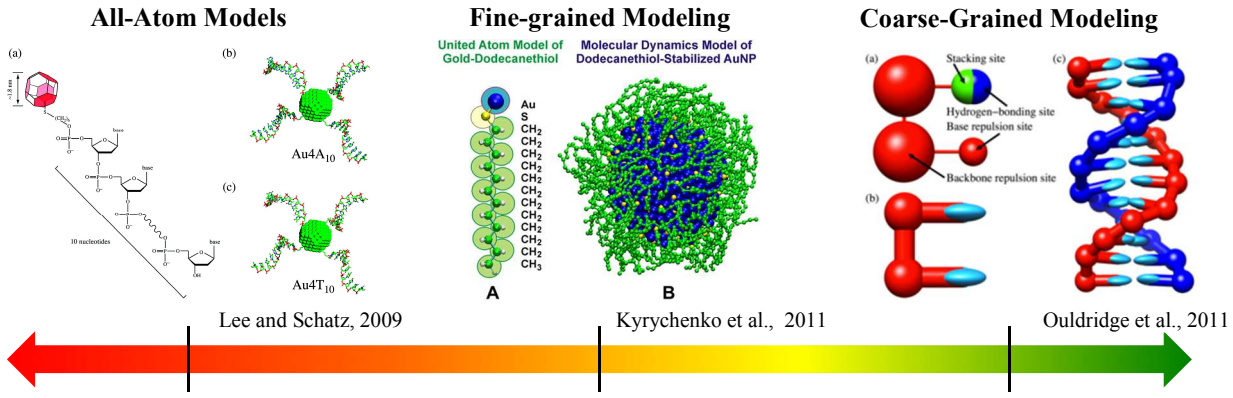

Figure 7. Continuum representing varying degrees of freedom and computational complexity for molecular modeling. The left represents all-atom models having a high number of degrees of freedom, corresponding greater computational complexity, greater detail of a smaller system, and shorter time scales. Moving towards coarse-grained modeling (right), the number of degrees of freedom decreases, allowing for longer time-scales, detail of more complexes processes of a larger system, and longer time scales. Adapted with permission from "Preparation, structure, and a coarse-grained molecular dynamics model for dodecanethiol-stabilized gold nanoparticles," by A. Kyrychenko et al., 2011, *Computational and Theoretical Chemistry, 977,* p. 37; "Molecular Dynamics Simulation of DNA-Functionalized Gold Nanoparticles, by O.-S. Lee & G. C. Schatz, 2009, *Journal of Physical Chemistry C, 113*, p. 2317; and "Structural, mechanical, and thermodynamic properties of a coarse-grained DNA model," by T. E. Ouldridge et al., 2011, *Journal of Chemical Physics, 134,* p. 085101-4.

Models have also been developed to help with the design process for hybridization-based DNA building blocks, explicitly for the purpose of modeling DNA origami (Castro et al., 2011; Sherman & Seeman, 2006). Sherman & Seeman (2006) have developed a geometrical scheme for the purpose of minimizing strain in origami structures (Sherman & Seeman, 2006), and Castro et al. (2011) developed a method to predict the structure of stressed DNA origami, treating dsDNA as an elastic rod (Bhushan et al., 2014; Castro et al., 2011; Kim, Kilchherr, Dietz, & Bathe, 2012). Although these tools are useful in the rational design process, they are not applicable to the self-assembly of the nanostructures (Ouldridge, 2011). However, like DNA origami has computer-aided software to simplify the design of nanostructures (Castro, Kilchherr,

Kim, Shiao, Wauer, Wortmann, Bathe, & Dietz, 2011; Kim, Kilchherr, Dietz, & Bathe, 2012), DNA-functionalized NP building blocks could also benefit from design software in the rational development of anisotropic nanostructures.

A model for the self-assembly of NP building blocks should occupy the middle ground between analytical and all-atom approaches (see Figure 7). Coarse-grained DNA models integrate many of the degrees of freedom of the DNA nucleotide (Ouldridge, 2011; Snodin et al., 2015). However, care must be taken in applying these models to a given problem because their approximations imply a compromise between accuracy, generality, and computational efficiency. Although DNA models utilizing approximately 10 coarse-grained units per nucleotide have been used to study the interaction of DNA with lipids (Corsi, Hawtin, Ces, Attard, & Khalid, 2010; Khalid, Bond, Holyoake, Hawtin, & Sansom, 2008), further reduction of the coarse-grained unit to approximately that of the nucleotide provides an effective compromise between resolution and the computational speed (Ouldridge, 2011). This simplified picture greatly increases time scales and the number of nucleotides that could be studied (Snodin et al., 2015).

A model for the self-assembly of NP building blocks should be a full 3D coarse-grained model mainly concerned with the formation of DNA duplexes involving single strands and B-DNA, which is believed to be the predominant form in cells with a diameter of 2 nm and a rise per base of 0.34 nm (Alberts et al., 2002; Ouldridge et al., 2011; Richmond & Davey, 2003). The goal of the model should be to describe processes relevant to the self-assembly of DNA nanostructures with the incorporation of NPs, with a view toward biological applications. Also, there should also be a good representation of the physicochemical properties of both ssDNA and dsDNA because DNA drives the self-assembly process and plays an important role in controlling the final product (Ouldridge et al., 2011). An excellent starting point for a coarse-grained model

of DNA-functionalized NP building blocks is Ouldridge's (2011) model of DNA, which represents ssDNA as a chain of rigid nucleotides with three interaction sites with anisotropic interactions described by potentials representing nucleotide connectivity in the strand, excluded volume, hydrogen-bonding, and base stacking (see Figure 8; Ouldridge, 2011; Schreck, Ouldridge, Romano, Louis, & Doye, 2015; Snodin et al., 2015; Srinivas, Ouldridge, Sulc, Schaeffer, Yurke, Louis, Doye, & Winfree, 2013). Since the development of this coarse-grained model, its parameters have been optimized for capturing the thermodynamic and mechanical fluctuations associated during duplex formation (Srinivas et al., 2013). This has resulted in the first demonstration of explicit stacking transitions in ssDNA and the only model to capture both hairpin and duplex formation (Ouldridge, 2011) as well as key insights into many different processes relevant to DNA nanotechnology and biophysics (Snodin et al., 2015). The model's most recent version is able to incorporate the major and minor grooves of DNA, to simulate large (kilobase-pair) structures, such as in DNA origami, and allows simulations in a range of salt concentrations, including physiological conditions ($[Na^+] \approx 0.15$ M; Snodin et al., 2015). Therefore, Ouldridge's coarse-grained DNA model's ability to capture DNA's structural, mechanical, and thermodynamic properties makes it a viable starting point to base a model for the self-assembly of DNA-functionalized NP building blocks (Armistead et al., 2015).

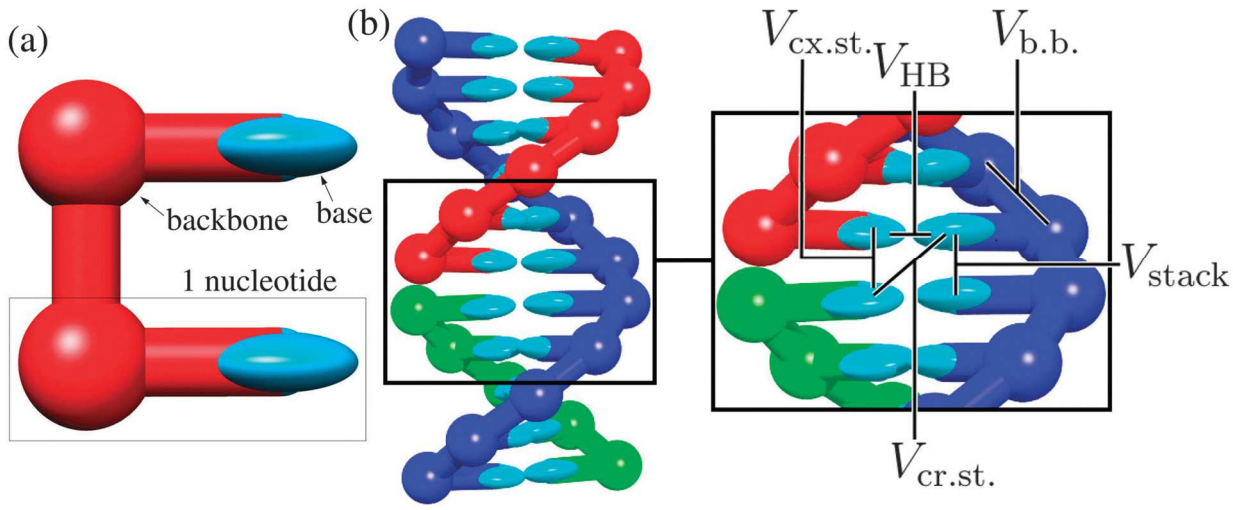

Figure 8. Schematic of oxDNA. (A) the model's basic unit of rigid nucleotides and (b) an 11-bp double helix that illustrates the various interactions. Adapted with permission from "Characterizing the bending and flexibility induced by bulges in DNA duplexes," by J. S. Schreck et al., 2015, *Journal of Chemical Physics, 124,* p. 165101-3.

1.5 Applications of Self-Assembled Multifunctional Nanocomposites

Nanostructure self-assembly holds great promise in producing new materials with improved properties (Aldaye & Sleiman, 2006; Kim & Deaton, 2013; Maier et al., 2001, Maier et al., 2003; Mastroianni et al., 2009, Rosi & Mirkin, 2005; Schmid, 2011), and the resulting structures are model systems for nanoscience because they allow the tuning of interactions between controlled numbers of NPs in groupings of varying compositional and spatial complexity (Mastroianni, Sivak, Geissler, & Alivisatos, 2009). As a result, innovations from multiple fields including medicine and engineering can be expected (Aldaye & Sleiman, 2006; Kim & Deaton, 2013; Maier et al., 2001, Maier et al., 2003; Mastroianni et al., 2009, Rosi & Mirkin, 2005; Schmid, 2011).

There is a growing interest in the self-assembly of noble metal nanoscrystals into nanocomposites of various shapes and structural configurations (Kim & Deaton, 2013; Tan, Campolongo, Luo, & Cheng, 2011; Wang, Brandl, Nordlander, & Halas, 2007). The ability to self-assemble nanocomposites opens the possibility of tuning their optical properties, producing customizable plasmonic nanomaterials (see Figure 5d; Kim & Deaton, 2013; Tan, Campolongo, Luo, & Cheng, 2011; Wang, Brandl, Nordlander, & Halas, 2007). The optical properties of nanomaterials are attributed to their unique surface plasmon resonances, which are strongly influenced by the NP's size, shape, material composition, and the local dielectric environment (Halas, Lal, Chang, Link, & Nordlander, 2011; Kim & Deaton, 2013; Nie, Petukhova, & Kumacheva, 2010; Tan, Campolongo, Luo, & Cheng, 2011; Wang, Brandl, Nordlander, & Halas, 2007). The ability to incorporate various metallic NPs into the appropriate building blocks for the bottom-up construction desired nanostructures would allow enhanced optical properties at multiple wavelengths for various miniaturized optical (Kim & Deaton, 2013; Schuller et al., 2010), electronic (Kim & Deaton, 2013; Ozbay, 2006; Shipway, Katz, & Willner, 2000), and photonic applications (Kim & Deaton, 2013; Maier, 2003), as well as and medical diagnostics and therapeutics (Kim & Deaton, 2013; Lal, Clare, & Halas, 2008; Tan et al., 2011; Yavuz et al., 2009).

Although significant advancements have been made in synthesizing these various NPs, there is still a gap in the field of technology for a method that offers substantial control for the rational self-assembly of well-defined molecule-like architectures. The realization of promising applications depends on the ability to control the interactions between NPs with different properties, which is determined by the spacing and relative positions of each NP (Kim & Deaton, 2013). However, the anisotropic mono-functionalization strategy is an excellent starting point to

be generalized for the precise positioning of these different NPs into plasmonic nanostructures for biotechnological applications and their translation into clinical practice. The ability to incorporate many various individual NPs into the DNA-functionalized building blocks and their successful assembly into a discrete structure promises a systematic examination of the nanoassembly's properties, potentially leading to further advances in the bottom-up design of nanomaterials (Hsu, 2010; Kim & Deaton, 2013).

1.6 Thesis Objectives

The field of nanotechnology needs an efficient method to accomplish the bottom-up self-assembly of NP building blocks into multifunctional nanoassemblies. A viable method for the self-assembly of complex nanocomposites is the sequential mono-functionalization of DNA to the surface of Au NPs developed by Kim et al. (2011). Even though this method has great promise to assemble NPs of various shapes, sizes, and compositions into discrete nanostructures for many applications, there are still challenges associated with reducing experimental trial and error. A possible direction to overcome this hurdle is to utilize coarse-grained modeling to simulate the self-assembly of the NP building blocks because it provides a compromise between accuracy and computational complexity to simulate the hybridization of DNA between building blocks. Therefore, the goal of this thesis is to validate the ability of the coarse-grained model for NP building blocks presented by Armistead et al. (2015) to simulate the self-assembly of the structures produced by Kim et al. (2011), Loweth et al. (1999), and Aldaye and Sleiman (2006; 2007, "*DNA-mediated"*; 2007, "*Dynamic*"). The hypothesis for this work is that if the coarse-grained model for Au NP building blocks is used to simulate the self-assembly of the previously manufactured nanostructures noted above, then the simulated interparticle distance, angles, and

visualizations obtained can be compared to the previous experimental data to test the validity of the model.

There are seven primary objectives for this study:

1. To verify the stability of the DMAP-MESA-Au NPs at the lowest salt concentration parameter available in the model due to the instability of the NPs that can occur with increasing salt concentrations.
2. To validate the model's ability to simulate the self-assembly of NP building blocks with increasing complexity of simulations.
3. To simulate the self-assembly of the Au NP building block configurations produced by Kim et al. (2011) into the diatomic, linear, t-shaped, square planar, square pyramidal, and octahedral nanoassemblies.
4. To examine the change in interparticle distances when the number of base pairs are varied within the simulations of the diatomic and linear nanostructures produced by Kim et al. (2011).
5. To test multiple diatomic structures simultaneously within a single simulation.
6. To continue validation of the model through the simulation of the structures simulated by Loweth et al. (1999) and Aldaye and Sleiman (2006; 2007, "*DNA-mediated"*; 2007, "*Dynamic*").
7. To simulate the self-assembly of linear and polygonal structures for later comparison to these fabricated structures for further validation of the model.

In addition, we have two secondary objectives:

1. To examine the simulated melting temperature profile of a diatomic structure.

2. To examine the effect of box size (effectively changing the concentration of the simulated nanostructures) on yield and list updates of the simulations of the six nanostructures produced by Kim et al. (2011).

Chapter 2: Model Description and Experimental Set-Up

A large component of this study on DNA-NP building blocks is based on coarse-grained modeling. Before presenting the results, first the model in this chapter is summarized. Section 2.1 is an introduction of the model for NP building blocks, specifically its philosophy, the potential, and the parameters for the interaction. Section 2.2 is a discussion of the simulation technique, which includes the instrumentation, procedure, and DNA sequences used to generate the simulations. Section 2.3 is a presentation of the experimental methods needed to fabricate the DMAP-MESA-Au NPs needed to verify the stability of the particles at the salt concentration used in the simulations.

2.1 Coarse-Grained Model for DNA-Functionalized NP Building Blocks

2.1.1 DNA-Au NP building block model. The building block model is an extension of the DNA model developed my Ouldridge et al. (2011) and improved by Snodin et al. (2015) to incorporate Au NPs for the simulation of DNA-NP building blocks (Armistead et al., 2015). The building block model incorporates a Au NP with the ability to attach up to six ssDNA to specific sites on its surface to the oxDNA2 model, resulting in a 3D, dynamical, coarse-grained representation of the building blocks produced by the anisotropic mono-functionalization strategy developed by Kim et al (2011) (Armistead et al., 2015). Each NP is modeled as a single spherical bead with 6 binding sites where the 5' side of the DNA oligonucleotide's backbone can be attached (Armistead et al., 2015). The nucleotides are represented as a single rigid body with three interaction sites (see Figure 8; Snodin et al., 2015), and the oligonucleotide and the Au NP are joined through a single rigid bond, representing the thiol linker (Armistead et al., 2015). Both

the Au NP and the 5' nucleotide have the ability to rotate about either side of the bond representing the thiol linker (J. Hendricks, personal communication, July 2015).

Since the NP building block model is an extension of the oxDNA2 model, it uses the pairwise potential presented by Snodin et al. (2015) and can be written as follows:

$$V_{oxDNA2} = \sum_{nearest\ neighbors} (V_{backbone} + V_{stack} + V'_{exc}) + \sum_{other\ pairs} (V_{HB} + V_{cross\ stack} + V_{exc} + V_{coax\ stack} + V_{DH})$$

The first summation describes the interaction between pairs of nearest neighbors with potentials representing the interactions for the covalent bonds for adjacent backbones ($V_{backbone}$), stacking interactions (V_{stack}), and excluded volume (V'_{exc}; Snodin et al., 2015). The second summation describes the interaction s between all other pairs in the simulation with potentials representing hydrogen bonding (V_{HB}), cross stacking ($V_{cross\ stack}$), excluded volume (V_{exc}), coaxial stacking ($V_{coax\ stack}$), and electrostatic interactions (V_{DH}; Snodin et al., 2015).

Since the Au NP and the thiol linker were added to the DNA model for simulating NP building blocks, parameters were adjusted in the following potentials described in Armistead et al. (2015) to accurately generate the interparticle distances of the nanostructure assembled by Kim et al. (2011):

$$V_{bond} = \frac{1}{2} k x^2 \quad (1)$$

$$V_{LJ} = 4\varepsilon \left[\left(\frac{\sigma}{r}\right)^{12} - \left(\frac{\sigma}{r}\right)^{6} \right] \quad (2)$$

$$V_{DH} = \sum_{ij} \frac{(qe)^2 exp\left[\left(-r_{ij} + r_{np}\right)/\lambda_{DH}\right]}{4\pi\varepsilon_0\varepsilon_r\left(r_{ij} - r_{np}\right)} \quad (3)$$

The potential represented by Equation (1) describes the bond between the oligonucleotide and the NP. Equation (2) represents the steric hindrance between the oligonucleotide and the Au NP. Equation (3) represents the potential for the electrostatic interactions between the oligonucleotide and the NP (Armistead et al., 2015). The Debye Length ($\lambda_{DH(T,I)}$) described in Armistead et al. (2015) for Equation (3) is as follows:

$$V_{DH}(T,I) = \sqrt{\frac{\varepsilon_0 \varepsilon_r k_B T}{2N_A e^2 I}} \qquad (4)$$

The coarse-grained model uses a constant NP diameter of 2.83 nm (Armistead et al., 2015), which is based on the Au NPs presented in Kim et al. (2011). The linker for DNA's attachment is described by Equations (1) and (2) to make the linker very rigid (Armistead et al., 2015). The effective charge q of the NP needed to accurately simulate the interparticle distances of each structure in Kim et al. (2011) in Equation (3) was found to be q = 1.875 (Armistead et al., 2015). A schematic of self-assembled mono-functionalized Au NPs is presented in Figure 9. The diatomic structure consists of two Au NPs shown as yellow beads, each with six possible interaction sites denoted by six blue bars on the surface of the yellow bead. In this example, only one attachment site is used corresponding to the single DNA strand attached to the Au NP, which is mono-functionalized to the 5' side of the oligonucleotide.

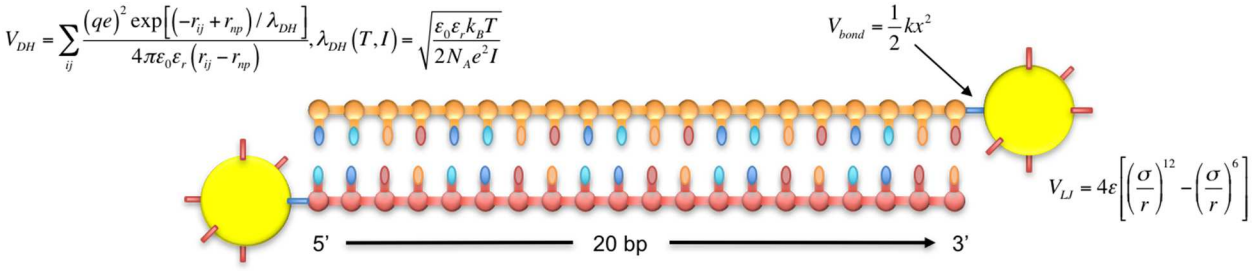

Figure 9. Schematic of the coarse-grained model for NP building blocks. The Au NP is represented by the yellow circle, the blue bars indicate the thiol linker that bonds the ssDNA to the Au NP, the red bars indicate the five other possible attachment sites for ssDNA, and the orange and red bead strings represent complimentary DNA sequences, consisting of 20 nucleotides. The harmonic potential describes the DNA attachment site, the Lennard-Jones potential for the NP excluded volume, and the Dubye-Hückel potential for the electrostatic interactions of the NP.

2.1.2 Instrumentation

Hardware. Set-up and initiation of simulations were done using a MacBook Pro (15-inch, Mid 2009). The computer had a 2.66 GHz Intel Core 2 Duo processor, 8 GB 1067 MHz DDR3 RAM, and a NVIDIA GeForce 9600M GT 256 MB graphics card. After the initiation of a simulation, a simulation was computed for a desired walltime, using the Arkansas High Performance Computing Cluster. The Arkansas High Performance Computing Cluster is a hardware and storage resource companion for computational science. The simulations ran on the Razor cluster, which consists of three sub clusters. Once a simulation exceeded the walltime, analysis and visualization of the simulation was done on the MacBook Pro.

Software. The MacBook Pro 2009 uses the operating system OSX. To set up and initiate the simulations, the program Terminal was used. After the simulations finished, molecular graphics and analyses were performed with the UCSF Chimera package. Chimera is developed by the Resource for Biocomputing, Visualization, and Informatics at the University of

Califronia, San Francisco (supported by NIGMS P41-GM103311; Pettersen et al., 2004). The program svnX (Version 0.9.13; SvnX, 2016) was used for storage of all the files created for the simulations.

2.1.3 Procedure for simulations. Before setting up a simulation, a folder was created and given a name to designate and keep track of the desired simulation. Two files, NBLOCK.pbs and sequences.txt, were used to design the simulation. NBLOCK.pbs is what was used to start a job on the AHPCC. In this file, several variables could be adjusted for the simulation, including sodium chloride concentration, temperature, and box size. The NPs and their sequences were designated in the sequences.txt file. Each NP building block was designated as *N* and the sequences for that NP building block were typed below the *N*. Up to six lines of sequences could be typed in below the *N*, representing the possible six single strands of DNA that could be added to the surface of an NP building block (see Figure 10). Once the simulation had been designed and the file found in Terminal, the command *qsub NBLOCK.pbs* was used to start the simulation.

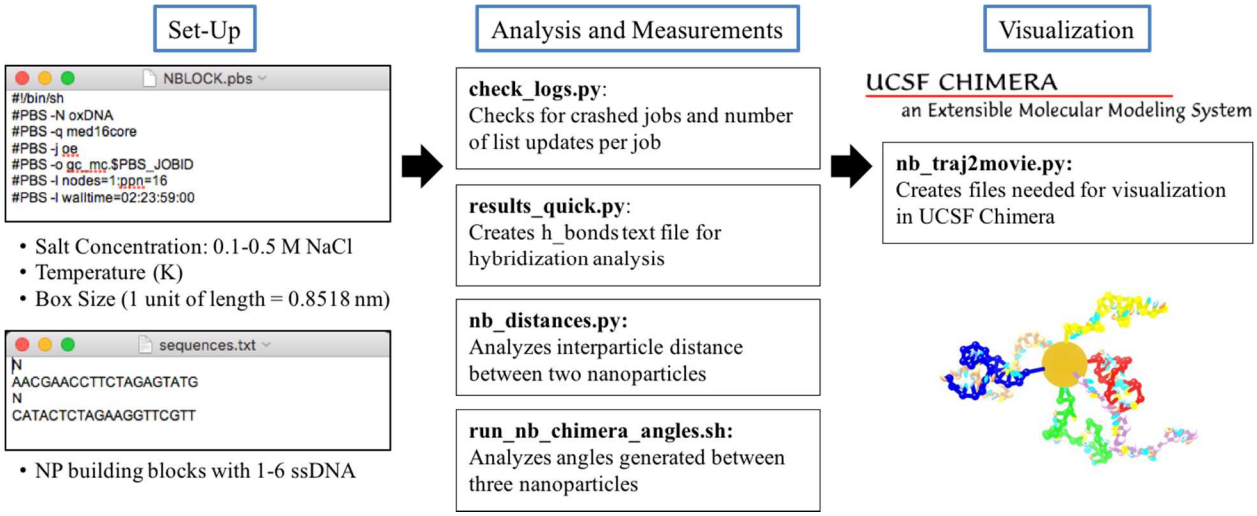

Figure 10. Procedures to set-up, initialize, analyze, and visualize simulations. The files NBLOCK.pbs and sequences.txt are used to set-up the simulation. The files check_logs.py, results_quick.py, nb_distances.py, and run_nb_chimera_angles.sh were utilized to analyze each simulation. Once analysis indicated a complete structure, nb_traj2movie.py was used to create the files necessary to visualize the simulation. Molecular graphics and analyses were performed with the UCSF Chimera package. Chimera is developed by the Resource for Biocomputing, Visualization, and Informatics at the University of Califronia, San Francisco (supported by NIGMS P41-GM103311; Pettersen et al., 2004).

After the walltime had been reached for the simulation, which was limited to 3 days by the AHPCC cluster, analysis was done on the desired simulation. Four files were used to view the relevant data from the simulation: (a)check_logs.py, (b) results_quick.py, (c) nb_distances.py, and (d) run_nb_chimera_angles.sh (see Figure 10). Check_logs.py was used to check whether a job has crashed and it also gave the number of list updates completed during the walltime for each job. Result_quick.py checked each job for the simulation for possible duplex formation and created a file called h_bonds_by_job.txt, which gave the strand ID number, the ID number of the strand that it had formed hydrogen bonds with, and the number of base-pairs involved in the bonding. Nb_distances.py was used to find the distances between NPs given in

nanometers. Run_nb_chimera_angles.sh utilized the h_bond_by_job.txt file to display the angles between three particles within a given structure.

When a job showed promise for a finished structure based on the desired number of duplexes to be formed, the job was committed to the svn, and the nb_traj2movie.py file to create two new files from the job called trajectory.dat.pdb and trajectory.dat.com, which were also committed to the svn. After these two files were created, the program UCSF Chimera was used to visualize the simulation (see Figure 10). This was accomplished by going into Tools, going to MD/Ensemble Analysis, and selecting MD Movie. A dialog box appeared to browse for the necessary trajectory.dat.pdb file. Once this file was found, the Per-Frame drop-down menu in the MD Movie: PDB trajectory dialog box was used to select Define script where the Insert text file button in the Per-Frame Commands dialog box could be used to find the corresponding trajectory.dat.com file. This file changed the view of the simulation, giving the NP its Au color and each strand its own color.

2.2 Experimental Methods for the Synthesis of DMAP-MESA-Au NPs

Capping ligands are used to control the aggregation, growth, stability, and behavior of NPs, and monodispersal of the NPs is due to the electrostatic repulsive force associated with them. The capping ligands used in the sequential anisotropic mono-functionalization strategy were DMAP and MESA. First, the Au NPs were protected by a monolayer DMAP (DMAP-Au NPs) based on the protocol developed by Gittins and Caruso (2001). Next, the DMAP-Au NPs were exposed to a controlled ligand exchange with MESA to synthesize DMAP-MESA-Au NPs (Kim & Kim, 2010).

The aqueous phase DMAP-Au NPs were synthesized by ligand exchange and phase transfer from toluene to water based on the Brust-Schiffrin method (Briñas, Maetani, & Barchi, 2013; Gandubert & Lennox, 2005). The first step to synthesize the DMAP-Au NPs involves mixing a toluene solution of tetraoctylammonium bromide (TOAB; 600 mg in 20 mL; Briñas, Maetani, & Barchi, 2013) with an aqueous solution of $HAuCL_4$ (100 mg in 8 mL; yellow color; see Figure 11) in a 100 mL conical flask. This mixture was vigorously stirred until the color changed from yellow to orange indicating complete phase transfer of the gold salt into toluene (Briñas, Maetani, & Barchi, 2013). Next, a freshly prepared solution of sodium borohydride (140 mg) in 30 mL of dH_2O was added slowly, and the mixture was quickly stirred for 2 minutes at room temperature. With this addition, the mixture changed from a light red color to red-ruby. After incubation at room temperature for 2 hours, the ruby-red solution was transferred into a separation conical flask and allowed to settle for 20 minutes (Briñas, Maetani, & Barchi, 2013; Gandubert & Lennox, 2005). Next, the byproduct at the bottom of the flask was removed and the ruby-red solution retained. The solution was washed with 0.1 M H_2SO_4, 0.1 M NaOH, and dH_2O, and each washing step was repeated three times. The volume was adjusted to 25 mL with toluene.

Figure 11. Observations of color change during the synthesis of TOAB-Au.

A freshly prepared solution of DMAP (600 mg) in 25 mL of dH_2O was added to the TOAB-Au in toluene, resulting in a phase transfer indicated by the color transferring into the aqueous phase. The ruby-red TOAB-Au-DMAP was collected at the bottom of a separation conical flask to discard the toluene. Then, the solution was washed with toluene three more times (Briñas, Maetani, & Barchi, 2013).

The MESA ligands were added to the DMAP monolayer based on the ligand exchange method described by Kim and Kim (2010). Fifty µL of a freshly prepared solution of MESA (9.8 mg) in 1 mL of dH_2O was pipetted as a drop onto the lid of a 1.5 mL micro-centrifuge tube containing 1 mL of the DMAP-Au NP solution. After closing the cap, the micro-centrifuge tube was quickly shaken and placed on a shaker and incubated for 15 hours. Then the solution was

washed with 10 mL of dichloromethane and shaken for 1 minute. Once the dichloromethane was removed, the remaining solution was subjected to flowing N_2 over the surface for 1 minute and the solution stored at 4ºC (Kim & Kim, 2010).

A UV/Vis spectrophotometer was used to characterize the spectra of the DMAP-Au and the DMAP-MESA-Au NPs to prove the attachment of the ligands for each type of NP. The wavelength peaks of the newly synthesized DMAP-Au NPs were compared to the DMAP-MESA-Au NPs (see Figure 12), revealing a peak wavelength for the DMAP-Au NPs of 526 nm and a blue shift to a 520 nm peak for the DMAP-MESA-Au NPs. The DMAP-Au spectra appeared to be wider than the curve for the DMAP-MESA-Au, signifying that DMAP alone was a weaker ligand than a mixed monolayer of DMAP and MESA and could easily aggregate due to its sensitivity to light or temperature.

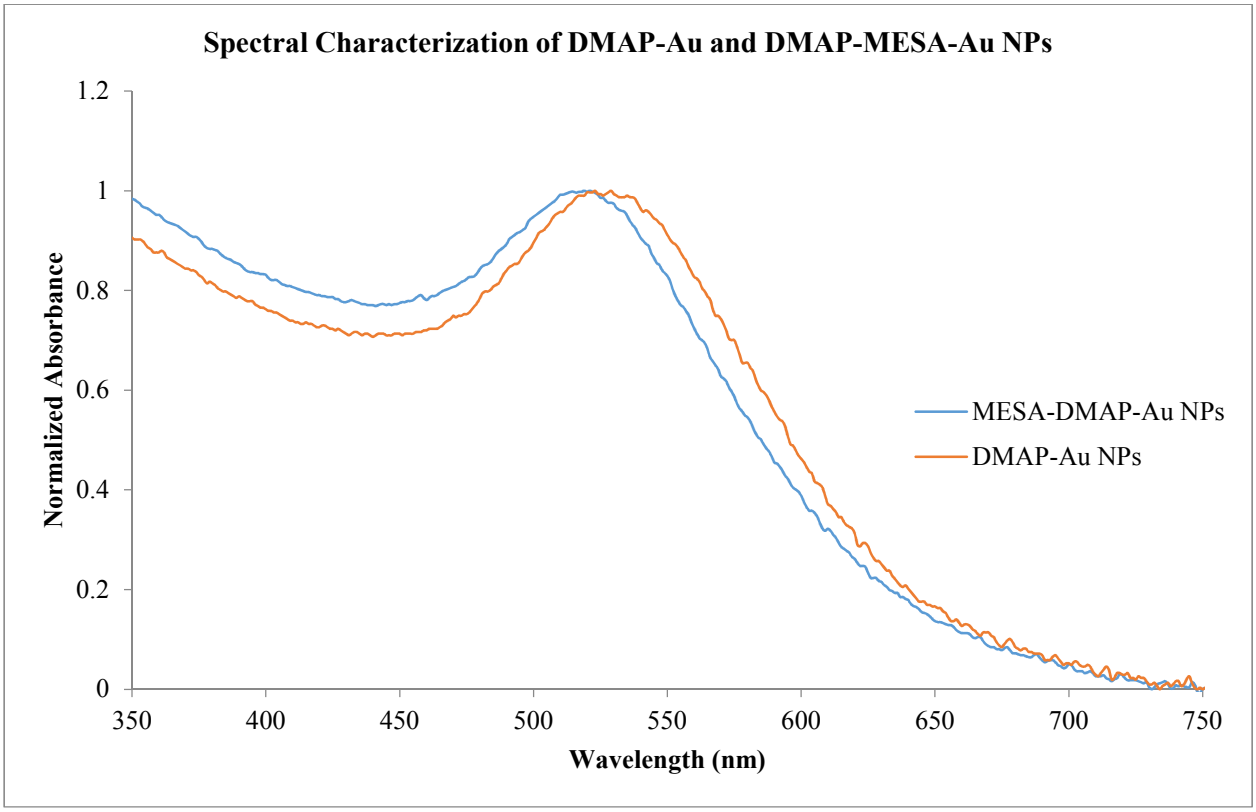

Figure 12. Comparison of spectra of synthesized DMAP-Au and DMAP-MESA-Au NPs with spectrophotometer. The peak wavelength for the DMAP stabilized Au NPs is 526 nm. After the ligand exchange to attach MESA to the surface, the peak shifts to the left and narrows.

Chapter 3: Stability of Au NPs for the NP Building Block Model

OxDNA2 is designed to handle a range of salt concentrations ([Na^+] = 0.1-0.5 M; Snodin et al., 2015). However, in the mono-functionalization developed by Kim et al. (2011), the building blocks were synthesized in 0.01 M phosphate buffer (Kim et al., 2011). Therefore, the first step in validating a model for Au NP building blocks was to determine if the NPs are stable within the range of concentrations required in the model. Since salt concentrations can affect the stability of the NPs and cause aggregation (Liu & Jiang, 2007), the range of concentrations used in the experiment only went up to 0.1 M NaCl to limit the possibility of destabilizing the Au NPs.

Using the procedure outlined in the Chapter 2, DMAP-MESA-Au NPs were synthesized to examine their stability in salt concentrations varying from 0 to 100 mM NaCl, using water as the control. The salt concentration was varied to include concentrations of 10, 50, and 100 mM. The four samples used in the experiment are summarized in the Table 1 below.

Table 1: Summary of Volumes used Salt Stability Experiment

Volumes Used for Testing Salt Concentration on DMAP-MESA-Au Nanoparticles				
Sample	**Au NP (uL)**	**H_2O (uL)**	**1 M NaCl (uL)**	**[NaCl]**
1	250	250	0	-
2	250	245	5	10 mM
3	250	225	25	50 mM
4	250	200	50	100 mM

To determine the stability of the DMAP-MESA-Au NPs, each sample was incubated for a 24-hr period after the salt was added to the Au NPs. At different time points during the incubation period, UV/VIS spectrophotometry and observation of the samples were used to verify whether the NPs had aggregated. If a particular salt concentration caused aggregation of

the Au NPs, there would be a change in the color of the sample from their red color to a more purple color (Liu & Jiang, 2007). The UV/VIS spectrophotometer was used to determine whether there was a significant change in the spectra of the sample, also indicating possible aggregation (Liu & Jiang, 2007). If the samples were to destabilize, the spectrophotometer would show a red shift in the spectra away from 520 nm and a broadening of the peak. The spectra generated from the 24-hr incubation of the samples are shown in Figure 13, which confirmed that the DMAP-MESA-Au NPs were stable in the presence of at least 100 mM NaCl. None of the samples showed the required red shift and broadening of the 520 nm peak for Au NPs to indicate aggregation. This was also verified by each sample's original red color at the end of the incubation period.

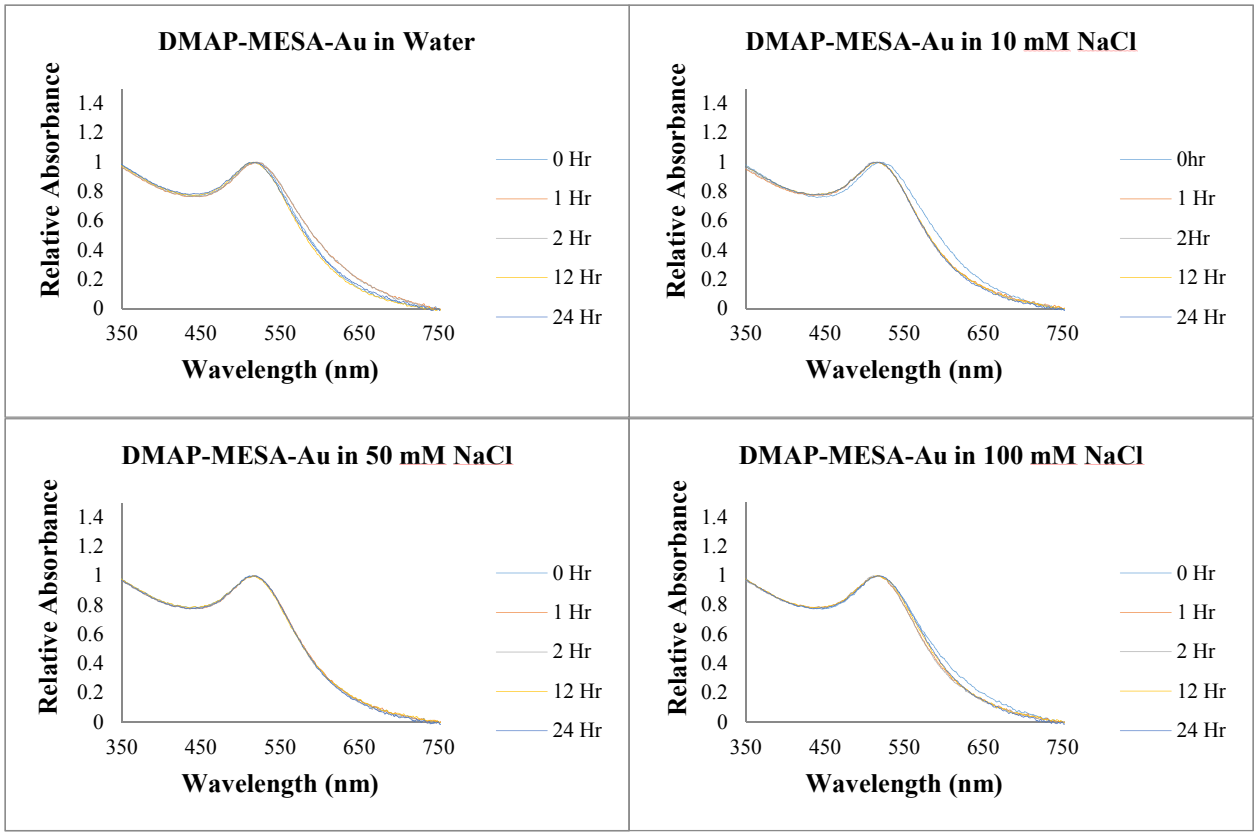

Figure 13. Effect of salt concentration on DMAP-MESA-Au NP. The DMAP-MESA-Au NPs were incubated for 24 hr in water (top-left), 10 mM NaCl (top-right), 50 mM NaCl (bottom-left), and 100 mM NaCl (bottom-right). Spectral analysis showed no change over the 24-hr period.

Since the DMAP-MESA-Au NPs were shown to be stable in at least 100 mM NaCl, the model would be validated to use the NPs at 100 mM NaCl throughout the course of the simulations for the self-assembly of NP building blocks. The next step in the validation of the model was to begin simulating the self-assembly of Au NP building blocks into discrete nanostructures.

Chapter 4: Validating Simulations of DNA-Linked Nanoparticle Building Blocks

In this study, the NP building block model was used to simulate the self-assembly of the NP building blocks into the six structures self-assembled by Kim et al. (2011): (a) diatomic, (b) linear, (c) T-shaped, (d) square planar, (e) square pyramidal, and (f) octahedral. Before simulating the self-assembly of the building blocks into their corresponding structures, several steps were followed to first validate the model.

In this chapter, the model was used to accomplish a few key objectives. The objectives included validating self-assembly of the building blocks, simulating the structures manufactured by Kim et al. (2011), self-assembling structures of varying numbers of bases, and simulating multiple structures simultaneously. Also, there were two secondary objectives that involved producing a melting temperature profile for the diatomic structure and to examine changing the box size of simulations.

4.1 Simulating DNA-Functionalized Au NP Building Block Configurations

Before simulating the self-assembly of Au NP building blocks into the structures produced by Kim et al. (2011), we verified that all six building block configurations, which were based on the building blocks presented by Kim et al. (2011), could be successfully simulated and visualized, shown in Figure 14. From the figure, the building blocks are shown to have a single gold colored sphere, representing the Au NP, and the expected relative orientations of the ssDNA on the surfaces of each Au NP. The simulations also show the flexible nature of ssDNA.

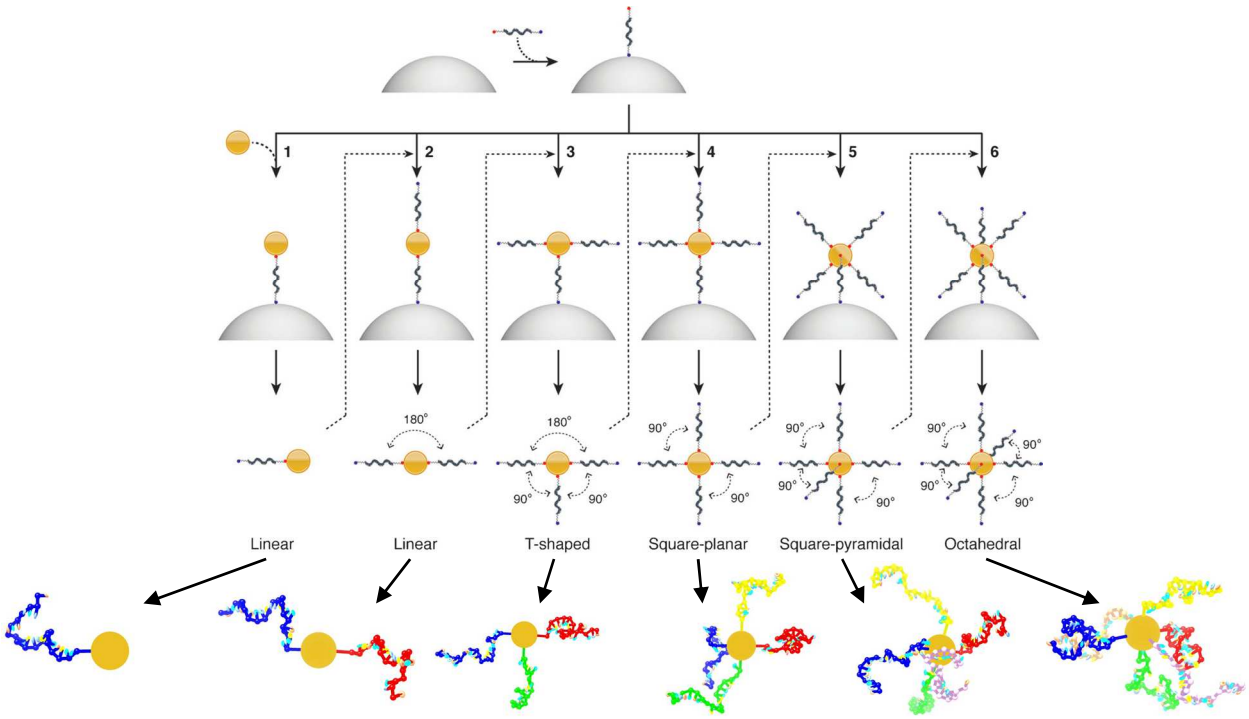

Figure 14. Simulated results of each Au NP building block configurations compared to the schematic of the NP building block configurations. Each arrow points to the corresponding simulated building block configuration. Adapted with permission from "DNA-Linked Nanoparticle Building Blocks for Programmable Matter," by J.-W. Kim et al., 2011, *Angewandte Chemie International Edition, 50,* p. 9186.

Now that the model has been verified to simulate each building block configuration, the next step is to simulate duplex formation between a simple system of building blocks.

4.2 Validation of Duplex Formation

Duplex formation is an important aspect of the self-assembly process – one that must be validated to ensure accuracy of the model. OxDNA2 was designed to accurately show the self-assembly process and thermodynamic and mechanical properties associated with ssDNA, duplex formation, and the double helical form. Since a Au NP and new interactions for that particle and

the attachment of ssDNA to the particle, we needed to verify whether our model could also capture the process of duplex formation between building blocks. This validation step consisted of simulating the simplest possible system of building block, two mono-functionalized linear building blocks, and simulate them at room temperature. Next, the same system would be simulated with non-complementary strands. Finally, a more complex system consisting of two bi-functionalized linear building blocks would be simulated to verify that duplex formation is specific to strands that are complementary to each other among other non-complementary strands. After the validation steps, we wanted to examine the effect of varying temperature on the yield of self-assembly of the diatomic structure.

4.2.1 Mono-functional linear NP building blocks. To validate duplex formation, the simplest system to simulate is two mono-functionalized linear NP building blocks. The self-assembly of this system would result in a diatomic structure with two Au NPs and one DNA double helix. This experiment consisted of two parts: the first being a simulation using complementary strands and the second using non-complementary strands. Using complementary strands in the first part should drive the self-assembly of the two building blocks, resulting in the desired diatomic assembly with a duplex. The complementary sequences of the strands used to verify duplex formation are summarized in Table 2.

Table 2: Complementary strands used to self-assembled diatomic structure from mono-functionalized Au NP linear building blocks (Kim et al., 2011).

NP Building Block	Strand	Sequences
1	**0**	5'-Thiol-AACGAACCTTCTAGAGTATG-Amine-3'
2	**1**	5'-Thiol-CATACTCTAGAAGGTTCGTT-Amine-3'

After simulating the first system with complementary strands for the 3-day period, the final configuration of the simulation was visualized, as shown in Figure 15. In the figure, the two mono-functionalized building blocks started out separated in the simulation. By the end of the simulation, the building blocks self-assemble into the desired structure, due to the complementarity of the strands.

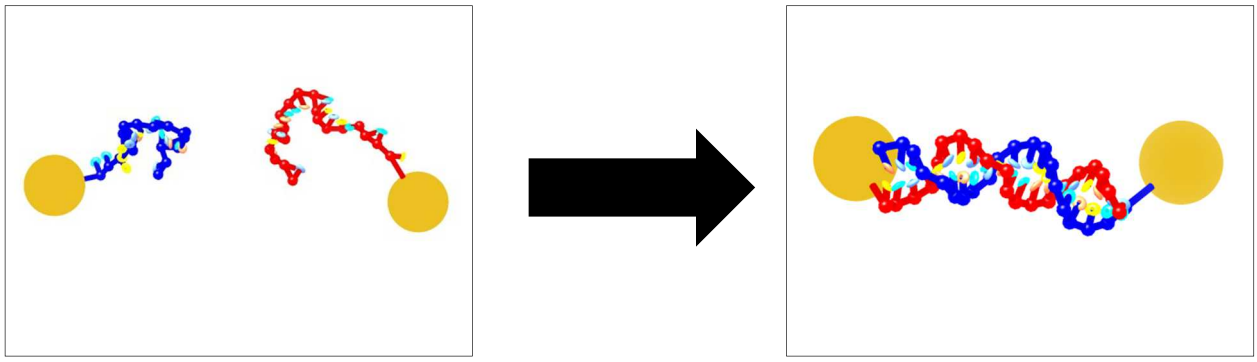

Figure 15. Simulation of the self-assembly of complementary mono-functionalized NP building blocks. The left shows the initial positions of the two separated mono-functionalized Au NP building blocks at the beginning of the simulation, and the right shows the final self-assembled structure at the end of the simulation.

The formation of a duplex in this simulation confirmed that our model was able to self-assemble two building blocks into the desired structure. Although the complementary strands were able to drive the self-assembly of the building blocks, this simulation did not confirm whether the model was able to distinguish between complementary and non-complementary strands.

In the second part of this experiment, non-complementary strands were used to test the opposite of the first simulation: non-complementary strands should not drive the two building

blocks to form a duplex, resulting in the diatomic structure. The non-complementary strands used in the simulation are summarized in Table 3.

Table 3: Non-complementary strands used to prevent the self-assembly of mono-functionalized Au NP linear building blocks (Deaton, Kim, & Chen, 2003).

NP Building Block	Strand	Sequences
1	**0**	5'-Thiol-GATCCTATATCTTAATGCAC-Amine-3'
2	**1**	5'-Thiol-CCTTGGATTTATCTTCGACA-Amine-3'

After simulating the two mono-functionalized Au NP building blocks with non-complementary strands for the same 3-day period, the simulation was visualized and the results are shown in Figure 16. The simulation resulted in the two Au NP building blocks staying separated, verifying that the model would not form duplexes between non-complementary strands.

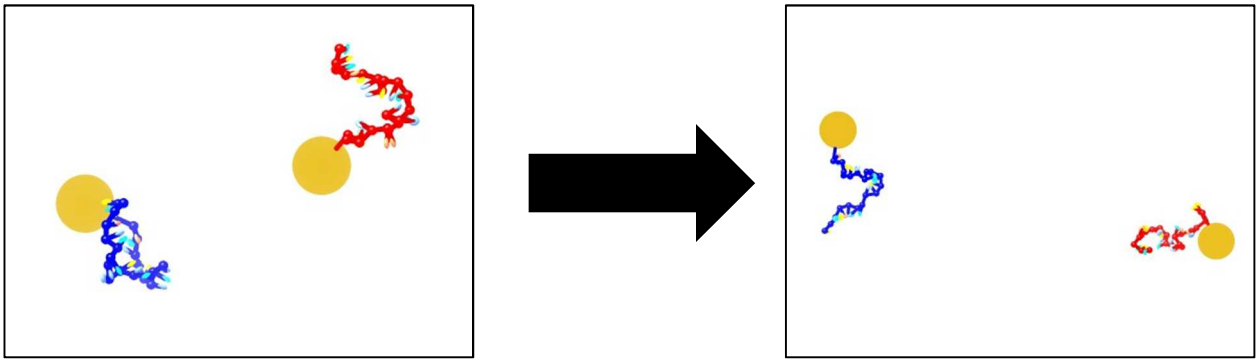

Figure 16. Simulation of non-complementary mono-functionalized NP building blocks. The left shows the initial positions of the two mono-functionalized Au NP building blocks, and the right shows the final positions of the building blocks at the end of the simulation.

Together these simulations were successful in verifying that self-assembly only occurs in the presence of complementary strands resulting in the desired diatomic structure. This marked the first step in verifying duplex formation in the coarse-grained model for NP building blocks.

4.2.2 Bi-functional linear Au NP building blocks. The next step in validating duplex formation was to use a slightly more complex system than what was used previously. The purpose of this experiment was to show that duplex formation was specific to complementary strands in the presence of non-complementary strands. This means that in a system containing more strands than just the pair of complementary strands, only the desired complementary strands would be expected to hybridize to each other and the other two strands should not hybridize to one of these strands and should not hybridize to each other. In this system, bi-functionalized linear building blocks were designed with the sequences from Table 2 and Table 3 and summarized in Table 4. There are four total strands: two that are complementary (Strands 0 and 2) and two others that are neither complementary to the desired duplex nor complementary to each other (Strands 1 and 3). Strands 0 and 1 are attached to the first building block, and Strands 2 and 3 are on the second building block, forming the two bi-functionalized linear building block configurations.

Table 4: Sequences used in duplex formation of bi-functional NP building blocks (Deaton, Kim, & Chen, 2003; Kim et al., 2011).

NP Building Block	Strand	Sequences (5' → 3')
1	**0**	AACGAACCTTCTAGAGTATG
	1	GATCCTATATCTTAATGCAC
2	**2**	CATACTCTAGAAGGTTCGTT
	3	CCTTGGATTTATCTTCGACA

After the simulation finished, it was visualized to show the self-assembly process of the building blocks. Figure 17 shows the initial and final positions of the building blocks. The strands in the figure are different colors: Strand 0 is Blue, Strand 1 is Red, Strand 2 is Green, and Strand 3 is Yellow. The simulation verifies formation of the desired duplex. To verify that the desired duplex was formed, a total of 64 simulations were done, and the hybridization of all strands in each system were examined. Out of the 64 simulations, 68.8% resulted in the formation of a diatomic structure at the end of the 3-day simulations.

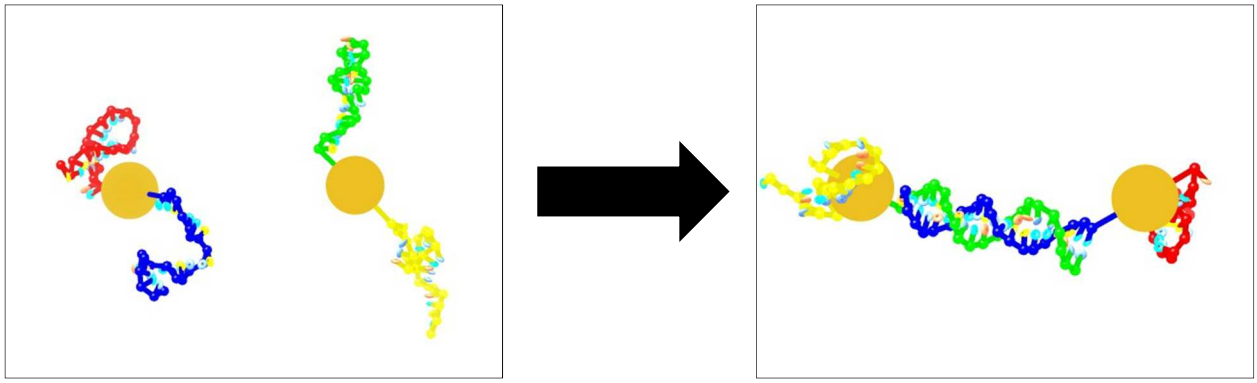

Figure 17. Simulated self-assembly of bi-functionalized NP building blocks. The left shows the initial positions of the bi-functionalized Au NP building blocks in the simulation, and the right shows the final self-assembled structure at the end of the simulation.

Figure 18 shows the results of the relative frequency of hybridization among the four strands across the 64 simulations. In the figure, 114 different hybridizations occurred across the 10 possible hybridizations in the 64 simulations. For example, “0-0” represents Strand 0 binding to itself, and “0-2” represents Strand 0 binding to Strand 2, the desired duplex formation. The left axis shows the relative frequency of each hybridization out of the 114, represented by the blue

bars. The right axis shows the number of base pairs present in each hybridization, represented by the red dots. The graph shows the desired duplex having the highest relative frequency and highest number of base pairs present in each of those formations. The results for "0-2" are significantly greater than all of the other possibilities.

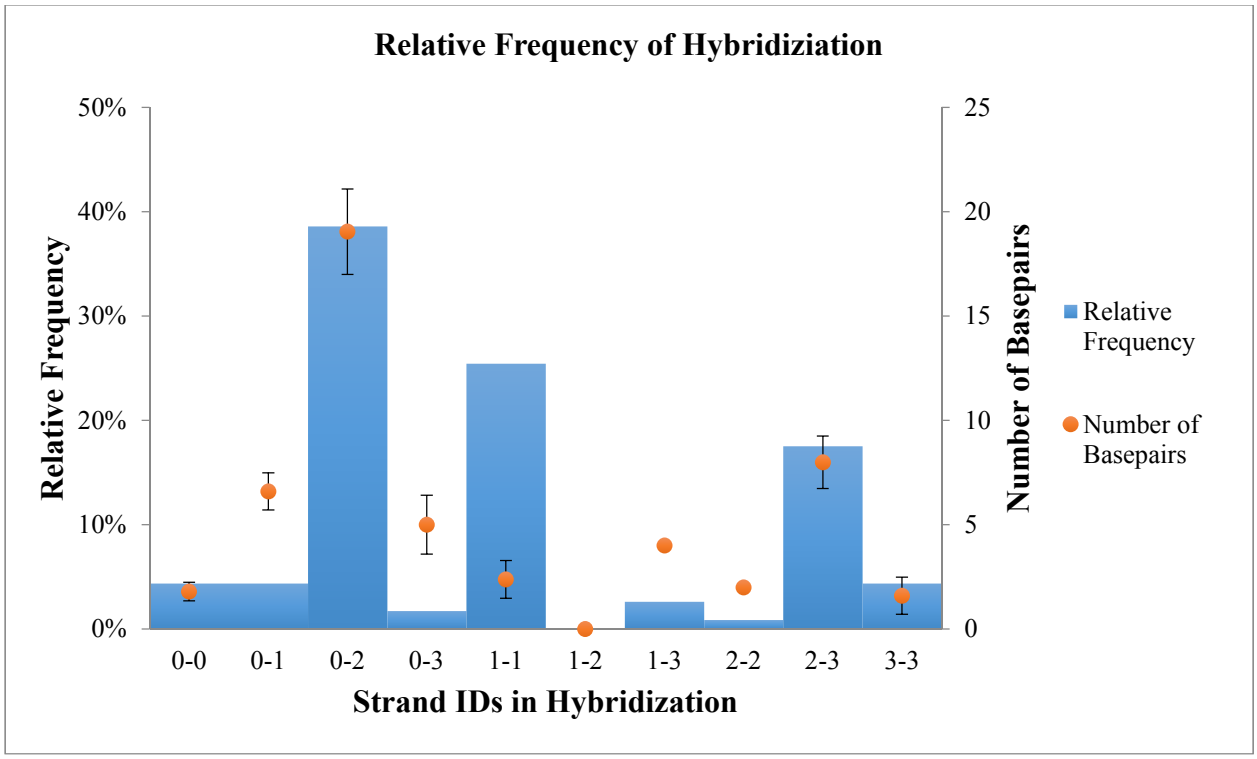

Figure 18. Relative frequency of hybridization of bi-functionalized NP building blocks. The x-axis shows the possible combinations of hybridized strand IDs. The combination "0-2" represents the desired complementary duplex formation. The left axis represents the relative frequency of hybridization across all simulations and is measured with the blue bars. The right axis represents the number of base pairs that occur in each hybridization and are measure with the red dots, with the highest possible number of base pairs in hybridization being 20.

This step in the validation process further proves the model's ability to correctly self-assemble a desired structure and to distinguish between complementary and non-complementary

DNA sequences. These abilities are important for a model with the purpose of aiding the rational design of nanostructures using NP building blocks.

4.2.3 Melting temperature profile with diatomic structure. After the validation of duplex formation, we wanted to examine the effects of temperature of duplex formation for the diatomic structure. The oxDNA2 model has been shown to accurately portray thermodynamic properties of DNA (Snodin et al., 2015). Therefore, the building block model should also demonstrate thermodynamics of the building blocks. The effect of temperature on the simulated self-assembly of NP building blocks with this model has not been examined. Since non-functionalized dsDNA undergoes reversible melting within a 20 K range, DNA-NP aggregates have been shown to have a narrower reversible melting temperature (T_m) range, and the melting of the aggregates is slightly higher than the bulk DNA T_m (Jin et al., 2003; Lee & Schatz 2009), the simulated self-assembly of the NP building blocks should reflect these properties. Therefore, in the experiment, the T_m profile for the diatomic structure should have a narrower that would have a T_m that would be shifted to a slightly higher temperature than the T_m of isolated DNA.

The model allows the user to change the desired temperature of the system. To generate the profile, the simulation involved the self-assembly of the diatomic structure for 3-day periods for multiple simulations at temperatures ranging from room temperature (298 K) to 375.6 K. The T_m profile is shown in Figure 19. The number of self-assembled structures at each temperature studied divided by the total number of simulations for that temperature determined the duplex yield at that temperature. There were at least 32 simulations done at each temperature to generate the data for the T_m profile. The sequences used in the simulations were the complementary sequences taken from Table 2 in section 4.2.1, utilized for the self-assembly of the diatomic structure.

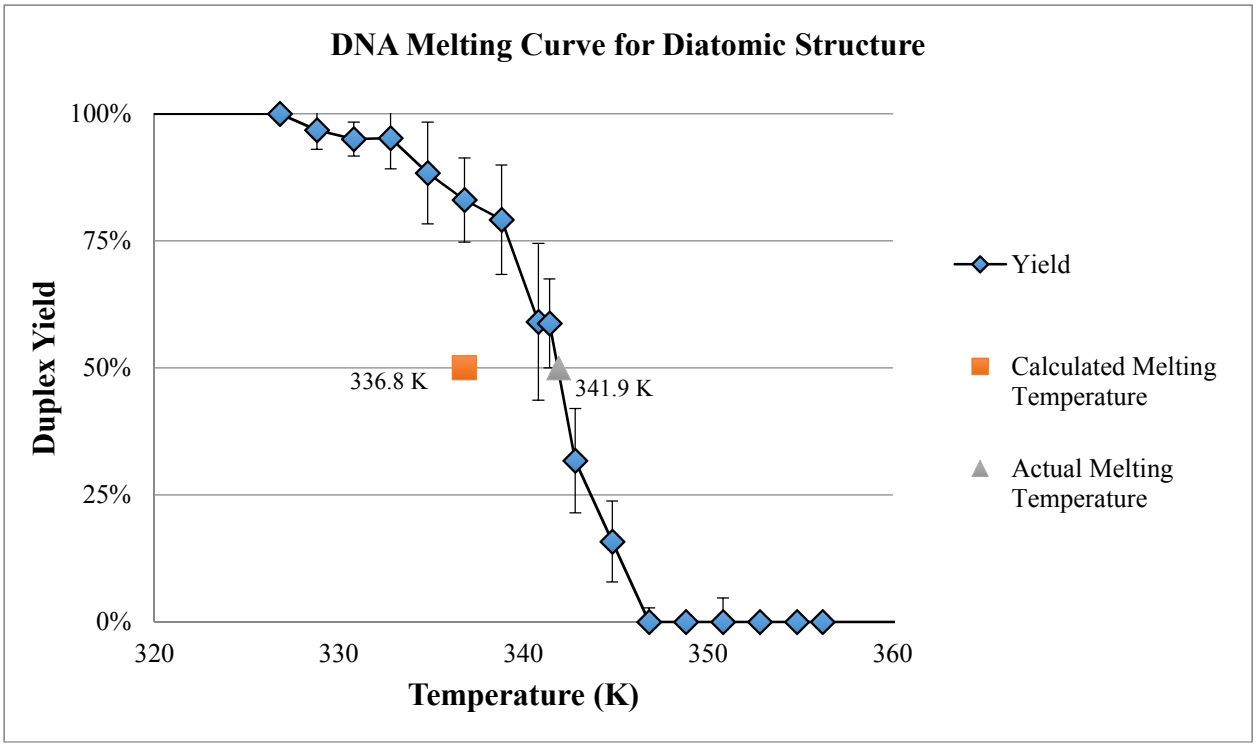

Figure 19. DNA melting profile for diatomic structure. The x-axis shows the temperature in Kelvin, and the y-axis shows the duplex yield for each temperature simulated. The red square is the melting temperature for free DNA calculated using the OligoAnalyzer tool from Integrated DNA Technologies. The green triangle is the calculated melting temperature of the profile generated through the simulations.

Figure 19 shows the resulting melting curve. The curve shows a T_m range of 20 K with a melting temperature for the diatomic structure of 341.9 K. Using Integrated DNA Technologies' OligoAnalyzer Tool, the melting temperature of the isolated DNA duplex was determined to be 336.8 K. Therefore, the profile shows a melting temperature of 5.1 K higher than the isolated DNA melting temperature. The results of these simulations correlate with what has been found in previous molecular dynamics simulations and experiments for DNA-linked NP aggregates (Jin et al., 2003; Lee & Schatz 2009) with respect to the higher T_m of the simulated diatomic structure but not with respect to the narrower expected T_m range.

4.3 Validation of DNA-Linked NP Building Block Structures

Once production of the desired duplex formation was verified, it was possible to move on to validation of the model through simulating the six DNA-linked nanoparticle building structures previously fabricated using the anisotropic mono-functionalization strategy developed by Kim et al. (2011). Using this technique, they were able to fabricate the six DNA-functionalized nanoparticle building block configurations, and hybridized each building block configuration with a mono-functionalized Au NP containing a complementary strand, producing six structures (Kim et al., 2011). As per their experimental technique, each simulation would be run at 298 K, but each simulation would initially consist of one of the six building block configurations and the required number of separate mono-functionalized Au NPs which would be given the opportunity self-assemble into the desired final structure. These sequences are the same ones used in the previous experiments and summarized in Table 2 (Kim et al., 2011).

The final configurations of the simulations are shown in Figure 20. In the figure, a) and b) are the diatomic and linear structures, respectively; c) and d) are the t-shaped and square planar structures, respectively; and e) and f) are the square pyramidal and octahedral structures, respectively. The visualizations show that the model was successful in simulating the self-assembly of the NP building blocks into the expected nanoassemblies. The visualizations of the self-assembled structures give an idea of the relative rigidity of the DNA duplexes and the mobility of the Au NP at the duplex termini.

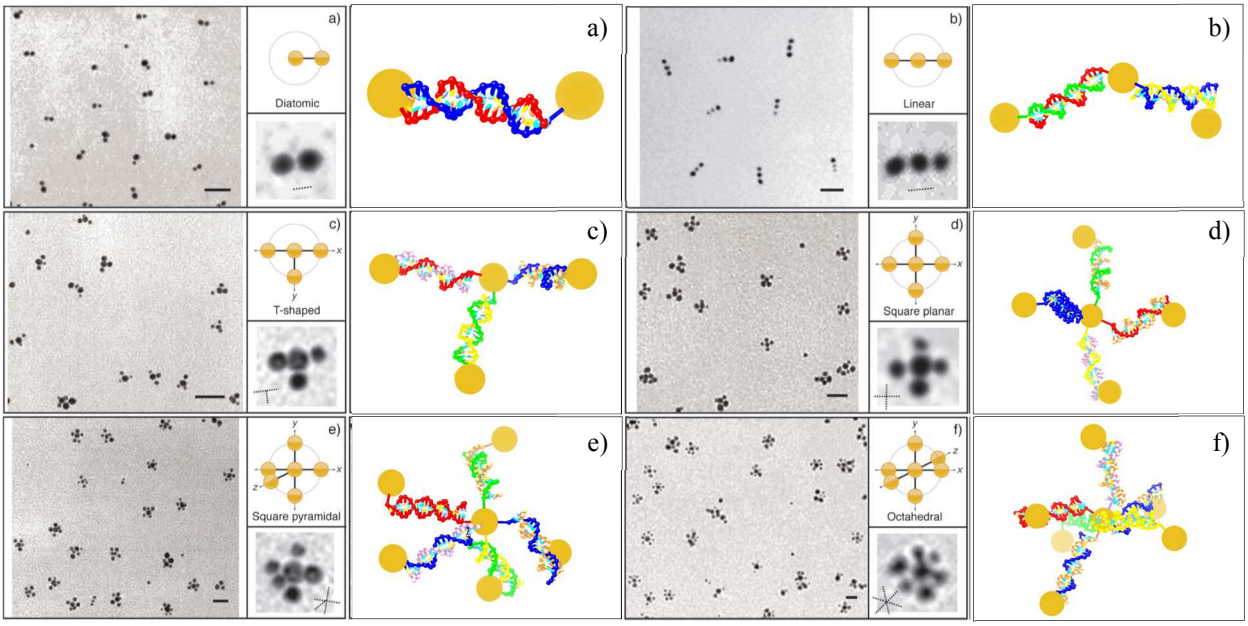

Figure 20. Summarized representation of the molecular geometry of DNA-linked gold nanoparticle structures, their self-assembled simulations, TEM micrographs and their expected schematic representation. A) is diatomic; b) is Linear; c) is T-shaped; d) is Square Planar; e) Square Pyramidal; f) is Octahedral. Adapted with permission from "DNA-Linked Nanoparticle Building Blocks for Programmable Matter," by J.-W. Kim et al., 2011, *Angewandte Chemie International Edition, 50,* p. 9188.

Further validation was performed by comparing the interparticle distances and angles produced by each of the simulated self-assembled structures to the previous data generated by from the TEM images (see Table 5; Kim et al., 2011). All interparticle spacing produced in the simulations for the diatomic, linear, t-shaped, and square planar structures, falls within the bottom of the range of interparticle spacing generated from the TEM images, but the average interparticle distance of the simulated structure was less than the averages measure by TEM of the fabricated structures. The modeled interparticle distances were, however, very consistent from structure to structure as were those measured from the fabricated structures. There were also significant difference between the micrographs and the simulations with respect to the

angles generated by the structures, with the simulated structures show different average angles when compared to the fabricated structures, and the simulated structures show a wider range of angles generated by the fabricated structures.

Table 5: Comparison of the physical characteristics of fabricated (Kim et al., 2011) and simulated NP building blocks structures.

Comparison of Nanostructure Data							
nBLOCK		**1 DNA: Diatomic**	**2 DNA: Linear**	**3 DNA: T-Shaped**	**4 DNA: Square Planar**	**5 DNA: Square Pyramidal**	**6 DNA: Octahedral**
Interparticle Spacing (nm)	**Modeled**	7.36 (± 1.55)	7.39 (± 1.47)	7.84 (± 1.54)	7.90 (± 1.40)	7.95 (± 1.37)	8.07 (± 1.34)
	Fabricated	9.3 (± 4.12)	9.7 (± 3.83)	9.5 (± 3.44)	10.1 (± 4.39)	-	-
Angles (^{0})	**Modeled**	-	83.80 (± 41.0)	112.13 (± 32.4) or 101.54 (± 34.0)	103.20 (± 32.9) or 97.57 (± 32.3)	95.28 (± 41.8) or 87.19 (± 40.1)	109.82 (± 40.5) or 87.03 (± 37.1)
	Fabricated	-	173.9 (± 9.88)	174.6 (± 8.76) or 85.9 (± 9.12)	171.8 (± 11.24) or 83.8 (± 8.24)	-	-

The coarse-grained model for NP building blocks was successful in simulating the self-assembly of each building block into the geometric structures demonstrated by Kim et al. (2011). The model indicated the capability to visualize the self-assembly process and measure structural information, which enables comparison of simulations to the results of those structures engineered by other researchers, making it a potential valuable tool in the research process.

4.3.1 Effect of concentration on simulations. To further study the performance of our model, we examined the effect of varying the NP building block concentration on yield of the

simulated nanoassemblies from Kim et al. (2011) by decreasing the simulation box size. The experiment consisted of simulating the self-assembly of structures over a 3-day period and increasing the original concentration by 25, 50, and 100 times. Figure 21 shows the results of changing this variable on structure and duplex formation during the simulated timeframe.

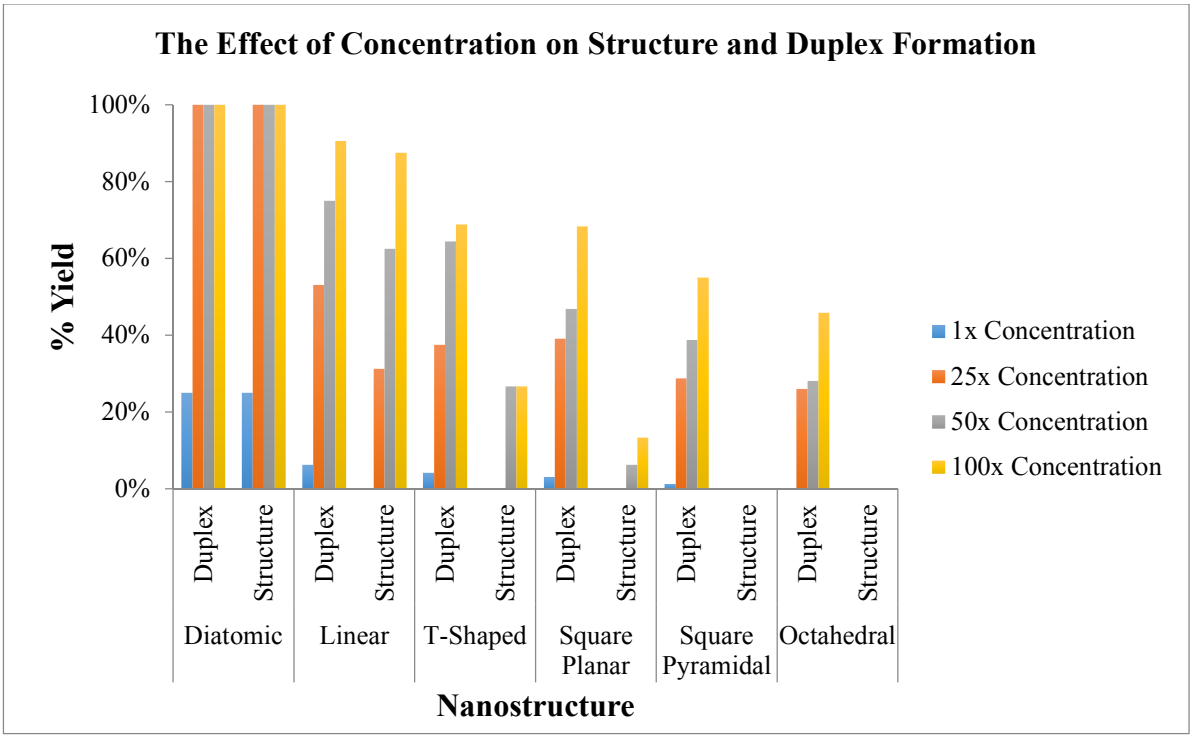

Figure 21. Effect of concentration on structure and duplex formation of DNA-linked NP building block structures. The x-axis separates each structure and contains labels for either duplex or structure. The left axis represents the percentage yield for either duplex or structure formation. There are bars for each concentration used in the simulations: blue for the initial concentration, red for 25 times concentration, green for 50 times concentration, and purple for 100 times concentration.

For a given structure, increasing the concentration by decreasing the box size resulted in an increase in yield of both the possible duplexes and structures throughout each series of

simulations for each nanoassembly. Also, for a given concentration, the yield of nanostructures decreases as the structural complexity increases, keeping the simulation timeframe equal.

The next analysis for the variation of concentration is examining the number of list updates that occur during a 3-day period for each structure at each concentration. The number of particles includes each nucleotide and each NP. For example, there are 42 particles involved in the simulation of the self-assembly of the diatomic structure, 20 nucleotides per DNA strand and two NPs. Figure 22 shows the effect of concentration on the number of list updates during simulations.

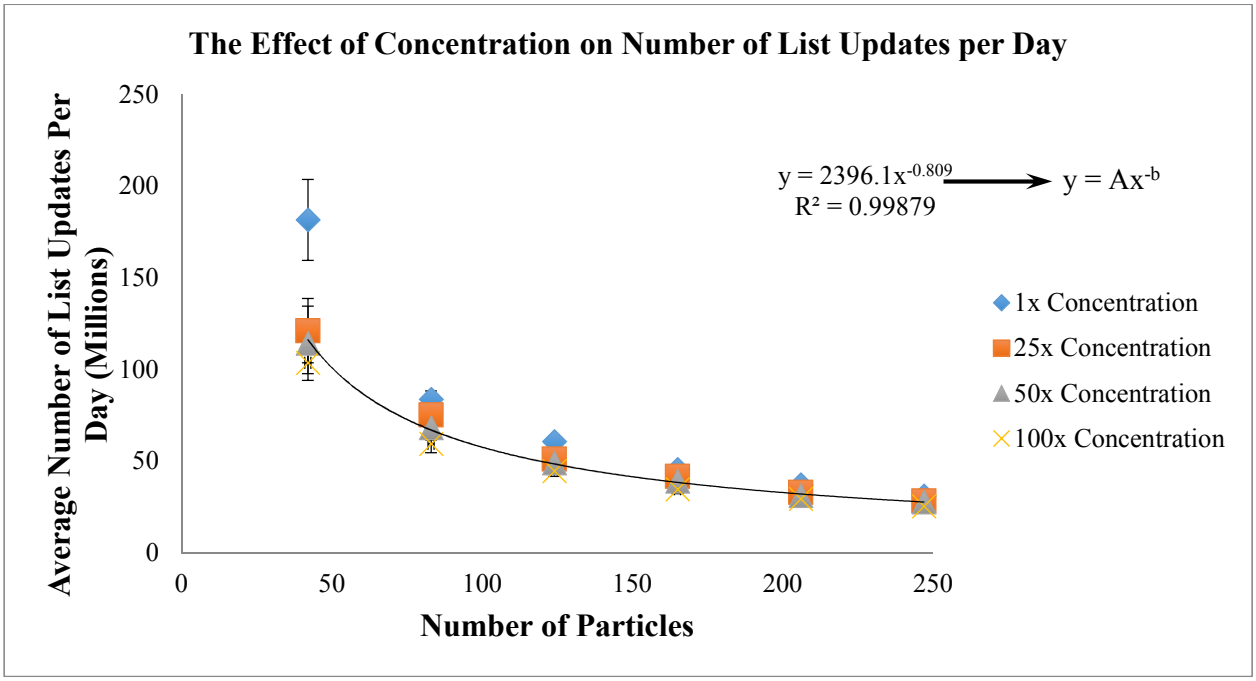

Figure 22. Effect of concentration on rate of list updates of simulations. Each DNA-linked building block structure was simulated at different concentrations. Each point on the graph represents the number of list updates that occurred per day for a given simulation of the self-assembled structures by Kim et al. (2011) for a given box size. The y-axis shows the number of list updates per day in millions, and the x-axis represents the number of particles in a simulation.

The results in Figure 22 shows that higher numbers of particles need to be simulated longer to achieve the same number of list updates as a smaller particle system at a given concentration. The decrease in average number of list updates with increasing the number of particles can be approximated by a power curve.

4.4 Design Control in Simulations

The purpose of the following experiments was to show the different kinds of control that a user of this model has in the design of NP building blocks. First, we examined varying the interparticle distance of a diatomic structure. Then, we simulated the linear structure to show that combinations of interparticle spacings can be utilized in the simulations of various structures. Finally, we used the diatomic structure to simulate multiple structures (up to six) in a simulated system, keeping the concentration constant for each system.

4.4.1 Varying interparticle spacing with diatomic structure. For this experiment, we used DNA sequences from Yu et al. (2010) to simulate three different interparticle distances in a diatomic structure based on the number of base pairs in a particular duplex. We hypothesized that we could control the interparticle spacing of the Au NPs by varying the number of base pairs of the duplex intended to assemble the building blocks into a diatomic structure. The chosen DNA sequences were 10, 16, and 20 bases (see Table 6) and was expected to have interparticle distances of 6.23, 8.27, and 9.63 nm, respectively, based on the rise per base of B-DNA.

Table 6: Summary of sequences from Yu et al. (2010) used for varying interparticle distance of diatomic structures.

Structure	Sequences (5' → 3')
10-Base Dimer	GCGATCGCGG
16-Base Dimer	CCTCCTAGATTAGGTT

20-Base Dimer	AACGAACCTTCTAGAGTATG

The model was successful in simulating each structure with varying interparticle distances. The visualized results of the simulations are summarized in Figure 23. The DNA duplexes seem to be relatively rigid with most of the mobility occurring at the attachment site of the Au NP to DNA.

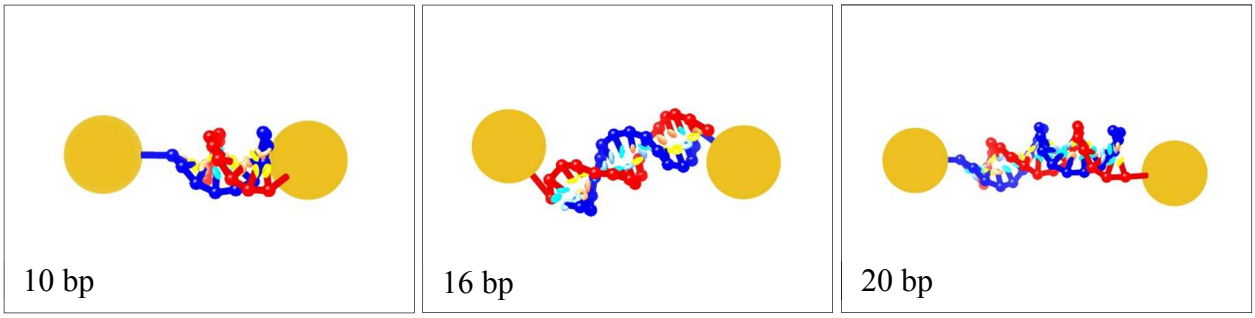

Figure 23. Varied interparticle spacing of diatomic structure. The left shows the 10-base pair diatomic; the middle shows the 16-base pair diatomic; the right shows the 20-base pair diatomic.

The simulated interparticle distances were calculated for comparison to the expected interparticle distances. The interparticle distances for each structure are summarized in Table 7. The modeled distances were shorter than the theoretical interparticle distances.

Table 7. Interparticle spacing between NPs in diatomic structures of varying lengths.

Structure	10-Base Dimer	16-Base Dimer	20-Base Dimer
Interparticle Spacing (nm)	4.26 ± 1.48 nm	5.67 ± 1.95 nm	7.36 ± 1.55 nm

Although the interparticle distances did not reflect what would be expected, the model has shown the ability to control the interparticle spacing by varying the number of base pairs in each sequence. Now that control over interparticle distance has been demonstrated, a combination of a variety of interparticle distances should also be utilized in a single structure.

4.4.2 Combinations of interparticle spacing with linear structure. The second experiment to demonstrate control of interparticle spacing was the self-assembly linear structures with combinations of interparticle spacing. From this premise, we decided to create two groups of simulations. The first group consisted of homogeneous spacings of the previous interparticle distances formed from the 10-, 16-, and 20-base diatomics simulated in the previous experiment. Therefore, this group consisted of three linear structures with each containing two duplexes of equal length, resulting in 10-10 base pair, 16-16 base pair, and 20-20 base pair linear structures. The second group consisted of the heterogeneous structures where each linear structure utilized a combination of spacings based on the three interparticle distances, resulting in a 10-16 base pair, 10-20 base pair, and 16-20 base pair structures. The sequences used in the simulations are the same sequences in Table 6.

After successfully simulating the self-assembly of the six aforementioned structures, they were visualized, and the results were grouped into Figure 24. In the figure, the nanoassemblies with homogeneous spacings are denoted by (a), (b), and (c), and the nanoassemblies with heterogeneous spacings are denoted by (d), (e), and (f). Once again, the structures show a fairly rigid DNA duplex with much of the mobility in the structure occurring at the DNA-NP interface. The simulation also indicates the model's ability to self-assemble structures with multiple designed interparticle distances.

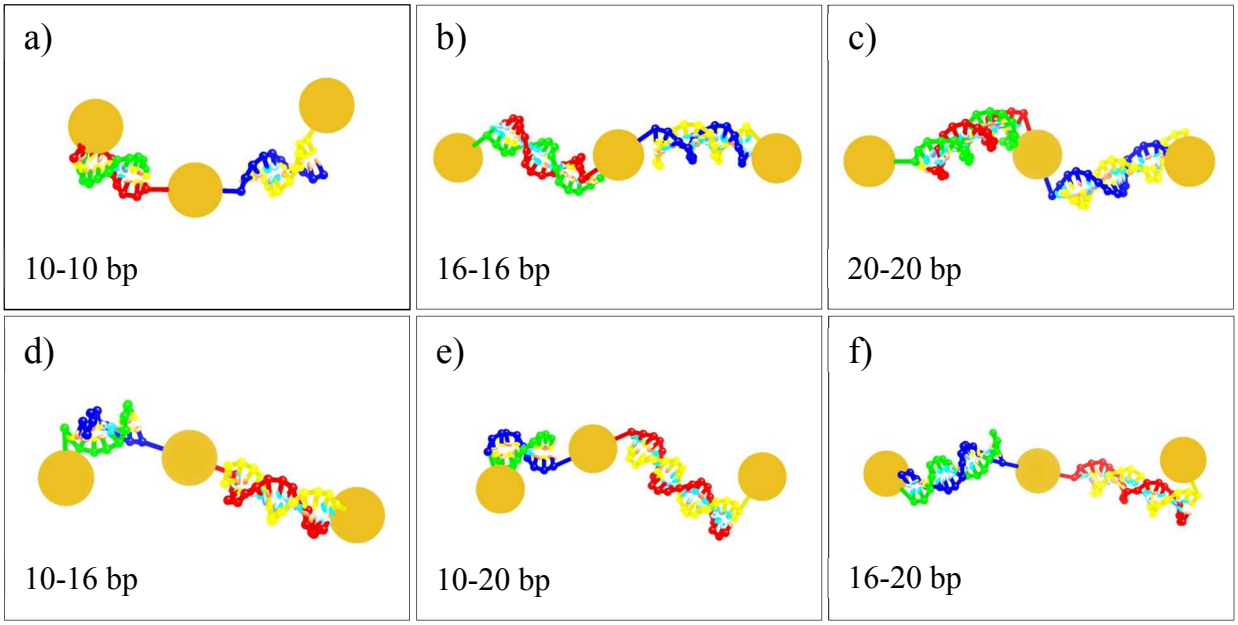

Figure 24. Homogeneous and heterogeneous combinations of interparticle spacing within linear self-assemblies. The top visualizations are the linear assemblies with homogeneous spacings (a-c), and the bottom visualizations are the linear assemblies with heterogeneous spacings (d-f).

To verify that the self-assembled structures include the correct interparticle distances, the distances were measured and summarized in the Table 8. The calculated interparticle distances for the linear assemblies were similar to the distances calculated in the previous diatomic assemblies for each corresponding number of base pairs. This suggests that the utilization of multiple interparticle distances can be controlled with this model as well.

Table 8. Interparticle distances within homogeneous and heterogeneous linear assemblies.

Homogeneous	10-10 Linear		16-16 Linear		20-20 Linear	
Interparticle Spacing (nm)	4.77 ± 1.23		6.09 ± 1.64		7.39 ± 1.47	
Heterogeneous	**10-16 Linear**		**10-20 Linear**		**16-20 Linear**	
	10 bp	16 bp	10 bp	20 bp	16 bp	20 bp
Interparticle Spacing (nm)	4.37 ± 1.46	6.25 ± 1.45	4.96 ± 1.29	7.57 ± 1.58	6.14 ± 1.45	7.64 ± 1.38

4.4.3 Simulating multiple diatomic structures simultaneously. The third experiment that was performed to show control of simulation design consisted of simulating the self-assembly of multiple structures simultaneously. In a laboratory setting, the manufacturing of nanoscale structures result in numerous structures within a single sample. The ability to simulate the self-assembly of a multitude of structures at once makes the model useful for simulating realistic systems. For this experiment, we used the simplest self-assembled structure, diatomic, as the focus. The experiment consisted of six different simulations, varying the number of possible structures up to six diatomics for 3 days each.

After the simulations were finished, the final positions of the building blocks were visualized for comparison (see Figure 25). Each simulation ran for a 3-day period and only four of the simulations self-assembled into all of the possible structures (Figure 25 a-d). Figures 25e and 25f had five and six possible structures, respectively, but one diatomic structure was unable to self-assemble.

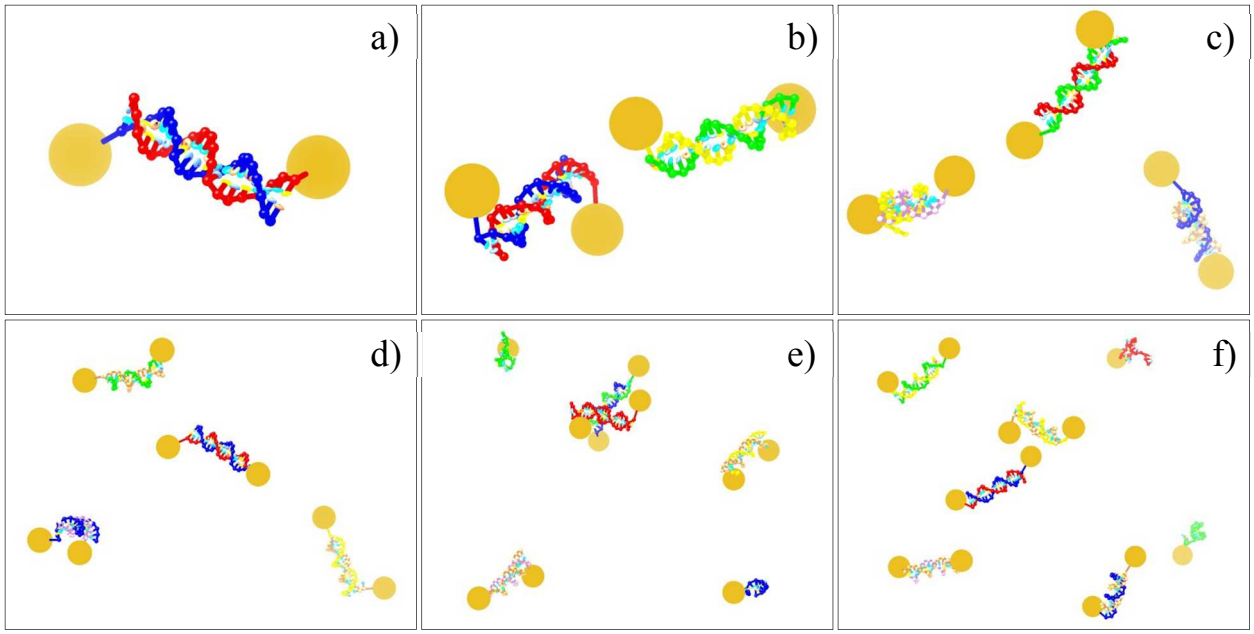

Figure 25. Diatomic self-assemblies simulated simultaneously. From (a) to (f), the number of diatomic structures simulated increases by one up to six structures. A-d) shows all the diatomic structures fully assembled. E-f) shows all but one structure full assembled.

Chapter 5: Validation & Generalization of the NP Building Block Model

To extend the validation of the NP building block model, simulating self-assembly should be applied to a broader selection of previously engineered nanostructures. In order to accomplish this objective, the model was used to simulate the self-assembly of building blocks into the homodimer and homotrimer structures developed by Loweth et al. (1999). After simulating their structures, we continued to examine the potential for possible 1D structures by simulating the self-assembly of nanoparticle building block chain aggregates with up to six building blocks. Next, we simulated self-assembly of the 2D polygonal structures fabricated by Aldaye and Sleiman (2006; Aldaye & Sleiman, 2007, "DNA-mediated"; Aldaye & Sleiman, 2007, "Dynamic"). Finally, we simulated the self-assembly of some additional 2D structures, which included the regular polygons consisting of up to six building blocks with either the bi-functional linear building block or the t-shaped building block. The table below shows the noncrosshybridizing sequences developed by Deaton et al. (2003) that were used to simulate the linear chain aggregates and regular polygons.

Table 9: Noncrosshybridizing library (Deaton et al., 2003) used to self-assemble NP building blocks into chains, regular polygons, and platonic solids. Only one sequence is shown from the complementary pairs.

#	Sequence
1	CTTTGGATTTATCTTCGACA
2	GATCCTATATCTTAATGCAC
3	AACGAACCTTCTAGAGTATG
4	GCACAATTAGGCACTAACCC
5	GGACCCTGTATAACATACAA
6	CATAAAAAGTTAATAAGTTA
7	ATCAGTTGTTGTTAAATTAC
8	ATTTTAAGACTATCTCTTAG
9	CATACTTTGTAAGTAATTAT
10	AGTAACTTCAACCATAGGCC
11	GTATTAATTTCCATCTAAAA
12	GGTCTCTGTACTTTCTGACT
13	AGGTTTAATTAGTCAAATAG
14	CTTCTCTATATAATATTTCA
14	AGACATAATTTTATATACTC

5.1 Simulating 1D Self-Assembly

The first step taken to generalize the coarse-grained model was to simulate the self-assembly of 1D structures previously fabricated by other researchers. The 1D structures chosen for this step in the validation process were the homodimers and homotrimer from Loweth et al.'s (1999) paper, "*DNA-Based Assembly of Gold Nanocrystals*.". Once the 1D structures from this work had been simulated and compared to the fabricated structures, the model was used to simulate 1D structures from dimer to hexamer, providing simple structures to be experimentally produce to verify the model's predictive ability for the creation of nanostructures.

5.1.1 DNA-based assembly of gold nanocrystals. For these simulations, we focused on four structures, which used only one size of nanoparticle. The researchers made three homodimers, which were each 18, 28, and 38 bp, and a homotrimer. The sequences used to make each of the four structures can be found in Table 10. The homodimers that were constructed are

similar to the diatomic structure constructed by Kim et al. (2011), but Loweth et al. (1999) varied the number of base pairs between each dimer and used 10-nm Au NPs. The homotrimer consisted of three 5-nm Au NPs where one of the particles was functionalized to a template strand. Both of the other two NPs were mono-functionalized to shorter ssDNA, which were complementary to a section of the third particle's template strand.

Table 10: Sequences used from Loweth et al. (1999) for the simulation of the self-assembly of homodimers and homotrimers.

Structure		Sequences (5' → 3')
Homodimer	**18-Basepair**	CAGTCAGGCAGTCAGTCA
	28-Basepair	ATGGCAACTATACGCGCTAGAGTCGTTT
	38-Basepair	ACGTCACGCTAGTCAGTCATCTTGCACTATGTCCTTGA
Homotrimer		GCGCTAGAGTCGTTT
		AAACGACTCTAGCGCTAAACGACTCTAGCGC

We began by simulating the self-assembly of the mono-functionalized building block into the three homodimer structures (see Figure 26). As shown, the structures exhibit a fairly rigid duplex between two Au NPs, and the NPs seem to be quite mobile about the DNA-NP attachment site, representing the flexible nature of the thiol modification on ssDNA.

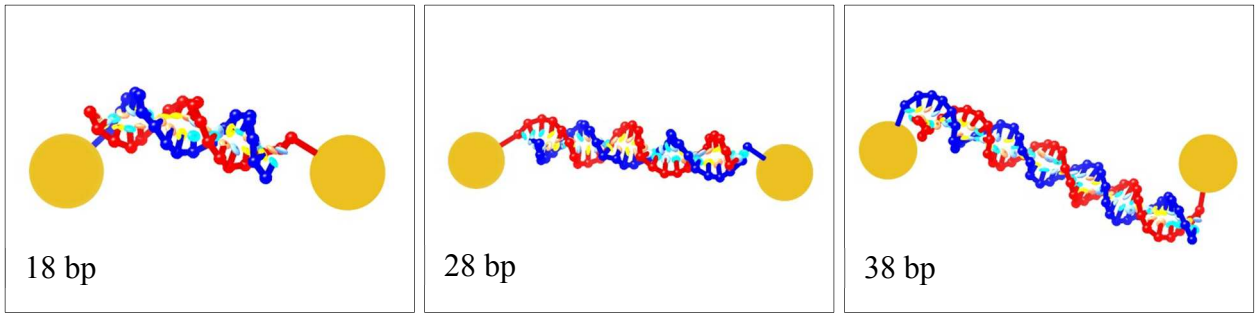

Figure 26. Simulated homodimer self-assemblies consisting of 18 bp (left), 28 bp (center), and 38 bp (right).

The lengths of the dsDNA were expected to be 6.12, 9.52, and 12.92 nm for the 18-, 28-, and 38-base pair sequences base on a rise per base of .34 nm of DNA (Loweth et al., 1999). From the simulations, the interparticle distances obtained from each of the three homodimer structures were calculated (see Table 11). The 18-bp homodimer interparticle distance was 6.20 ± 1.41 nm, the 28-bp homodimer interparticle distance was 8.94 ± 1.41 nm, and the 38-np homodimer interparticle distance was 10.84 ± 1.41 nm. Loweth et al. (1999) observed distances between the NP edges averaging 1.2 nm with distances ranging from 0-6 nm for the 18-bp homodimer, 1.5 nm with distances ranging from 0-6 nm for the 28-bp homodimer, and 5.8 nm with distances ranging from 0-15 nm for the 38-bp homodimer. In order to convert the interparticle distances calculated from the simulations, the diameter of the NP (2.83 nm) was subtracted from the interparticle distance, resulting in edge to edge calculations. The variation in values for the distances can be attributed to the flexibility of the thiol linker, possible minor bending of the dsDNA, and the difference in NP diameters. Loweth et al. (1999) noted that the process of depositing the structures onto the TEM grids may also affect the spacing. The distances in the table show that the model was able to produce distances between the NP edges with the range of observed distances.

Table 11. Interparticle distances of homodimers consisting of 18, 28, and 38 base pairs.

Structure		18-Base Pair	28-Base Pair	38-Base Pair
Interparticle Distance (nm)	Modeled	6.20 ± 1.41 nm	8.94 ± 1.73 nm	10.84 ± 1.70 nm
Distance Between NP Edges (nm)	Modeled	3.37 nm (0.35-6.04 nm observed)	6.11 nm (3.12-8.51 nm observed)	8.01 nm (3.58-11.27 nm observed)
Distance Between NP Edges (nm)	Fabricated	1.2 nm (0-6 nm observed)	1.5 nm (0-6 nm observed)	5.8 nm (0-15 nm observed)

Next, the model was used to simulate the self-assembly of the homotrimer structure. Up to this point in the simulations, a structure had not been self-assembled containing a template strand in which two other strands were intended to bind. Using the longer sequence for the homotrimer structure in Table 10 as the template strand and the other shorter sequence for the other two NPs, the model was successful in simulating the self-assembly of the homotrimer structure. The visualized results of the simulated homotrimer assembly are presented in Figure 27. In the figure, the simulated homotrimer is being compared to the schematic and TEM images that Loweth et al. (1999) had generated from their self-assembly of the structure. The major difference between the simulation and Loweth et al.'s structure is the difference in NP diameters. Loweth et al used NPs 5 nm in diameter and the simulations utilized a diameter of 2.83 nm.

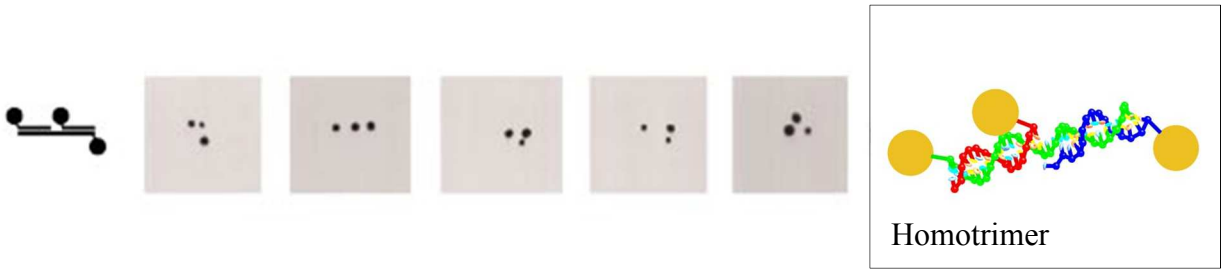

Figure 27. Comparison of simulated homotrimer self-assembly to the homotrimer schematic and TEM micrographs. Schematic and TEM images are of a 5-nm homotrimer, using strategy A from Figure 3. The simulation utilizes NPs with 2.83-nm diameters. Adapted with permission from "DNA-Based Assembly of Gold Nanocrystals," by C. J. Loweth, 1999, *Angewandte Chemie International Edition, 38,* p. 1810.

The interparticle distances were not reported for the homotrimer, but the distances calculated in the simulations averaged 5.64 ± 1.35 nm. The simulations showed mobility in spatial arrangement of the particles similar to what is shown in Figure 27, ranging from collinear to triangular orientations (Loweth et al., 1999).

5.1.2 NP building block chain aggregates. After simulating 1D structures that had previously been engineered in a laboratory setting, the model was used to generate simulations of 1D self-assemblies using the mono- and bi-functionalized linear configurations developed with the anisotropic mono-functionalization strategy (Kim et al., 2011). The intent of simulating these structures was to provide a series of 1D self-assembled structures that could be created in the laboratory that could be later compared to the simulations. The reason for this was to generate more data to reinforce the validity of the coarse-grained NP building block model.

There were five structures simulated for the 1D NP building block chain aggregates. Two of these structures were similar to the diatomic and linear structures originally constructed by Kim et al. (2011), but one of the duplexes in the trimer structure was different than the linear

structure. The other three structures consisted of a (a) tetramer, (b) pentamer, and (c) hexamer. structure consisted of the mono-functionalized linear building block configurations or a combination of the bi-functionalized linear building block and the mono-functionalized building block. The three pairs of strands used in the simulations were Sequences 1, 2, and 3 from the noncrosshybridizing library in Table 9 (Deaton et al., 2003). Each of the finished assemblies of the five 1D structures is shown in Figure 29.

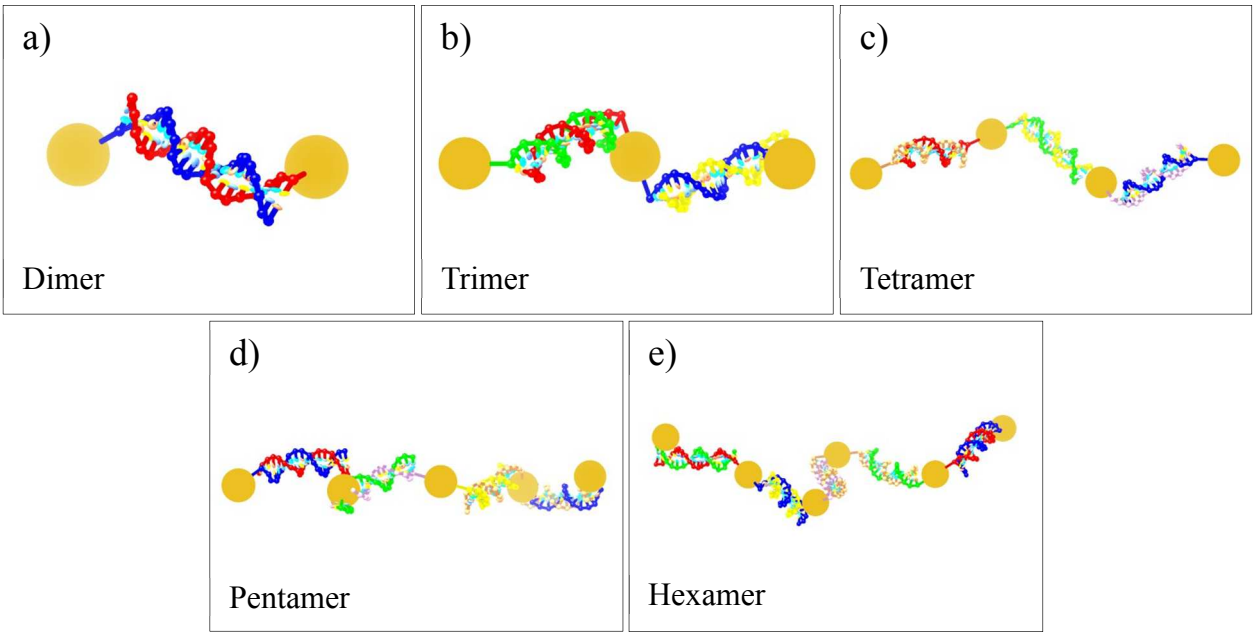

Figure 28. Visualizations of simulated 1D linear NP building block chain aggregates. The five structures are (a) dimer, (b) trimer, (c) tetramer, (d) pentamer, and (e) hexamer.

The simulations show flexibility in each of the structures. The interparticle distances between each pair of NPs in each of the structures is summarized in Table 12. Each structure shows similar interparticle distances between each NPs closest neighbors.

Table 12. Interparticle distances of the linear NP building block chain aggregates.

Structure	Dimer	Trimer	Tetramer	Pentamer	Hexamer
Interparticle Distance (nm)	7.43 ± 1.54 nm	7.39 ± 1.47 nm	7.69 ± 1.55 nm	7.16 ± 1.53 nm	7.71 ± 1.58 nm

5.2 Simulating 2D Self-Assembly

The next logical step after simulating 1D self-assembly was to move on to 2D self-assembly to further the validation process. After 1D self-assembly, moving on to 2D self-assembly was a reasonable direction for the validation process. Like the 1D self-assembly done in the previous section, the simulations done in this section followed the same format of validation using previous work and then moving on to simulating new structures using the building block configurations from the mono-functionalization strategy (Kim et al., 2011). In this section, the works of Aldaye and Sleiman (2006; Aldaye & Sleiman, 2007, "DNA-mediated"; Aldaye & Sleiman, 2007, "Dynamic") are used to validate the model. Due to the current state of the model, the self-assembly of the 2D nanostructures could not be simulated using the same building blocks Aldaye and Sleiman used. Therefore, the goal of these simulations was to simulate the self-assembly of similar structures produced by Aldaye and Sleiman (2006; Aldaye & Sleiman, 2007, "DNA-mediated"; Aldaye & Sleiman, 2007, "Dynamic"). The first structure simulated was the DNA hexagon constructed in the paper, "*Sequential Self-Assembly of a DNA Hexagon*." The second and third structures were the triangle and square created in the paper, "*DNA Mediated Patterning of Gold Nanoparticles*." After simulating these structures, the NP building block configurations were used to make a triangle, square, pentagon, and hexagon using two different NP building blocks for 2D self-assembly.

5.2.1 Sequential self-assembly of a DNA hexagon. The first 2D structure simulated was the DNA hexagon (Aldaye & Sleiman, 2006). The design of Aldaye and Sleiman's building blocks are different compared to the NP building blocks for the coarse-grained model. The sequences used for each building block to self-assemble the hexagon are summarized in Table 9. This hexagon design would utilize the bi-functionalized linear NP building blocks and simulated in sequence like the hexagon designed by Aldaye and Sleiman (Aldaye & Sleiman, 2006).

Table 13: Sequences used for the sequential self-assembly of NP building blocks into a hexagon (Aldaye & Sleiman, 2006).

NP Building Block		Sequences (5' → 3')
1	0	CGATCTTGTGGCATTAG
	1	CATTAGCTCGCAGGACG
2	2	CTAATGCCACAAGATCG
	3	CTGGTTCTCTCAAGTAG
3	4	GACACCTAGTGCACACG
	5	CTACTTGAGAGAACCAG
4	6	CGTGTGCACTAGGTGTC
	7	CTAACCGATACTCGTTG
5	8	CTCAGTTGTGACTTATG
	9	CAACGAGTATCGGTTAG
6	10	CATAAGTCACAACTGAG
	11	CGTCCTGCGAGCTAATG

The simulation of the DNA hexagon consisted of six different simulations, each representing a different point in the sequential assembly of the hexagon from the first building block to the final assembly. The visualized results of each simulation is summarized and compared to the schematic of Aldaye and Sleiman's sequential assembly of the DNA hexagon in Figure 29 (Aldaye & Sleiman, 2006). There is considerable flexibility in the overall structure in each simulation, but even without the use of an organic vertex (Aldaye & Sleiman, 2006), the model's building blocks are capable of self-assembling into the cyclic hexagonal structure.

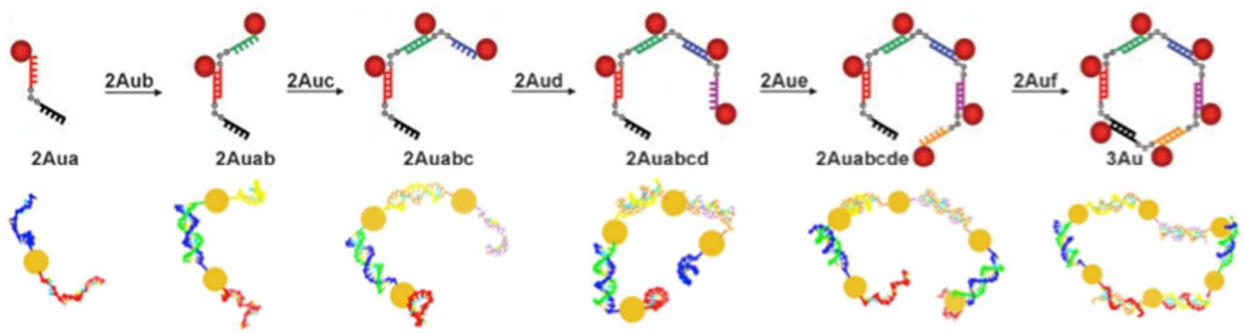

Figure 29. Comparison of the simulated structures to the schematic representing each step in the sequential self-assembly of the DNA hexagon. Both the red and gold spheres represent gold nanoparticles. The schematic uses building blocks mono-functionalized with an oligonucleotide connected to another nucleotide by a organic vertex. Due to the current constraints of the model, the simulations utilize the bi-functionalized linear building block to self-assemble the hexagon. Adapted with permission from "Sequential Self-Assembly of a DNA Hexagon as a Template for the Organization of Gold Nanoparticles," by F. A. Aldaye and H. F. Sleiman, 2006, *Angewandte Chemie International Edition, 45,* p. 2205.

Since the building blocks are capable of generating the cyclic structure needed to form the hexagon, it should be possible to simulate other 2D polygonal structures. Further, since the building blocks developed by the anisotropic mono-functionalization strategy have not been shown to self-assemble into polygonal structures, it would be a promising area of investigation for further validation of the model and added potential to the technique.

5.2.2 DNA mediated patterning of Au NPs. The next two structures to help in 2D validation of the model were the triangle and square constructed by Aldaye and Sleiman (2007, "DNA-mediated"; 2007, "Dynamic"). A similar issue was encountered with the self-assembly of the triangle and square as occurred with the DNA hexagon. Currently, the model does not have the ability to simulate the cyclic template strand used to construct the triangular and square structures (Aldaye & Sleiman, 2007, "DNA-mediated"; Aldaye & Sleiman, 2007, "Dynamic").

Instead, the bi-functionalized linear NP building blocks were used to generate the triangle and square (Kim et al., 2011).

The sequences used for each building block are taken from the noncrosshybridizing library in Table 7 (Deaton et al., 2003). Table 14 shows the sequences used for each structure and to which NP building block the sequence was attached. This resulted in the edges of each structure consisting of 20 base pairs, making it smaller than the structures engineered by Aldaye and Sleiman (Aldaye & Sleiman, 2007, "DNA-mediated"; Aldaye & Sleiman, 2007, "Dynamic").

Table 14: Sequences used for the self-assembly of bi-functionalized linear NP building blocks into triangles and squares (Deaton et al., 2003).

Structure	NP Building Block	#	Sequences (5' → 3')
Triangle	**1**	0	AACGAACCTTCTAGAGTATG
		1	AACGAACCTTCTAGAGTATG
	2	2	CATACTCTAGAAGGTTCGTT
		3	GATCCTATATCTTAATGCAC
	3	4	CATACTCTAGAAGGTTCGTT
		5	GTGCATTAAGATATAGGATC
Square	**1**	0	AACGAACCTTCTAGAGTATG
		1	GATCCTATATCTTAATGCAC
	2	2	AACGAACCTTCTAGAGTATG
		3	GTGCATTAAGATATAGGATC
	3	4	CATACTCTAGAAGGTTCGTT
		5	CCTTGGATTTATCTTCGACA
	4	6	CATACTCTAGAAGGTTCGTT
		7	TGTCGAAGATAAATCCAAGG

The final simulated self-assembled structures can be found in Figure 30. The figure shows the comparison of the schematics and TEM images of the triangles and squares developed by Aldaye and Sleiman's technique (Aldaye & Sleiman, 2007, "DNA-mediated"; Aldaye & Sleiman, 2007, "Dynamic") to the finished simulations for the triangle and square self-assembled

from bi-functionalized NP building blocks. There is a high amount of mobility shown at each vertex where the NP resides, which is due to the flexibility of the thiol linker in the model.

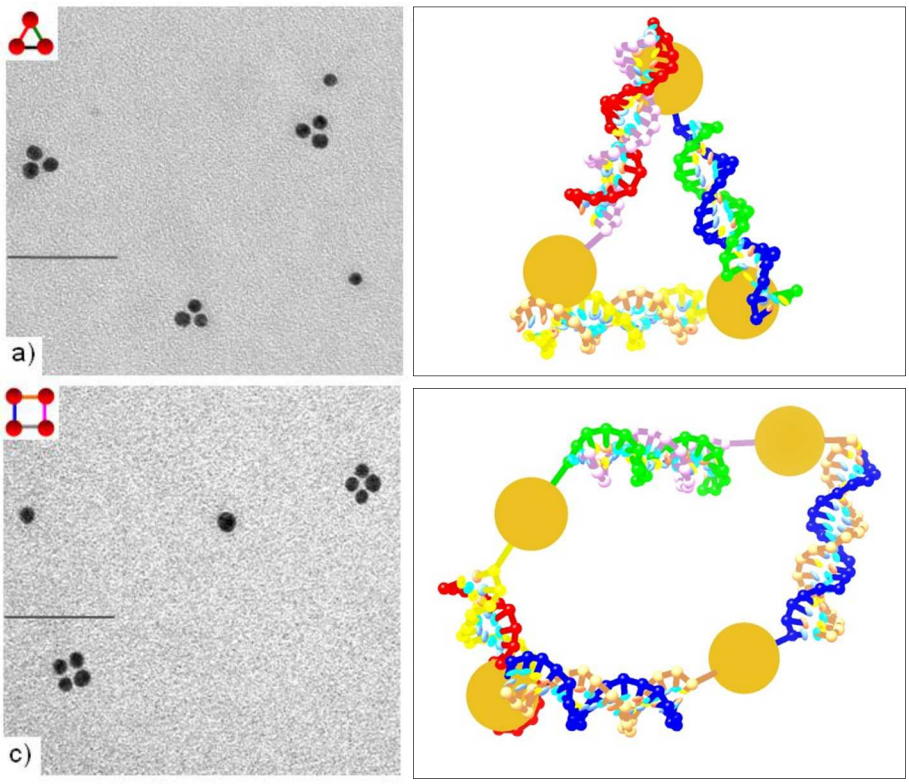

Figure 30. Comparison of simulated structures to schematic and TEM images of triangles (a) and squares (b). The schematic and TEM images are of the structures assembled using a cyclic DNA template. Due to the constraints of the model, the simulations utilize the bi-functionalized linear building block to generate the triangle and square. Adapted with permission from "Sequential Self-Assembly of a DNA Hexagon as a Template for the Organization of Gold Nanoparticles," by F. A. Aldaye and H. F. Sleiman, 2006, *Angewandte Chemie International. Edition, 45,* p. 2205.

The interior angles, interparticle distances, and circumradii of the two simulated structures are summarized in Table 15. The interparticle distances of connected NPs are similar to the other calculations for the duplexes consisting of 20 base pairs, 6.82 ± 1.46 nm for the triangle and 7.23 ± 1.30 nm for the square. The model has the ability to find the distances

between NPs across from each other in a square, so this was used to find the circumradius. Since the interparticle distance of NPs across duplexes could be considered as the edges of the square and those edges averaged 7.23 nm, the circumradius of the self-assembled square would be expected to be about 5.11 nm. Instead, the average circumradius of the square was found to be 4.27 nm. This means that from a 2D view, the square fills in a smaller than expected circle, leading to smaller interior angles. This suggests that the simulated self-assembled square's structure is more of a dynamic, puckered 3D structure than a flat 2D square. This was confirmed by the average interior angles of the square being 75.71 ± 32.59 degrees.

Table 15. Interparticle distances, circumradii, and interior angles of the triangle and square self-assembled with bi-functionalized linear NP building blocks.

Structure	Triangle	Square
Interparticle Distance (nm)	6.82 ± 1.46 nm	7.23 ± 1.30 nm
Circumradius (nm)	-	4.27 ± 1.35 nm
Interior Angles (^{0})	-	75.71 ± 32.59

5.2.3 NP building block regular polygons. After simulating the structures similar to the triangles, squares, and hexagons that were constructed by Aldaye and Sleiman (2006; Aldaye & Sleiman, 2007, "DNA-mediated"; Aldaye & Sleiman, 2007, "Dynamic"), the NP building block configurations were used to simulate the regular polygons: triangle, square, pentagon, and hexagon. These four structures were self-assembled using either the 1D bi-functionalized linear building block or the 2D T-shaped building block (Kim et al., 2011). These configurations were used because each configuration utilizes a different angle from the relative orientation of the strands attached to the surface of the Au NP: the linear building block has DNA strands 180 degrees apart and the t-shaped building block has a strand that is 90 degrees away from the other

two strands. These simulations would provide insight to the angles that could be achieved with the different building blocks and the behavior of these 2D polygonal structures.

The structures were self-assembled using Sequences 1, 2, 3, and 4 from the noncrosshybridizing library in Table 9 (Deaton et al., 2003) and summarized for each structure in Table 16 below. In the structures self-assembled with the linear building block, all of the strands were intended to hybridize with a complementary sequence. In the structures self-assembled with the t-shaped building block, the second strand for each building block was a sequence that did not have an intended target. The triangle and square constructed with the linear building block were the same structures simulated for comparison to Aldaye and Sleiman's triangle and square (Aldaye & Sleiman, 2007, "DNA-mediated"; Aldaye & Sleiman, 2007, "Dynamic").

Table 16. Summarization of DNA sequences used for the self-assembly of 2D polygonal structures with either the bi-functionalized linear or t-shaped building blocks (Deaton et al., 2003).

Structure	Linear Building Block	#	Sequence (5' → 3')	T-Shaped Building Block	#	Sequence (5' → 3')
Triangle	1	0	AACGAACCTTCTAGAGTATG	1	0	AACGAACCTTCTAGAGTATG
		1	AACGAACCTTCTAGAGTATG		1	CTTTGGATTTATCTTCGACA
	2	2	CATACTCTAGAAGGTTCGTT		2	AACGAACCTTCTAGAGTATG
		3	GATCCTATATCTTAATGCAC	2	3	GATCCTATATCTTAATGCAC
	3	4	CATACTCTAGAAGGTTCGTT		4	CTTTGGATTTATCTTCGACA
		5	GTGCATTAAGATATAGGATC		5	CATACTCTAGAAGGTTCGTT
				3	6	CATACTCTAGAAGGTTCGTT
					7	CTTTGGATTTATCTTCGACA
					8	GTGCATTAAGATATAGGATC
Square	1	0	AACGAACCTTCTAGAGTATG	1	0	AACGAACCTTCTAGAGTATG
		1	GATCCTATATCTTAATGCAC		1	ACTAGACCAAGAAATTTAGA
	2	2	AACGAACCTTCTAGAGTATG		2	GATCCTATATCTTAATGCAC
		3	GTGCATTAAGATATAGGATC	2	3	AACGAACCTTCTAGAGTATG
	3	4	CATACTCTAGAAGGTTCGTT		4	ACTAGACCAAGAAATTTAGA
		5	CTTTGGATTTATCTTCGACA		5	GTGCATTAAGATATAGGATC
	4	6	CATACTCTAGAAGGTTCGTT	3	6	CATACTCTAGAAGGTTCGTT
		7	TGTCGAAGATAAATCCAAAG		7	ACTAGACCAAGAAATTTAGA
					8	CTTTGGATTTATCTTCGACA
				4	9	CATACTCTAGAAGGTTCGTT

					10	ACTAGACCAAGAAATTTAGA
					11	TGTCGAAGATAAATCCAAAG
Pentagon	1	0	AACGAACCTTCTAGAGTATG	1	0	AACGAACCTTCTAGAGTATG
		1	AACGAACCTTCTAGAGTATG		1	ACTAGACCAAGAAATTTAGA
	2	2	CATACTCTAGAAGGTTCGTT		2	AACGAACCTTCTAGAGTATG
		3	GATCCTATATCTTAATGCAC	2	3	CATACTCTAGAAGGTTCGTT
	3	4	CATACTCTAGAAGGTTCGTT		4	ACTAGACCAAGAAATTTAGA
		5	GATCCTATATCTTAATGCAC		5	GATCCTATATCTTAATGCAC
	4	6	CTTTGGATTTATCTTCGACA	3	6	CATACTCTAGAAGGTTCGTT
		7	GTGCATTAAGATATAGGATC		7	ACTAGACCAAGAAATTTAGA
	5	8	GTGCATTAAGATATAGGATC		8	GATCCTATATCTTAATGCAC
		9	TGTCGAAGATAAATCCAAAG	4	9	CTTTGGATTTATCTTCGACA
					10	ACTAGACCAAGAAATTTAGA
					11	GTGCATTAAGATATAGGATC
				5	12	GTGCATTAAGATATAGGATC
					13	ACTAGACCAAGAAATTTAGA
					14	TGTCGAAGATAAATCCAAAG
Hexagon	1	0	AACGAACCTTCTAGAGTATG	1	0	AACGAACCTTCTAGAGTATG
		1	GATCCTATATCTTAATGCAC		1	ACTAGACCAAGAAATTTAGA
	2	2	GTGCATTAAGATATAGGATC		2	GATCCTATATCTTAATGCAC
		3	GTGCATTAAGATATAGGATC	2	3	GTGCATTAAGATATAGGATC
	3	4	GATCCTATATCTTAATGCAC		4	ACTAGACCAAGAAATTTAGA
		5	AACGAACCTTCTAGAGTATG		5	GTGCATTAAGATATAGGATC
	4	6	CATACTCTAGAAGGTTCGTT	3	6	GATCCTATATCTTAATGCAC
		7	CTTTGGATTTATCTTCGACA		7	ACTAGACCAAGAAATTTAGA
	5	8	TGTCGAAGATAATCCAAAG		8	AACGAACCTTCTAGAGTATG
		9	TGTCGAAGATAATCCAAAG	4	9	CATACTCTAGAAAGGTTCGTT
	6	10	CCTTGGATTTATCTTCGACA		10	ACTAGACCAAGAAATTTAGA
		11	CATACTCTAGAAGGTTCGTT		11	CTTTGGATTTATCTTCGACA
				5	12	TGTCGAAGATAAATCCAAAG
					13	ACTAGACCAAGAAATTTAGA
					14	TGTCGAAGATAAATCCAAAG
				6	15	CTTTGGATTTATCTTCGACA
					16	ACTAGACCAAGAAATTTAGA
					17	CATACTCTAGAAGGTTCGTT

After preparing the simulations, they simulated for a 3-day period until the structures finished. Then, the simulations were visualized to show the desired self-assembled polygonal structures (see Figure 31). All of the intended 2D polygonal structures were successfully self-assembled in the simulations. The simulations also showed high mobility over the course of the simulations. Both of the triangular structures (Figure 31a-b) displayed planar orientations for the Au NPs with most of the movement coming from the mobility of the DNA attachment sites. The

squares (Figure 31c-d) exhibited some puckering, making the bond angles seem smaller than the intended 90 degrees associated with the square. The simulated pentagons and hexagons (Figure 31e-i) also showed some puckering, resulting in more 3D conformations. The movement of the NPs within the polygonal structures resembled the movement associated with cycloalkane conformations. Therefore, the self-assembled polygonal structures take on fluctuating 3D conformations.

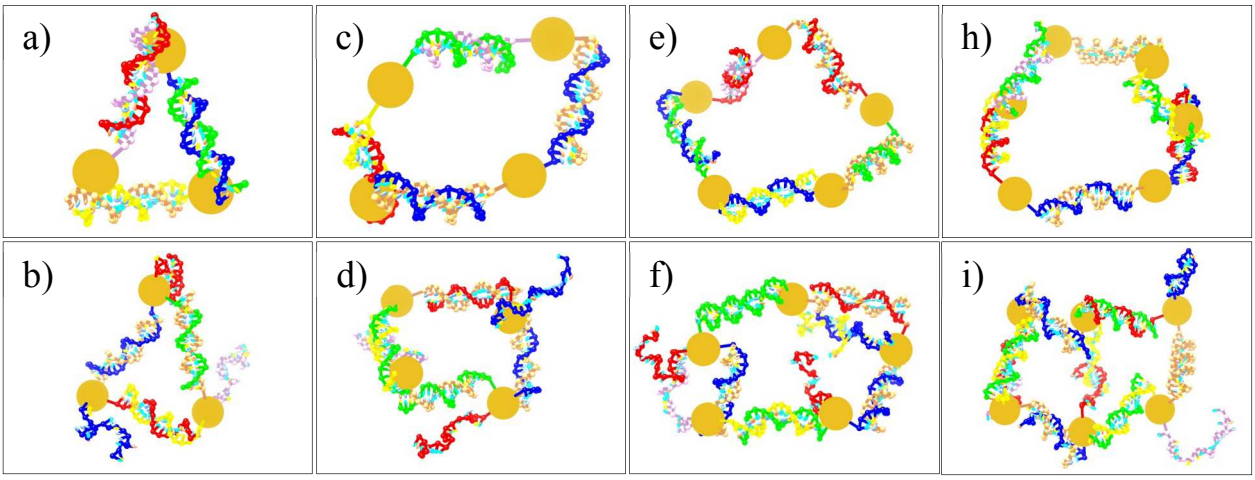

Figure 31. Visualizations of simulated self-assembled 2D regular polygonal structures. A-B) show triangles self-assembled using linear and t-shaped NP building block configurations, respectively. C-D) show squares self-assembled using linear and t-shaped NP building block configurations, respectively. E-F) show pentagons self-assembled using linear and t-shaped NP building block configurations, respectively. H-I) show hexagons self-assembled using linear and t-shaped NP building block configurations, respectively.

To examine the structural information for each simulated structure, the interparticle distances, circumradii, and interior angles of each were measured and the data summarized in Table 17. Like the results from the NP building block chain aggregates, the interparticle distances of each connected NP within the polygonal structures were all similar because each of

the duplexes consisted of 20 base pairs. It was possible to determine the circumradii for the squares and hexagons because the model calculates the interparticle distance between all pairs of NPs within the simulation. Since the simulated self-assembled square with the t-shaped building blocks had sides of 7.37 ± 1.62 nm, we would expect the circumradius to be about 5.21 nm. Instead, the measured circumradius is 4.60 ± 1.43 nm, which is less than the expected circumradius. There is also less of a reduction from the expected circumradius than what occurred with the square self-assembled from the bi-functionalized linear building blocks, indicating that the square assembled from the t-shaped building blocks could have a flatter conformation. This could be the result of the steric effects of adding a third DNA strand to the building block and the 90-degree relative orientation of the target strands on the NP versus the 180-degree orientation utilized with the bi-functionalized building block. The average interior angle was also affected, increasing to 82.21 ± 34.50 degrees from 74.71 ± 32.59 degrees with the addition of the third strand.

The hexagons displayed similar behavior to the squares. The hexagon self-assembled with the bi-functionalized building block exhibited an interparticle distance of 7.35 ± 1.62 nm, which would result in an expected circumradius of 7.35 nm. The circumradius calculated from the simulations were found to be 5.04 ± 1.48 nm. The hexagon self-assembled with the t-shaped building blocks displayed an interparticle distance of 7.61 ± 1.40 nm with an expected circumradius of 7.61, but it also had a smaller value of 5.28 ± 1.39 nm. The reduction in circumradius is only slightly more for the hexagon self-assembled from the bi-functionalized building block. This is reflected in the measurements for the interior angles: 88.87 ± 1.46 degrees for the hexagon self-assembled with the bi-functionalized building block and 89.16 ± 34.59 degrees for the hexagon self-assembled with the t-shaped building block.

Table 17. Summarization of the interparticle distances, circumradius and interior angles of the 2D polygonal structures self-assembled with either bi-functionalized linear or t-shaped building blocks.

NP Building Block Structure	Triangle Linear	Square Linear	Pentagon Linear	Hexagon Linear
Interparticle Distance (nm)	6.82. ± 1.46 nm	7.23 ± 1.30 nm	7.32 ± 1.43 nm	7.35 ± 1.62 nm
Circumradius (nm)	-	4.27 ± 1.35 nm	-	5.04 ± 1.48 nm
Interior Angles (^{0})		75.71 ± 32.59	88.64 ± 38.76	88.87 ± 1.46
NP Building Block Structure	**Triangle T-Shaped**	**Square T-Shaped**	**Pentagon T-Shaped**	**Hexagon T-Shaped**
Interparticle Distance (nm)	7.61 ± 1.73 nm	7.37 ± 1.62 nm	7.68 ± 1.47 nm	7.61 ± 1.40 nm
Circumradius (nm)	-	4.60 ± 1.43 nm	-	5.28 ± 1.39 nm
Interior Angles (^{0})		82.21 ± 34.50	83.32 ± 30.68	89.16 ± 34.59

The model has been further validated through the simulation of structures previously engineered by Loweth et al. (1999) and Aldaye and Sleiman (2006; Aldaye & Sleiman, 2007, "DNA-mediated"; Aldaye & Sleiman, 2007, "Dynamic"). There have also been numerous simulations of structures, which have not been constructed experimentally. These simulations for the 1D chain aggregates and 2D polygonal structures provide modeled nanostructures to be fabricated in the lab for further validation of the model. which could lead to further improvements in the coarse-grained model for the self-assembly of NP building blocks into nanostructures.

The results for the simulated self-assembly of the structures developed by Loweth et al. (1999), the 1D chain aggregates and 2D polygonal structures were successful. Utilizing the 20-base sequences developed by Deaton et al. (2003), the chain aggregates and polygonal structures exhibited interparticle distances similar to the other simulations with 20-bp duplexes. The data obtained indicates that the NPs within the nanostructures have high mobility. The polygonal

structures, except for the triangles, do not take on a planar 2D structure, but rather 3D conformations that change over time. This information could be lost when attempting to characterize self-assembled structures using a TEM. Therefore, the model acts as a complementary tool for the analysis of the structure and behavior of self-assembled structures and an efficient way to test a multitude of structures in a relatively short amount of time.

Chapter 6: Conclusions, Discussions, & Future Work

This thesis concerned the validation and generalization of a coarse-grained model designed to self-assemble Au NPs decorated with DNA strands in specific orientations into discrete nanoassemblies. The coarse-grained DNA model, developed by Ouldridge (2011) and later improved by Snodin et al. (2015), was extended to simulate DNA nanoassemblies with attached Au NPs (Armistead et al., 2015) based on the nanostructures produced experimentally using the sequential mono-functionalization strategy of ssDNA to the surface of Au NPs by Kim et al. (2011). The coarse-grained model for Au NP building blocks utilizes the properties of DNA to drive the self-assembly of the building blocks into a desired structure. The simulated self-assembly of the nanostructures produced by Kim et al. (2011), Loweth et al. (1999), and Aldaye and Sleiman (2006; Aldaye & Sleiman, 2007, "DNA-mediated"; Aldaye & Sleiman, 2007, "Dynamic") was used to aid in the preliminary validation in of the building block model. Also, the model was utilized to generate simulated self-assemblies of 1D and 2D structures using various building blocks to show further potential of the coarse-grained model. Below the key findings are summarized and the implications discussed.

6.1 Summary and Discussion

6.1.1 Stability of Au NPs for NP building block model. In Chapter 3, it was verified that the DMAP-MESA-Au NPs were stable in the presence of 0.1 M NaCl, which is the lowest available concentration offered by the model. Once it was verified that the Au NPs were stable in a salt concentration available in the model, validation of the model could begin. This salt concentration was chosen due to the tendency of increasing salt concentrations to destabilize the

NPs and cause uncontrolled aggregation. To extend this experiment, it would be beneficial to determine the salt concentration that causes aggregation.

6.1.2 Validation of DNA-linked NP building blocks. Chapter 4 involved the initial implementation of a coarse-grained model for the self-assembly of Au NP building blocks. The model was validated through the simulation of the nanostructures self-assembled using the sequential anisotropic mono-functionalization strategy (Kim et al., 2011). The technique was used to engineer six building block configurations: (a) mono-functionalized linear, (b) bi-functionalized linear, (c) t-shaped, (d) square planar, (e) square pyramidal, and (f) octahedral (see Figure 6; Kim et al., 2011). Each building block was termed based on the orientation of the attached ssDNA.

Before the simulation of the self-assembly of the DNA-linked NP building block structures, each configuration was simulated and visualized to verify the successful creation of each configuration in the model. Next, two mono-functionalized NP building blocks were used to test for self-assembly in the presence of complementary strands and test for lack of self-assembly in the presence of non-complementary strands. Then, a more complicated system was used to test for complementary self-assembly, utilizing bi-functionalized NP building blocks consisting of one complementary strand and one non-complementary strand each. These series of simulations were successful in showing that the model favored complementary self-assembly over non-complementary self-assembly in the construction of a nanostructure.

Next, a series of simulations were done to examine the T_m of a diatomic structure, showing a slight right shift in the T_m when compared to the T_m of free duplex DNA, but a range of melting temperature values of 20 K., correlating with what had been seen experimentally with respect to a right shift in the presence of DNA-NP aggregates but in contradistinction to the

narrowing of the temperature range (Jin et al., 2003; Lee & Schatz, 2009). The difference could be attributed to, at least in part, to the presence of only one DNA strand per Au NP in the simulation. Additionally, it might also be partially due to the need to adjust the thermodynamic parameters of the model. Therefore, this represents an avenue for future investigations. For example, replicate the simulation as a laboratory experiment to produce a melting curve for the self-assembled diatomic structure.

Once these initial experiments had been completed, the validation of the model through the self-assembly of the different Au NP building block configurations with a mono-functionalized Au NPs began. These simulations were successful in showing the self-assembly of the building blocks into the structures developed by Kim et al. (2011). The major differences found were smaller averages and less variation in the interparticle spacing and there were discrepancies in the average angles with more variation occurring in the simulations. This could be attributed to the calculations from the simulations being compared to the measured interparticle distances of the structure from a TEM image. The differences in the variation of interparticle spacing could be occurring due to the Au NPs having more mobility in the experimental structures, creating the increased variation in values. It could be possible to either change the parameter for the Au NP's effective charge or to increase the available movement at either side of the thiol linker. . The discrepancies in the angles could have occurred due to how the angles are calculated in the model compared to the how they are measured in the 2D TEM image. The model calculations of the angles are made through finding the shortest angle occurring among three NPs, restricting the measured angles to 180 degrees or less, whereas in the TEM image all of the angles would be measured either clockwise or counterclockwise to generate each angle. The results indicate that further investigation is needed into the interparticle

spacing and angles produced by the structures. One possible direction would be to use UV/Vis spectrophotometry to measure the spectra of each structure in a 0.1 mM NaCl solution and, then, compare the spectra to modeled spectra based on the information gathered from the relative positions of the Au NPs in the simulations. This could provide a better way to validate the model because the systems would be the same for the nanostructures.

After simulation of the structures developed by Kim et al. (2011), a series of simulations were conducted to examine the effect of changing the box size (changing the concentration of the building blocks) would have on the formation of a finished structure. This creates a realistic view of the simulation environment because in an experimental setting, changing the concentration can have an effect on the results. This process also provided a way to optimize the concentration when simulating a structure on a CPU to achieve self-assembly in a more reasonable timeframe. The results showed that decreasing the box size resulted in more duplexes forming within the 3-day period for a given structure. Also, the number of list updates that occurred was shown to be approximated with a power curve for a given structure within the 3-day period, decreasing as the number or particles in the simulation increased and as the concentration increased.

After investigating on the effect that varying concentration had on simulating self-assembly, the control over the design of nanostructures in the model was examined. This included varying the interparticle distance within the diatomic structure, utilizing combinations of interparticle spacing within a linear structure, and simulating multiple diatomic structures simultaneously. Controlling interparticle distance is crucial for the design of specific nanoassemblies for any given application because it effects the properties of the nanostructure, which influences its function (Kim & Deaton, 2013). Three interparticle distances were simulated based on varying the number of base pairs in the intended DNA duplex, resulting in

three simulated diatomic structures with 10, 16, and 20 base pairs with clearly distinct interparticle distances. This displayed the model's ability to simulate self-assembly of varying lengths of DNA sequences.

More complex structures will potentially need to utilize multiple interparticle distances to realize multiple functions simultaneously in a single structure. As an example of utilizing multiple spacings between Au NPs within a nanoassembly, the model was used to simulate the linear nanostructure with different combinations of the interparticle distances previously simulated with the diatomic nanostructure. Consequently, six different simulations were performed resulting in three structures of homogeneous distances with either 10, 16, or 20 bp and three structures of heterogeneous distances with 10 bp paired with either 16 or 20 bp and 16 bp paired with 20 bp. These structures all had distances similar to what was measured in the diatomic simulations, showing consistency in interparticle spacing with varying lengths of oligonucleotides and resulting in distinct interparticle distances measured across each duplex.

The simulations previously mentioned in the report consisted of systems where only one structure was self-assembled. Experimentally, producing a desired structure would result in numerous nanoassemblies within the sample. Therefore, simulating a single structure in a simulated environment is not realistic. Simulating multiple diatomic structures simultaneously would be more realistic and provide more insight into the self-assembly process among building blocks. The model was used to conduct a series of simulations varying the number of diatomic structures from one to six in a single system within a 3-day period. The visualizations of these simulations indicated the model's ability to simulate more than one structure within a simulation. However, the larger system caused a lower number of list updates within the timeframe. Therefore, the increasing computational complexity due to the larger number of particles in the

simulation resulted in one structure not being assembled in both the five-diatomic and six-diatomic systems. Potentially, the coarse-grained model could be utilized to simulate the self-assembly of much larger systems, including either multiple of the same nanostructures or larger nanoassemblies. Additionally, due to the highly parallel structure of a graphics processing unit (GPU), it could be beneficial to develop a GPU adaptation for the model to simulate these larger and more complicated systems since GPU's are more efficient at processing large blocks of visual data (Teo, Perilla, Shahoei, McGreevy, & Harrison, 2014).

The coarse-grained model for the self-assembly of NP building blocks has been effective in simulating the self-assembly of the DNA-linked NP building block nanostructures developed by Kim et al. (2011). Also, the model showed the ability to aid in the purposeful design of nanostructures by exhibiting varying interparticle distances within structures and simulating multiple structures simultaneously. Even though some progress was made utilizing the coarse-grained model for the self-assembly of NP building blocks, an investigation should be made into utilizing the modeling of plasmonic spectra of the simulated nanoassemblies to help improve the model's results, since it would be possible to compare the modeled spectra to an experimental sample of the same conditions (Nordlander, Oubre, Prodan, Li, & Stockman, 2004). Also, the simulated diatomic and linear nanostructures with the varying interparticle distances should be fabricated and characterized to verify the model's results.

6.1.3 Validation and generalization of the NP building block model. In Chapter 5, the model was used to simulate 1 and 2D structures to further validate the model and provide new structures to be manufactured for comparison. The chapter began with simulations of three homodimer structures of varying DNA lengths and a homotrimer structure that was previously produced by Loweth et al (1999). The model successfully simulated the self-assembly of the

homodimer structures. However, the simulations used the 2.83-nm Au NP diameter instead of the 10-nm Au NP diameter used in the experimental samples. The model was able to measure the interparticle distances generated in each of the homodimer nanostructures, but the experimental measurements were of the distance from one NP edge to the closest edge of its pair. For better comparison of the distances, the calculations made with the model were adjusted to measure the distance from one NP edge to the other by subtracting the radius of each NP. Although the average distance between simulated NP edges was greater than the average distances observed from NP edge to NP edge, the range of simulated edge to edge distances were similar to the range of observed edge to edge distances, especially for the 18-bp homodimer. However, Loweth et al. (1999) noted that deposition of the nanostructures on the TEM grid could influence the observed distances, which could contribute to the differences between the simulated distance to the observed distances. Another factor that should be considered is the largest observed edge to edge distance of the 38-bp homodimer being longer than the theoretical largest edge to edge distance of 12.92 nm based on the length of the DNA duplex. A final consideration is the difference in the size of the NPs simulated compared to the size of the NPs used in the study, as well as the variability in sizes of the NPs about the average size, which could affect the measurements of the distances.

The model was also able to simulate the self-assembly of homotrimer produced by Loweth et al. (1999) using a template strand mono-functionalized to a Au NP with two complementary regions for two mono-functionalized linear building blocks to hybridize. Once again, this simulation used a Au NP diameter of 2.83 nm, whereas the NPs in the study were 5 nm in diameter (Loweth et al., 1999). The model also showed similar conformations as what was shown in the TEM images. The researchers did not report interparticle distances of the

homotrimer, but the model was used to calculate interparticle distances of 5.64 ± 1.35 nm. Even though successful simulation of self-assembly occurred of the structural design, it would still be interesting to simulate the self-assembly of the structure with the 5-nm Au NPs reported in the study. This would also allow simulations of heterotrimeric structures seen in the paper (Loweth et al., 1999).

The next series of simulations consisted of using the Au NP building blocks to simulate nanoparticle chain aggregates ranging from dimer to hexamer, using a DNA duplex length of 20 bp. The purpose for simulating these linear structures was to provide structures that could be self-assembled experimentally and compared to the model results. These structures showed high mobility of the NPs throughout the nanostructure during the simulations and generated similar interparticle distances seen in previous simulations across the 20-bp DNA duplex. This shows a consistency of the model to produce similar interparticle distance given a particular length of oligonucleotide.

After simulating the 1D structures, the model was used to simulate similar 2D structures produced by Aldaye and Sleiman (2006; 2007). These researchers were able to develop their own unique building blocks to self-assembled hexagons (Aldaye & Sleiman, 2006), triangles, and squares (Aldaye & Sleiman, 2007). Their hexagons used Au NPs mono-functionalized to ssDNA, which was connected to a second DNA arm by an organic vertex as its building blocks, which were self-assembled sequentially (Aldaye & Sleiman, 2006). The triangles and square were self-assembled utilizing ssDNA mono-functionalized Au NPs that had complementary sequences to the regions of premade cyclic ssDNA templates (Aldaye & Sleiman, 2007). Presently, the model does not have the capability to replicate the self-assembly of these structures in the same way Aldaye and Sleiman had demonstrated because the model does not

utilize the same building blocks. Instead, the bi-functionalized linear NP building blocks were used to simulate the construction of the 2D polygonal structures. The bi-functionalized linear NP building blocks were able to be simulated into the self-assembled polygonal structures. After using the model to calculate the interparticle distances and angles of the nanoassemblies, except for the triangle, they were found to have more 3D conformations. This demonstrates that the model is able to provide additional structural information about a resulting nanoassembly in comparison to a 2D TEM image. Furthermore, it would be interesting to self-assemble the hexagon, triangle, and square based on the design of the NP building blocks used in these simulations.

The final study of simulations involved the comparison of the self-assembly of triangles, squares, pentagons, and hexagons, using either the bi-functionalized linear building block or the t-shaped building block from Kim et al. (2011). The purpose of these simulations was to examine the effects of using different building blocks to self-assemble the same structural design. It is important to note that the bi-functionalized linear building block utilizes a 180-degree angle between DNA strands, whereas the t-shaped building block utilizes a 90-degree angle between DNA strands (Kim et al., 2011). This was to examine whether there were any angle restrictions that would keep the building blocks from self-assembling into the correct structure. For example, the square nanoassembly was designed to have edges of equal DNA lengths with angles of 90 degrees between NPs. Therefore, the DNA strands on the bi-functionalized linear building block would have to self-assemble into the required 90 degrees from the 180-degree angle preferred by steric hindrance (Kim et al. 2011). The model was able to simulate the self-assembly of all the structures successfully. The visualizations showed that the structures display more of a 3D conformation compared to the expected 2D shape, except for the triangular assembly. This was

verified by the calculated average angles and the variance among the NPs for the square, pentagon, and hexagon being less than the theoretical interior angles of each regular polygonal nanostructure. This study should be continued by experimentally self-assembling the polygonal nanostructure with their corresponding NP building blocks, providing more data to be compared to the data obtained from these simulations.

Although the validation of the model by the simulations of the self-assembly of NP building blocks conducted in this study suggest that the model has progressed toward being a potentially complementary tool to the analysis and design of nanoassemblies, the structures in this report need to be produced experimentally, spectrally characterized, and compared to the simulation data. After the analysis of the experimental data and comparison to the results of the simulations, appropriate adjustments of the model parameters should be considered.

6.1.4 Contributions. Our research has shown that the model has the capability of controlling the interparticle distances between NPs within a nanostructure. There are also tools that have been incorporated into the model to measure interparticle distance, angles, the number of bp hybridized within a duplex, and to visualize a 3D representation of the self-assembly simulation. With these capabilities, the model has been shown to be valuable resource in the nanostructure design process. Furthermore, it was also revealed that is possible to simulate many different nanostructure designs in a relatively short amount of time, making it an efficient tool for examining many ideas in parallel. Also, there have been many simulated self-assembled nanostructures which could be self-assembled experimentally for comparison to aide in further validation of the NP building block model and to begin to discern its predictive ability to design nanostructures.

6.1.5 Limitations. Although the utility of the self-assembly model was found to be significant, there were some limitations found as well. In its present state, the model can only simulate the self-assembly of nanostructures with one size of NP (2.83 nm in diameter), which is the average size of NP used in the sequential anisotropic mono-functionalization strategy (Kim et al., 2011). It would be beneficial to be able to select other NP sizes or select a range of NP sizes within a simulation to extend the flexibility of the model producing broader range of NP building blocks. This would reduce the limitation currently imposed by the model on researchers' ability to validate the model against previous experimentally self-assembled Au NP structures and the current lack of ability to adjust Au NP size, reducing the potential library for Au NP building blocks. Furthermore, the option to select different NP sizes would require the appropriate adjustment in parameters for a given NP size.

Another limitation was the inability to simulate free ssDNA as a scaffold or template strand within a system. This would allow further validation of the model with simulations for the structures developed by Alivisatos et al. (1996) and Loweth et al. (1999), and possibly the ability to simulate DNA origami structures (Rothemund, 2006). Finally, computational speed and the restriction to 3-day walltimes for simulations became a limitation. As the systems increased in the number of particles, the number of list updates decreased, which meant that these larger systems needed to simulated for longer periods of time to achieve the self-assembled structure. In this study, the simulations had to be restarted in 3-day intervals to allow the simulations to complete self-assembly. Being able to use a GPU to compute the progression of simulations could greatly reduce the time needed for more complex simulations to achieve a final self-assembled structure (Teo et al, 2014).

Although there were some limitations in the current version of the coarse-grained model, the benefits of the model greatly outweigh its limitations. Therefore, the model should be improved to resolve the current limitations and add to its utility for the self-assembly of anisotropic multifunctional nanocomposites.

6.2 Future Work

While this thesis has revealed the potential of simulating the self-assembly of NP building blocks by using the building blocks developed by Kim et al. (2011) to construct various nanostructures, many opportunities for extending the scope of this thesis remain (see Figure 32). First, validation of the model should be done through the fabrication of the structures simulated in this report. If the results of fabrication do not reflect what was seen in the model, the appropriate adjustments to the parameters of the model should be implemented accordingly to improve the model's accuracy. If the results do reflect what was seen in the simulations, the abilities of the model should be expanded for further investigation into the behavior of self-assembly of the NP building blocks into various nanostructures and aid in the design of multifunctional nanocomposites.

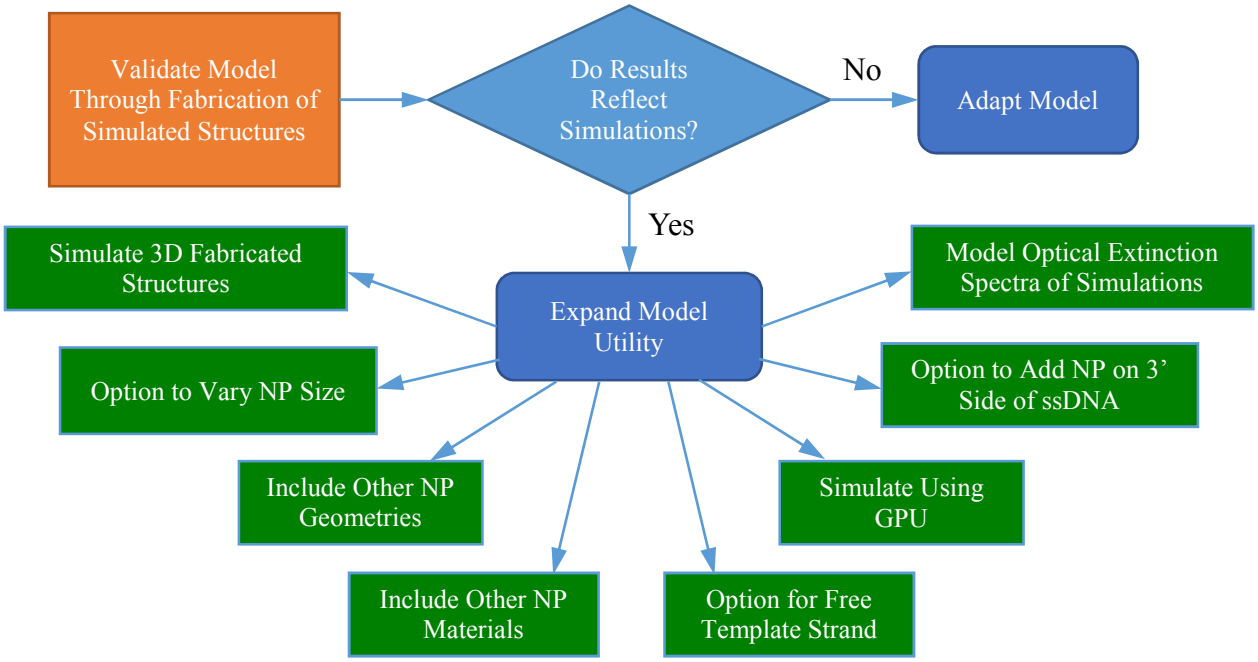

Figure 32. Workflow diagram of options for future development of the coarse-grained model for the self-assembly of NP building blocks.

The first direction these investigations could undertake is the simulation of previously fabricated 3D Au NP nanoassemblies, which could begin with the Au NP pyramids experimentally produced by Mastroianni et al. (2009) for further validation of the model. Simulating these structures would give the coarse-grained model more data to be used in comparison with experimental results to fine tune its parameters.

Another direction would be to include more design inputs for building blocks in the coarse-grained model, including the ability to change the size of individual NPs, apply additional NP geometries, and include other NP materials besides Au. A suitable place to start would be the library of NPs reported in Tan et al. (2011). Another possibility would be to add the capability to perform simulations using free ssDNA (Alivisatos et al., 1996; Rothemund, 2006). This would

enable simulations of the parallel and antiparallel dimers and parallel homotrimers produced by Alivisatos et al. (Alivisatos et al., 1996) and the ability to simulate DNA-origami structures through the use of a scaffold or free template strand where the staple strands are functionalized to the Au NPs (Rothemund, 2006). Finally, the ability to add NPs to the 3' side of ssDNA would allow the model to cater to other methods for self-assembly developed by other researchers (Alivisatos et al., 1996). These options would also allow for the simulation of more structures to validate the model, specifically those manufactured by Alivisatos et al. (1996) and Loweth et al. (1999).

Two other options for further development of the model are adaption of the model for GPU simulation and the ability to produce modeled extinction spectra of the simulated self-assembled structures. The GPU would enable the model to simulate much larger systems in shorter timeframes (Teo et al., 2014), which would further enhance the utility of the model for the rational design of nanocomposites for many applications. Since the coarse-grained model simulates the NP building blocks in a salt solution and the characterization of optical properties is done with a UV/Vis spectrophotometer in a liquid sample, modeling the extinction spectra of the simulated self-assembled structures would enable researchers to see whether their proposed structure is suitable for plasmonic applications (Nordlander, Oubre, Prodan, Li, & Stockman, 2004). The use of an appropriate theoretical approach, such as plasmon hybridization (Prodan, Radloff, Halas, & Nordland, 2003), could be used to predict the optical properties of Au NP pairs since the optical properties are dependent on the size, shape, and or spacing between the NPs (Loweth et al., 1999). Also, it would permit researchers to compare spectra of their manufactured structures to the spectra of the simulated structures, which could result in optimization of the model to self-assemble the correct interparticle spacing between NPs for more accurate modeling

since a nanostructure's plasmon band is dependent on the size, shape, and spacing of the NPs within the structure.

6.3 Conclusion

The coarse-grained model for the self-assembly of NP building blocks is a modeling tool that aims to enhance the purposeful design of multifunctional nanostructures by creating a 3D virtual representation of the self-assembly process of the building blocks and the ability to calculate structural properties of interparticle distance and angles (Armistead et al., 2015). This report extends the work of Armistead et al. (2015) with additional model validation, demonstrates the potential capabilities of the model, and presents new structures to be manufactured for further validation. Although there are current limitations, the coarse-grained NP building block model shows promise for future utility as a valuable aid to the nanoassembly design process.

References

[1] Adleman, L. M. (1998). Computing with DNA. Scientific American, 279(8), 34-41.

[2] Alberts B, Johnson A, Lewis J, et al. Molecular Biology of the Cell. 4th edition. New York: Garland Science; 2002. The Structure and Function of DNA. Available from: http://www.ncbi.nlm.nih.gov/books/NBK26821/

[3] Aldaye, F. A., & Sleiman, H. F. (2006). Sequential self-assembly of a DNA hexagon as a template for the organization of gold nanoparticles. Angewandte Chemie International Edition, 45(14), 2204-2209.

[4] Aldaye, F. A., & Sleiman, H. F. (2007, September). DNA-mediated patterning of gold nanoparticles into discrete structures: modularity, write/erase, and structural switching. In NanoScience+ Engineering (pp. 664203-664203). International Society for Optics and Photonics.

[5] Aldaye, F. A., & Sleiman, H. F. (2007). Dynamic DNA templates for discrete gold nanoparticle assemblies: control of geometry, modularity, write/erase and structural switching. Journal of the American Chemical Society, 129(14), 4130-4131.

[6] Aldaye, F. A., Palmer, A. L., & Sleiman, H. F. (2008). Assembling materials with DNA as the guide. Science, 321(5897), 1795-1799.

[7] Alivisatos, A. P. (1996). Perspectives on the physical chemistry of semiconductor nanocrystals. The Journal of Physical Chemistry, 100(31), 13226-13239.

[8] Alivisatos, A. P. (1996). Semiconductor clusters, nanocrystals, and quantum dots. Science, 271(5251), 933.

[9] Alivisatos, A. P., Johnsson, K. P., Peng, X., Wilson, T. E., Loweth, C. J., Bruchez, M. P., Jr., & Schultz, P. G. (1996). Organization of nanocrystal molecules' using DNA. Nature, 382(6592), 609-611.

[10] Armistead, C., Hendricks, J., Fochtman, T., Batta-Mpouma, J., Patitz, M., Deaton, R., Han, H., & Kim, J.-W. (2015). Coarse-grained simulation of DNA-linked nanoparticle

building blocks. Poster presented at the 9th IEEE International Conference on Nano/Molecular Medicine & Engineering, Honolulu, HI.

[11] Auyeung, E., Cutler, J. I., Macfarlane, R. J., Jones, M. R., Wu, J., Liu, G., Zhang, K., Osberg, K. D., & Mirkin, C. A. (2012). Synthetically programmable nanoparticle superlattices using a hollow three-dimensional spacer approach. Nature Nanotechnology, 7(1), 24-28.

[12] Bethune, D. S., Kiang, C. H., De Vries, M. S., Gorman, G., Savoy, R., Vazquez, J., & Beyers, R. (1993). Cobalt-catalysed growth of carbon nanotubes with single-atomic-layer walls. Nature, 363, 605-607.

[13] Bhushan, B., Luo, D., Schricker, S. R., Sigmund, W., & Sauscher, S. (Eds.). (2014) Handbook of Nanomaterials Properties. New York: Springer.

[14] Briñas, R. P., Maetani, M., & Barchi, J. J. (2013). A Survey of Place-exchange Reaction for the Preparation of Water-Soluble Gold Nanoparticles. Journal of Colloid and Interface Science, 392, 415–421. http://doi.org/10.1016/j.jcis.2012.06.042

[15] Bustamante, C., Marko, J. F., Siggia, E. D., & Smith, S. B. (1994). "Entropic elasticity of λ-phage DNA", Science 265, 1599-1600.

[16] Cai, W., Gao, T., Hong, H., & Sun, J. (2008). Applications of gold nanoparticles in cancer nanotechnology. Nanotechnology, Science and Applications, 2008(1).

[17] Cao, G. (2004). Nanostructures and Nanomaterials: Synthesis, Properties and Applications. Imperial College Press, London.

[18] Castro, C. E., Kilchherr, F., Kim, D.-N., Shiao, E. L., Wauer, T., Wortmann, P., Bathe, M., & Dietz, H. (2011). A primer to scaffolded DNA origami. Nature Methods, 8(3), 221-229.

[19] Chen, J. H., & Seeman, N. C. (1991). Synthesis from DNA of a molecule with the connectivity of a cube. Nature, 350(6319), 631-633.

[20] Claridge, S. A., Goh, S. L., Frechet, J. M., Williams, S. C., Micheel, C. M., & Alivisatos, A. P. (2005). Directed assembly of discrete gold nanoparticle groupings using branched DNA scaffolds. Chemistry of Materials, 17(7), 1628-1635.

[21] Claridge, S. A., Liang, H. W., Basu, S. R., Fréchet, J. M., & Alivisatos, A. P. (2008). Isolation of Discrete Nanoparticle−DNA Conjugates for Plasmonic Applications. Nano Letters, 8(4), 1202-1206.

[22] Collier, C. P., Vossmeyer, T., & Heath, J. R. (1998). Nanocrystal superlattices. Annual Review of Physical Chemistry, 49(1), 371-404.

[23] Corsi, J., Hawtin, R. W., Ces, O., Attard, G. S., & Khalid, S. (2010). DNA lipoplexes: Formation of the inverse hexagonal phase observed by coarse-grained molecular dynamics simulation. Langmuir, 26(14), 12119-12125.

[24] Cuenca, A. G., Jiang, H., Hochwald, S. N., Delano, M., Cance, W. G., & Grobmyer, S. R. (2006). Emerging implications of nanotechnology on cancer diagnostics and therapeutics. Cancer, 107(3), 459-466.

[25] Deaton, R., Kim, J.-W., & Chen, J. (2003). Design and test of noncrosshybridizing oligonucleotide building blocks for DNA computers and nanostructures. Applied Physics Letters, 82(8), 1305-1307.

[26] Drexler, K. E., (1986), Engines of Creation, Anchor Books.

[27] Erben, C. M., Goodman, R. P., & Turberfield, A. J. (2007). A self-assembled DNA bipyramid. Journal of the American Chemical Society, 129(22), 6992-6993.

[28] Feynman, R. P. (1960). There's plenty of room at the bottom. Engineering and Science, 23(5), 22-36.

[29] Fu, A., Micheel, C. M., Cha, J., Chang, H., Yang, H., & Alivisatos, A. P. (2004). Discrete nanostructures of quantum dots/Au with DNA. Journal of the American Chemical Society, 126(35), 10832-10833.

[30] Gandubert, V. J. & Lennox, R. B. (2005). Assessment of 4-(dimethylamino)pyridine as a capping agent for gold nanoparticles. Langmuir, 21(14), 6532-6539.

[31] Gittins, D. I., Caruso, F. (2001). Spontaneous phase transfer of nanoparticulate metals from organic to aqueous media. Angewandte Chemie International Edition, 40(16), 3001-3004.

[32] Halas, N. J., Lal, S., Chang, W. S., Link, S., & Nordlander, P. (2011). Plasmons in strongly coupled metallic nanostructures. Chemical Reviews, 111(6), 3913-3961.

[33] Hsu, C. W. (2010). Self-Assembly of DNA-Linked Nanoparticles (Doctoral dissertation, Wesleyan University).

[34] Iijima, S. & Ichihashi, T., (1993). Single-shell carbon nanotubes of 1-nm diameter, Nature, 363, 603-605.

[35] Iijima, S., (1991). Helical microtubules of graphic carbon, Nature, 406, 118-120.

[36] Jin, R., Wu, G., Li, Z., Mirkin, C. A., & Schatz, G. C. (2003). What controls the melting properties of DNA-linked gold nanoparticle assemblies? Journal of the American Chemical Society, 126(6) 1643-1654.

[37] John, K., & Bär, M. (2005). Alternative mechanisms of structuring biomembranes: self-assembly versus self-organization. Physical Review Letters, 95(19), 198101.

[38] Jones, M. R., Seeman, N. C., & Mirkin, C. A. (2015). Programmable materials and the nature of the DNA bond. Science, 347(6224), 1260901.

[39] Kelsall, R. W., Hamley, I. W., & Geoghegan, M. (Eds.). (2005). Nanoscale science and technology. Chichester: Wiley.

[40] Khalid, S., Bond, P. J., Holyoake, J., Hawtin, R. W., & Sansom, M. S. (2008). DNA and lipid bilayers: self-assembly and insertion. Journal of The Royal Society Interface, 5(Suppl 3), 241-250.

[41] Kim, B., Carignano, M. A., Tripp, S. L., & Wei, A. (2004). Cluster size analysis of two-dimensional order in colloidal gold nanoparticle arrays. Langmuir, 20(21), 9360-9365.

[42] Kim, D. N., Kilchherr, F., Dietz, H., & Bathe, M. (2012). Quantitative prediction of 3D solution shape and flexibility of nucleic acid nanostructures. Nucleic Acids Research, 40(77), 2862-2868.

[43] Kim, J. H., & Kim, J.-W. (2010). Simultaneously controlled directionality and valency on a water-soluble gold nanoparticle precursor for aqueous-phase anisotropic self-assembly. Langmuir, 26(24), 18634-18638.

[44] Kim, J.-W., & Deaton, R. (2013). Molecular Self-Assembly of Multifunctional Nanoparticle Composites with Arbitrary Shapes and Functions: Challenges and Strategies. Particle & Particle Systems Characterization, 30(2), 117-132.

[45] Kim, J.-W., Kim, J. H., & Deaton, R. (2011). DNA-Linked Nanoparticle Building Blocks for Programmable Matter. Angewandte Chemie International Edition, 50(39), 9185-9190.

[46] Kyrychenko, A., Karpushina, G. V., Bogatyrenko, S. I., Kryshtal, A. P., & Doroshenko, A. O. (2011). Preparation, structure, and a coarse-grained molecular dynamics model for dodecanethiol-stabilized gold nanoparticles. Computational and Theoretical Chemistry, 977(1), 34-39.

[47] Lal, S., Clare, S. E., & Halas, N. J. (2008). Nanoshell-enabled photothermal cancer therapy: impending clinical impact. Accounts of chemical research, 41(12), 1842-1851.

[48] Le, J. D., Pinto, Y., Seeman, N. C., Musier-Forsyth, K., Taton, T. A., & Kiehl, R. A. (2004). DNA-templated self-assembly of metallic nanocomponent arrays on a surface. Nano Letters, 4(12), 2343-2347.

[49] Lee, O. S., & Schatz, G. C. (2009). Molecular dynamics simulation of DNA-functionalized gold nanoparticles. The Journal of Physical Chemistry C, 113(6), 2316-2321.

[50] Li, H., Park, S. H., Reif, J. H., LaBean, T. H., & Yan, H. (2004). DNA-templated self-assembly of protein and nanoparticle linear arrays. Journal of the American Chemical Society, 126(2), 418-419.

[51] Li, X., Yang, X., Qi, J., & Seeman, N. C. (1996). Antiparallel DNA double crossover molecules as components for nanoconstruction. Journal of the American Chemical Society, 118(26), 6131-6140.

[52] Liu, Z., & Jiang, M. (2007). Reversible aggregation of gold nanoparticles driven by inclusion complexation. Journal of Materials Chemistry, 17(40), 4249-4254.

[53] Lodish, H., Berk, A., Kaiser, C. A., Krieger, M., Scott, M. P., Bretscher, A., Ploegh, H., & Matsudaira, P. (2000). Molecular cell biology (Vol. 4). New York: WH Freeman.

[54] Loweth, C. J., Caldwell, W. B., Peng, X., Alivisatos, A. P., & Schultz, P. G. (1999). DNA-based assembly of gold nanocrystals. Angewandte Chemie International Edition, 38(12), 1808-1812.

[55] Macfarlane, R. J., Lee, B., Jones, M. R., Harris, N., Schatz, G. C., & Mirkin, C. A. (2011). Nanoparticle superlattice engineering with DNA. Science, 334(6053), 204-208.

[56] Macfarlane, R. J., O'Brien, M. N., Petrosko, S. H., & Mirkin, C. A. (2013). Nucleic Acid-Modified Nanostructures as Programmable Atom Equivalents: Forging a New "Table of Elements". Angewandte Chemie International Edition, 52(22), 5688-5698.

[57] Maier, S. A., Brongersma, M. L., Kik, P. G., Meltzer, S., Requicha, A. A., & Atwater, H. A. (2001). Plasmonics—a route to nanoscale optical devices. Advanced Materials, 13(19), 1501-1505.

[58] Maier, S. A., Kik, P. G., Atwater, H. A., Meltzer, S., Harel, E., Koel, B. E., & Requicha, A. A. (2003). Local detection of electromagnetic energy transport below the diffraction limit in metal nanoparticle plasmon waveguides. Nature Materials, 2(4), 229-232.

[59] Mastroianni, A. J., Claridge, S. A., & Alivisatos, A. P. (2009). Pyramidal and chiral groupings of gold nanocrystals assembled using DNA scaffolds. Journal of the American Chemical Society, 131(24), 8455-8459.

[60] Mastroianni, A. J., Sivak, D. A., Geissler, P. L., & Alivisatos, A. P. (2009). Probing the conformational distributions of subpersistence length DNA. Biophysical Journal, 97(5), 1408-1417.

[61] Mirkin, C. A., Letsinger, R. L., Mucic, R. C., & Storhoff, J. J. (1996). A DNA-based method for rationally assembling nanoparticles into macroscopic materials. Nature, 382(6592), 607-609.

[62] Mura, C., & McCammon, J. A. (2008). Molecular dynamics of a κB DNA element: base flipping via cross-strand intercalative stacking in a microsecond-scale simulation. Nucleic Acids Research, 36(15), 4941-4955.

[63] Nie, Z., Petukhova, A., & Kumacheva, E. (2010). Properties and emerging applications of self-assembled structures made from inorganic nanoparticles. Nature Nanotechnology, 5(1), 15-25.

[64] Niemeyer, C. M. (2000). Self-assembled nanostructures based on DNA: towards the development of nanobiotechnology. Current Opinion in Chemical Biology, 4(6), 609-618.

[65] Niemeyer, C. M. (2001). Nanoparticles, proteins, and nucleic acids: biotechnology meets materials science. Angewandte Chemie International Edition, 40(22), 4128-4158.

[66] Nordlander, P., Oubre, C., Prodan, E., Li, K., & Stockman, M. I. (2004). Plasmon hybridization in nanoparticle dimers. Nana Letters, 4(5), 899-903.

[67] Nykypanchuk, D., Maye, M. M., van der Lilie, D., & Gang, O. (2008). DNA-guided crystallization of colloidal nanoparticles. Nature 451, 549-552.

[68] Ochekpe, N. A., Olorunfemi, P. O., & Ngwuluka, N. C. (2009). Nanotechnology and drug delivery part 1: background and applications. Tropical Journal of Pharmaceutical Research, 8(3).

[69] Orozco, M., Pérez, A., Noy, A., & Luque, F. J. (2003). Theoretical methods for the simulation of nucleic acids. Chemical Society Reviews, 32(6), 350-364.

[70] Ouldridge, T. E. (2011) Coarse-grained modelling of DNA and DNA self-assembly. (Doctoral dissertation, University of Oxford)

[71] Ouldridge, T. E., Louis, A. A., & Doye, J. P. (2011). Structural, mechanical, and thermodynamic properties of a coarse-grained DNA model. The Journal of Chemical Physics, 134(8), 085101.

[72] Ozbay, E. (2006). Plasmonics: merging photonics and electronics at nanoscale dimensions. Science, 311(5758), 189-193.

[73] Park, S. H., Yan, H., Reif, J. H., LaBean, T. H., & Finkelstein, G. (2004). Electronic nanostructures templated on self-assembled DNA scaffolds. Nanotechnology, 15(10), S525.

[74] Park, S. Y., Lytton-Jean, A. K., Lee, B., Weigand, S., Schatz, G. C., & Mirkin, C. A. (2008). DNA-programmable nanoparticle crystallization. Nature, 451(7178), 553-556.

[75] Pérez, A., Luque, F. J., & Orozco, M. (2007). Dynamics of B-DNA on the microsecond time scale. Journal of the American Chemical Society, 129(47), 14739-14745.

[76] Pettersen, E. F., Goddard, T. D., Huang, C. C., Couch, G. S., Greenblatt, D. M., Meng, E. C., & Ferrin, T. E. (2004). UCSF Chimera--a visualization system for exploratory research and analysis. Journal of Computational Chemistry, 25(13), 1605-12.

[77] Pileni, M. P. (2001). Nanocrystal self-assemblies: fabrication and collective properties. The Journal of Physical Chemistry B, 105(17), 3358-3371.

[78] Prodan, E., Radloff, C., Halas, N. J., & Nordlander, P. (2003). A hybridization model for the plasmon response of complex nanostructures. Science, 302(5644), 419-422.

[79] Richmond, T. J., & Davey, C. A. (2003). The structure of DNA in the nucleosome core. Nature, 423; 145-150.

[80] Rosi, N. L., & Mirkin, C. A. (2005). Nanostructures in biodiagnostics. Chemical Reviews, 105(4), 1547-1562.

[81] Rosvall, M., & Sneppen, K. (2006). Self-assembly of information in networks. Europhysics Letters, 74(6), 1109-1115.

[82] Rothemund, P. W. (2006). Folding DNA to create nanoscale shapes and patterns. Nature, 440(7082), 297-302.

[83] Rothemund, P. W., Papadakis, N., & Winfree, E. (2004). Algorithmic self-assembly of DNA Sierpinski triangles. Public Library of Science Biology, 2(12), 424.

[84] Schmid, G. (Ed.). (2011). Nanoparticles: from theory to application. John Wiley & Sons.

[85] Schreck, J. S., Ouldridge, T. E., Romano, F., Louis, A. A., & Doye, J. P. K. (2015). Characterizing the bending and flexibility induced by bulges in DNA duplexes. AIP: The Journal of Chemical Physics, 142, 165101-165103.

[86] Schuller, J. A., Barnard, E. S., Cai, W., Jun, Y. C., White, J. S., & Brongersma, M. L. (2010). Plasmonics for extreme light concentration and manipulation. Nature Materials, 9(3), 193-204.

[87] Seeman, N. C. (1998). Nucleic acid nanostructures and topology. Angewandte Chemie International Edition, 37(23), 3220–3238.

[88] Seeman, N. C. (2003). DNA in a material world. Nature, 421(6921), 427-431.

[89] Sharma, P. K., Dutta, R. K., & Pandey, A. C. (2011). Advances in multifunctional magnetic nanoparticles. Adv. Mater. Lett, 2(4), 246-263.

[90] Sherman, W. B., & Seeman, N. C. (2006). Design of minimally strained nucleic acid nanotubes. Biophysical Journal, 90(12), 4546-4557.

[91] Shih, W. M., Quispe, J. D., & Joyce, G. F. (2004). A 1.7-kilobase single-stranded DNA that folds into a nanoscale octahedron. Nature, 427(6975), 618-621.

[92] Shipway, A. N., Katz, E., & Willner, I. (2000). Nanoparticle arrays on surfaces for electronic, optical, and sensor applications. ChemPhysChem, 1(1), 18-52.

[93] Snodin, B. E., Randisi, F., Mosayebi, M., Šulc, P., Schreck, J. S., Romano, F., Ouldridge, T. E., Tsukanov, R., Nir, E., Louis, A. A., & Doye, J. P. K. (2015). Introducing improved structural properties and salt dependence into a coarse-grained model of DNA. The Journal of Chemical Physics, 142(23), 234901.

[94] Srinivas, N., Ouldridge, T. E., Šulc, P., Schaeffer, J. M., Yurke, B., Louis, A. A., Doye, J. P. K., & Winfree, E. (2013). On the biophysics and kinetics of toehold-mediated DNA strand displacement. Nucleic Acids Research, 41(22), 10341-10658.

[95] Storhoff, J. J., & Mirkin, C. A. (1999). Programmed materials synthesis with DNA. Chemical Reviews, 99(7), 1849-1862.

[96] SvnX [Computer Software]. (2016). Retrieved from http://www.lachoseinteractive.net/en/community/subversion/svnx/download/

[97] Swigon, D. (2009). The Mathematics of DNA Sturcture, Mechanics, and Dynamics. In Mathematics of DNA Structure, Function and Interactions (pp. 293-320). Springer New York.

[98] Tan, S. J., Campolongo, M. J., Luo, D., & Cheng, W. (2011). Building plasmonic nanostructures with DNA. Nature Nanotechnology, 6(5), 268-276.

[99] Teo, I., Perilla, J., Shahoei, R., McGreevy, R., & Harrison, C. (2014). GPU Accelerated Molecular Dynamics Simulation, Visualization, and Analysis. Beckman Institute for Advanced Science and Technology, University of Illinois at Urbana-Champaign

[100] Toffoli, T., & Margolus, N. (1991). Programmable matter: Concepts and realization. Physica D: Nonlinear Phenomena, 47(1-2), 263-272.

[101] Varadan, V. K., Pillai, A. S., Mukherji, D., Dwivedi, M., & Chen, L. (2010). Nanoscience and nanotechnology in engineering (pp. 50-51). World Scientific.

[102] Vollmer, M., & Kreibig, U. (1995). Optical properties of metal clusters. Springer Ser. Materials Science, 25.

[103] Wang, H., Brandl, D. W., Nordlander, P., & Halas, N. J. (2007). Plasmonic nanostructures: artificial molecules. Accounts of Chemical Research, 40(1), 53-62.

[104] Whitesides, G. M., & Boncheva, M. (2002). Beyond molecules: Self-assembly of mesoscopic and macroscopic components. Proceedings of the National Academy of Sciences, 99(8), 4769-4774.

[105] Wilson, M., Kannangara, K., Smith, G., Simmons, M., & Raguse, B. (2002). Nanotechnology: basic science and emerging technologies. CRC Press.

[106] Winfree, E. (1998). Algorithmic self-assembly of DNA (Doctoral dissertation, California Institute of Technology).

[107] Winfree, E., Liu, F., Wenzler, L. A., & Seeman, N. C. (1998). Design and self-assembly of two-dimensional DNA crystals. Nature, 394(6693), 539-544.

[108] Yang, X., Wenzler, L. A., Qi, J., Li, X., & Seeman, N. C. (1998). Ligation of DNA triangles containing double crossover molecules. Journal of the American Chemical Society, 120(38), 9779-9786.

[109] Yavuz, M. S., Cheng, Y., Chen, J., Cobley, C. M., Zhang, Q., Rycenga, M., Xie, J., Kim, C., Song, K. H., Schwartz, A. G., Wang, L. V., & Xia, Y. (2009). Gold nanocages covered by smart polymers for controlled release with near-infrared light. Nature Materials, 8(12), 935-939.

[110] Yu, W., Lee, J. S., Johnson, C., Kim, J.-W., & Deaton, R. (2010). Independent sets of DNA oligonucleotides for nanotechnology applications. IEEE Transactions on Nanobioscience, 9(1), 38-43.

[111] Zanchet, D., Micheel, C. M., Parak, W. J., Gerion, D., & Alivisatos, A. P. (2001). Electrophoretic isolation of discrete Au nanocrystal/DNA conjugates. Nano Letters, 1(1), 32-35.

[112] Zanchet, D., Micheel, C. M., Parak, W. J., Gerion, D., Williams, S. C., & Alivisatos, A. P. (2002). Electrophoretic and structural studies of DNA-directed Au nanoparticle groupings. The Journal of Physical Chemistry B, 106(45), 11758-11763.

[113] Zhang, D. Y., & Seelig, G. (2011). Dynamic DNA nanotechnology using strand-displacement reactions. Nature Chemistry, 3(2), 103-113.

[114] Zhang, S. (2003). Fabrication of novel biomaterials through molecular self-assembly. Nature Biotechnology, 21(10), 1171-1178.

[115] Zhang, Y., & Seeman, N. C. (1994). Construction of a DNA-truncated octahedron. Journal of the American Chemical Society, 116(5), 1661-1669.

[116] Zheng, J., Constantinou, P. E., Micheel, C., Alivisatos, A. P., Kiehl, R. A., & Seeman, N. C. (2006). Two-dimensional nanoparticle arrays show the organizational power of robust DNA motifs. Nano Letters, 6(7), 1502-1504.

Appendix A: Permissions from Publishers

Figures 1 and 2

License Number	3918451275986
License date	Jul 29, 2016
Licensed Content Publisher	John Wiley and Sons
Licensed Content Publication	Angewandte Chemie International Edition
Licensed Content Title	Nanoparticles, Proteins, and Nucleic Acids: Biotechnology Meets Materials Science
Licensed Content Author	Christof M. Niemeyer
Licensed Content Date	Nov 16, 2001
Licensed Content Pages	31
Type of use	Dissertation/Thesis
Requestor type	University/Academic
Format	Print and electronic
Portion	Figure/table
Number of figures/tables	2
Original Wiley figure/table number(s)	Figure 2, Figure 9
Will you be translating?	No
Title of your thesis / dissertation	Coarse-Grained Simulations of the Self-Assembly of DNA-Linked Gold Nanoparticle Building Blocks
Expected completion date	Sep 2016
Expected size (number of pages)	114
Publisher Tax ID	EU826007151

Figure 3A

License Number	3920000211599
License date	Aug 01, 2016
Licensed Content Publisher	Nature Publishing Group
Licensed Content Publication	Nature
Licensed Content Title	Organization of 'nanocrystal molecules' using DNA
Licensed Content Author	A. Paul Alivisatos, Kai P. Johnsson, Xiaogang Peng, Troy E. Wilson, Colin J. Loweth et al.
Licensed Content Date	Aug 15, 1996
Licensed Content Volume	382
Licensed Content Issue	6592
Type of Use	reuse in a dissertation / thesis
Requestor type	academic/educational
Format	print and electronic

Portion	figures/tables/illustrations
Number of figures/tables/illustrations	1
Figures	Figure 1
Author of this NPG article	no
Your reference number	
Title of your thesis / dissertation	Coarse-Grained Simulations of the Self-Assembly of DNA-Linked Gold Nanoparticle Building Blocks
Expected completion date	Sep 2016
Estimated size (number of pages)	114

Figures 3B, 4, and 27

License Number	3919670446289
License date	Jul 31, 2016
Licensed Content Publisher	John Wiley and Sons
Licensed Content Publication	Angewandte Chemie International Edition
Licensed Content Title	DNA-Based Assembly of Gold Nanocrystals
Licensed Content Author	Colin J. Loweth, W. Brett Caldwell, Xiaogang Peng, A. Paul Alivisatos, Peter G. Schultz
Licensed Content Date	Jun 8, 1999
Licensed Content Pages	5
Type of use	Dissertation/Thesis
Requestor type	University/Academic
Format	Print and electronic
Portion	Figure/table
Number of figures/tables	2
Original Wiley figure/table number(s)	Scheme 1, Figure 2
Will you be translating?	No
Title of your thesis / dissertation	Coarse-Grained Simulations of the Self-Assembly of DNA-Linked Gold Nanoparticle Building Blocks
Expected completion date	Sep 2016
Expected size (number of pages)	114

Figures 3C and 29

License Number	3919671142377

License date	Jul 31, 2016
Licensed Content Publisher	John Wiley and Sons
Licensed Content Publication	Angewandte Chemie International Edition
Licensed Content Title	Sequential Self-Assembly of a DNA Hexagon as a Template for the Organization of Gold Nanoparticles
Licensed Content Author	Faisal A. Aldaye, Hanadi F. Sleiman
Licensed Content Date	Feb 27, 2006
Licensed Content Pages	6
Type of use	Dissertation/Thesis
Requestor type	University/Academic
Format	Print and electronic
Portion	Figure/table
Number of figures/tables	2
Original Wiley figure/table number(s)	Scheme 1, Figure on Page 2204
Will you be translating?	No
Title of your thesis / dissertation	Coarse-Grained Simulations of the Self-Assembly of DNA-Linked Gold Nanoparticle Building Blocks
Expected completion date	Sep 2016
Expected size (number of pages)	114

Figures 3D and 30

Date: Sun, Jul 31, 2016 at 9:40 PM
Subject: Reprint Permission
To: reprint_permission@spie.org

Title: DNA-mediated patterning of gold nanoparticles into discrete structures: modularity, write/erase and structural switching
Author: Faisal A. Aldaye and Hanadi F. Sleiman
Volume: 6642
Issue: 664203
Page Numbers: 1-8
What I would like to reproduce: Figure 4
Where I'll republish the requested material: Thesis

Figure 3E

Title: Pyramidal and Chiral Groupings of Gold Nanocrystals Assembled Using DNA Scaffolds

Author: Alexander J. Mastroianni, Shelley A. Claridge, A. Paul Alivisatos

Publication: Journal of the American Chemical Society

Publisher Date: Jun 1, 2009

"Permission/License is granted for your order at no charge"

Figures 3F and 14

License Number	3920000818811
License date	Aug 01, 2016
Licensed Content Publisher	John Wiley and Sons
Licensed Content Publication	Angewandte Chemie International Edition
Licensed Content Title	DNA-Linked Nanoparticle Building Blocks for Programmable Matter
Licensed Content Author	Jin-Woo Kim, Jeong-Hwan Kim, Russell Deaton
Licensed Content Date	Sep 2, 2011
Licensed Content Pages	6
Type of use	Dissertation/Thesis
Requestor type	University/Academic
Format	Print and electronic
Portion	Figure/table
Number of figures/tables	2
Original Wiley figure/table number(s)	Figure 1, Figure 3
Will you be translating?	No
Title of your thesis / dissertation	Coarse-Grained Simulations of the Self-Assembly of DNA-Linked Gold Nanoparticle Building Blocks
Expected completion	Sep 2016

date	
Expected size (number of pages)	114

Figures 5 and 6

License Number	3920001012101
License date	Aug 01, 2016
Licensed Content Publisher	John Wiley and Sons
Licensed Content Publication	Particle & Particle Systems Characterization
Licensed Content Title	Molecular Self-Assembly of Multifunctional Nanoparticle Composites with Arbitrary Shapes and Functions: Challenges and Strategies
Licensed Content Author	Jin-Woo Kim, Russell Deaton
Licensed Content Date	Feb 11, 2013
Licensed Content Pages	16
Type of use	Dissertation/Thesis
Requestor type	University/Academic
Format	Print and electronic
Portion	Figure/table
Number of figures/tables	2
Original Wiley figure/table number(s)	Figure 1, Figure 2
Will you be translating?	No
Title of your thesis / dissertation	Coarse-Grained Simulations of the Self-Assembly of DNA-Linked Gold Nanoparticle Building Blocks
Expected completion date	Sep 2016
Expected size (number of pages)	114

Figure 7

License Number	3920001303033
License date	Aug 01, 2016
Licensed Content Publisher	Elsevier
Licensed Content	Computational and Theoretical Chemistry

Publication	
Licensed Content Title	Preparation, structure, and a coarse-grained molecular dynamics model for dodecanethiol-stabilized gold nanoparticles
Licensed Content Author	Alexander Kyrychenko, Galina V. Karpushina, Sergey I. Bogatyrenko, Alexander P. Kryshtal, Andrey O. Doroshenko
Licensed Content Date	15 December 2011
Licensed Content Volume	977
Licensed Content Issue	1-3
Licensed Content Pages	6
Type of Use	reuse in a thesis/dissertation
Portion	figures/tables/illustrations
Number of figures/tables/illustrations	1
Format	both print and electronic
Are you the author of this Elsevier article?	No
Will you be translating?	No
Order reference number	
Original figure numbers	Figure 4
Title of your thesis/dissertation	Coarse-Grained Simulations of the Self-Assembly of DNA-Linked Gold Nanoparticle Building Blocks
Expected completion date	Sep 2016
Estimated size (number of pages)	114
Elsevier VAT number	GB 494 6272 12

Figure 7

Title: Molecular Dynamics Simulation of DNA-Functionalized Gold Nanoparticles

Author: One-Sun Lee, George C. Schatz

Publication: The Journal of Physical Chemistry C

Date: Feb 1, 2009

"Permission/License is granted for your order at no charge"

Figure 7

License Number	3920010595431
License date	Aug 01, 2016

Licensed Content Publisher	AIP Publishing LLC
Licensed Content Publication	Journal of Chemical Physics
Licensed Content Title	Structural, mechanical, and thermodynamic properties of a coarse-grained DNA model
Licensed Content Author	Thomas E. Ouldridge, Ard A. Louis, Jonathan P. K. Doye
Licensed Content Date	Feb 22, 2011
Licensed Content Volume	134
Licensed Content Issue	8
Requestor type	Student
Format	Print and electronic
Portion	Figure/Table
Number of figures/tables	1

Figure 8

License Number	3920010463587
License date	Aug 01, 2016
Licensed Content Publisher	AIP Publishing LLC
Licensed Content Publication	Journal of Chemical Physics
Licensed Content Title	Characterizing the bending and flexibility induced by bulges in DNA duplexes
Licensed Content Author	John S. Schreck, Thomas E. Ouldridge, Flavio Romano, et al.
Licensed Content Date	Apr 22, 2015
Licensed Content Volume	142
Licensed Content Issue	16
Requestor type	Student
Format	Print and electronic
Portion	Figure/Table
Number of figures/tables	1